

HYDRODYNAMIC PERFORMANCE ANALYSIS OF A CONTAINER SHIP IN INLAND WATERWAY OF BANGLADESH USING 3D NUMERICAL SIMULATION

By

Md. Al Amin Miazee

Student No.: 1014122010 P

Session: October 2014

A thesis submitted to the

Department of Naval Architecture and Marine Engineering

in partial fulfillment of the requirements for the degree of

MASTER OF SCIENCE

in

NAVAL ARCHITECTURE AND MARINE ENGINEERING



DEPARTMENT OF NAVAL ARCHITECTURE AND MARINE ENGINEERING

BANGLADESH UNIVERSITY OF ENGINEERING AND TECHNOLOGY

DHAKA-1000

1st March 2018

Certificate of Approval

The thesis entitled **Hydrodynamic Performance Analysis of a Container Ship in Inland Waterway of Bangladesh using 3d Numerical Simulation** submitted by **Md. Al Amin Miazee**, Student No.: 1014122010P, Session: October, 2014 to the Department of Naval Architecture and Marine Engineering, Bangladesh University of Engineering and Technology (BUET), Dhaka-1000, Bangladesh has been accepted as satisfactory in partial fulfillment of the requirements for the degree of **Master of Science** in Naval Architecture and Marine Engineering on **1st March, 2018**.

Board of Examiners

1. 

Dr. Goutam Kumar Saha
Professor and Head
Department of NAME, BUET, Dhaka-1000.

Chairman
(Supervisor)

2. 

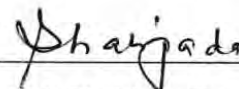
Dr. Goutam Kumar Saha
Professor and Head
Department of NAME, BUET, Dhaka-1000.

Member
(Ex-Officio)

3.  1.03.18

Dr. Md. Mashud Karim
Professor
Department of NAME, BUET, Dhaka-1000.

Member

4. 

Dr. Md. Shahjada Tarafder
Professor
Department of NAME, BUET, Dhaka-1000.

Member

5. 

Dr. Md. Abdur Rashid Sarkar
Professor
Department of Mechanical Engineering,
BUET, Dhaka-1000.

Member
(External)

Certificate of Research

This is to certify that the candidate has done this work and it was not submitted elsewhere for the award of any degree or diploma.



Supervisor

Dr. Goutam Kumar Saha

Professor and Head

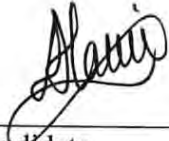
Department of Naval Architecture and Marine Engineering (NAME)

Bangladesh University of Engineering and Technology (BUET)

Dhaka-1000, Bangladesh

Declaration

I do hereby declare that I, the candidate, have done this work and it was not submitted elsewhere for the award of any degree or diploma.



Candidate

Md. Al Amin Miazee

Student No.: 1014122010 P

Department of Naval Architecture and Marine Engineering (NAME)

Bangladesh University of Engineering and Technology (BUET)

Dhaka-1000, Bangladesh

Acknowledgment

In the beginning, I would like to acknowledge the blessings of Almighty Allah, The Beneficent, and The Merciful for His divine help in completing this thesis successfully.

Then I would like to express my deep gratitude to my thesis supervisor, Dr. Goutam Kumar Saha, Professor and Head, Department of Naval Architecture and Marine Engineering (NAME), BUET, for his heartiest cooperation throughout the thesis. The work was mostly conducted at the high configured computers of NAME department. I am extremely thankful to him for providing me all necessary technical supports to perform my thesis work successfully. Without his guidance, wise suggestions, encouragement and great assistance this thesis may not be completed. Besides, I would like to mention the (CP#2084) project of Higher Education Quality Enhancement Program (HEQEP), UGC, Ministry of Education, Govt. of Bangladesh for providing necessary research facilities during the thesis work. In addition to my supervisor, I would like to thank all the members of my thesis committee: Prof. Dr. Md. Abdur Rashid Sarkar, Prof. Dr. Md. Mashud Karim, Prof. Dr. Md. Shahjada Tarafder for their insightful comments and encouragement which lead me to finish the thesis. I would like to give many thanks to all of my teachers of Department of NAME for their help during my period of study and staffs for their support and kindness. My sincere appreciation goes to all the developers of computer software used in this thesis including but not limited to SHIPFLOW CFD code, Origin, Microsoft Office.

Last but not least, I would like to acknowledge my gratitude to my father, mother and wife who have always encouraged me and provided all necessary facilities to elevate my knowledge up to this level, and without their support and guidance, it would be impossible for me to carry out the thesis work properly.

Md. Al Amin Miazee

Contents

Certificate of Approval	ii
Certificate of Research	iii
Declaration	iv
Acknowledgment	v
Contents	vi
List of Figures	ix
List of Tables	xii
Abstract	xiii
Nomenclature	xiv
1. Introduction	1
1.1 Background	1
1.2 Motivation	3
1.3 Literature Review	5
1.4 Objectives	6
1.5 Outline of the Methodology	7
2. Theory and Mathematical Formulation	8
2.1 Definition of Ship Resistance, Sinkage and Trim	8
2.1.1 Ship resistance	8
2.1.2 Sinkage	11
2.1.3 Trim	12
2.1.4 Shallow Water	12
2.2 Different Methods for the Prediction of Ship's Resistance	13
2.2.1 Empirical Methods	13
2.2.2 Use of the Methods	13
2.2.3 Physical Experiments: Model Testing	14
2.2.4 Numerical Methods: Computational Fluid Dynamics	15

2.3 Numerical Methods for Prediction of Ship Resistance, Sinkage and Trim using SHIPFLOW	18
2.3.1 Potential Flow Region	18
2.3.2 Boundary Layer Flow Region	20
2.3.3 Viscous Flow Region, RANS	23
2.3.3.1 Turbulence Modeling	25
2.3.3.2 Selection of Turbulence Modeling	26
2.3.3.3 Shear-Stress Transport (SST) $k-\omega$ model	26
2.3.3.4 Wall Functions vs. Near-Wall Model	29
2.4 SHIPFLOW CFD Software	30
2.4.1 XMESH	31
2.4.2 XPAN	31
2.4.3 XBOUND	32
2.4.4 XGRID	33
2.4.5 XCHAP	33
2.4.6 Co-ordinate system in SHIPFLOW	34
2.4.7 Initial and Boundary Conditions	35
2.4.8 Grid	36
2.4.9 Overlapping grids	37
2.5 Verification and Validation (V&V)	37
2.5.1 Verification	38
2.5.2 Validation	39
3. Geometry and Condition	41
3.1 Geometry and Principal Particulars	41
3.1.1 Case model-1: KRISO Container Ship (KCS) Hull	41
3.1.2 Case model-2: 158 TEU Container Ship Hull	43
3.2 Conditions	44
3.2.1 Conditions for Model Test Experiment	45

3.2.2 Conditions for Simulation in SHIPFLOW	46
3.2.3 Boundary Conditions in SHIPFLOW	47
4. Results and Discussions	48
4.1 Case Study 1: KRISO Container Ship (KCS) Hull	48
4.1.1 Verification & Validation for KCS Hull	50
4.2 Case Study 2: 158 TEU Container Ship Hull	52
4.2.1 Deep Water Resistance, Sinkage and Trim	53
4.2.1.1 Calculation of Resistance	53
4.2.1.2 Calculation of Sinkage and Trim	55
4.2.2 Shallow Water Resistance, Sinkage and Trim	62
4.2.2.1 Resistance	62
4.2.2.2 Sinkage and Trim	63
4.2.3 Squat Calculation	65
4.3 Case Study 3: Investigation of the Dhaka Chittagong Route for the Container Ship	66
5. Conclusions and Future Works	78
5.1 Conclusions	78
5.2 Future Works	79
References	80
A.1 SHIPFLOW input file for 158 TEU Container ship at 10 knot speed	85
A.2 SHIPFLOW output file for 158 TEU Container ship at 10 knot speed	86

List of Figures

Figure 1.1: Income, Costs, and Profit as functions of vessel speed (Dagkinis. 2015)	4
Figure 2.1: Definition of Ship Resistance	8
Figure 2.2: Components of resistance of ships	9
Figure 2.3: Boundary layer along the hull	10
Figure 2.4: Definition of sinkage and trim	12
Figure 2.5: Towing Tank at Gdansk University of Technology, Poland	15
Figure 2.6: Applications of CFD in Marine Hydrodynamics	16
Figure 2.7: Flow region	18
Figure 2.8: Hierarchy of turbulence models (Sadrehaghighi, 2018)	26
Figure 2.9: Wall functions vs. near-wall model	30
Figure 2.10: Cartesian coordinate system in SHIPFLOW	34
Figure 2.11: Boundary conditions for a typical flow domain	36
Figure 2.12: Examples of grid topologies	36
Figure 2.13: Sources of errors in computed results	38
Figure 3.1: Geometry of KCS hull	41
Figure 3.2: Lines plan of KCS hull	42
Figure 3.3: Geometry of 158 TEU container ship hull	43
Figure 3.4: Lines plan of 158 TEU container ship	44
Figure 3.5: Boundary conditions for KCS hull	47

Figure 4.1: Four sets of grids for KCS hull: (a) Fine, (b) Medium, (c) Coarse, (d) Vcoarse	49
Figure 4.2: Four sets of grids for 158 TEU container ship hull: (a) Fine, (b) Medium, (c) Coarse, (d) Vcoarse	52
Figure 4.3: Resistance coefficients (C_W , C_F) at varying Froude numbers	54
Figure 4.4: Prediction of resistance in SHIPFLOW and Towing Tank	55
Figure 4.5: Sinkage and trim variation with Froude numbers	56
Figure 4.6 (a): Kelvin wave pattern at the speed of 10 knots	57
Figure 4.6 (b): Wave profile at the speed of 10 knots (units are meter)	57
Figure 4.7 (a): Kelvin wave pattern at the speed of 9.5 knots	58
Figure 4.7 (b): Wave profile at the speed of 9.5 knots (units are meter)	58
Figure 4.8 (a): Kelvin wave pattern at the speed of 9 knots	59
Figure 4.8 (b): Wave profile at the speed of 9 knots (units are meter)	59
Figure 4.9 (a): Kelvin wave pattern at the speed of 8.5 knots	60
Figure 4.9 (b): Wave profile at the speed of 8.5 knots (units are meter)	60
Figure 4.10 (a): Kelvin wave pattern at the speed of 8 knots	61
Figure 4.10 (b): Wave profile at the speed of 8 knots (units are meter)	61
Figure 4.11: Resistance coefficients (C_W , C_F , C_T) at varying Froude numbers for medium deep water	63
Figure 4.12: Sinkage and Trim at different Froude numbers for medium deep water	64
Figure 4.13: Squat at different ship speeds	66
Figure 4.14: The map for inland waterways of Bangladesh	68
Figure 4.15: Dhaka to Chittagong waterway (magenta colored line)	69

Figure 4.16: Waterway from Pangaon inland container terminal, Dhaka to Chittagong port container terminal	70
Figure 4.17: Hydrographic Chart Index for Dhaka-Chittagong route (BIWTA Hydrographic Chart, 2018)	70
Figure 4.18: Enlarged figure of Hydrographic Chart CD 650 A (Ilisha region)	73
Figure 4.19: Enlarged figure of Hydrographic Chart ED 274 B (Chairman Ghat region)	74
Figure 4.20: Enlarged figure of Hydrographic Chart ED 274 A (Bhasanchar region)	75
Figure 4.21: Bangladesh Tide Tables, 2018 for Ilisha region (Meghna River, Char Ramdaspur)	76
Figure 4.22: Bangladesh Tide Tables, 2018 (Satal Khal, Sandhip)	77

List of Tables

Table 2.1: Coefficients in turbulence model	29
Table 3.1: Principal particulars for KCS hull	43
Table 3.2: Principal particulars for 158 TEU container ship	44
Table 3.3: Conditions for Resistance, Sinkage and Trim test of KCS model	45
Table 3.4: Parameters for completing the simulation in SHIPFLOW	46
Table 4.1: Grid sequence for the KCS hull	50
Table 4.2: V&V study of KCS hull for $R_e = 1.26 \times 10^7$ and $F_n = 0.260$	50
Table 4.3: Deep water resistance coefficients at various ship speeds	53
Table 4.4: Computed and experimental values of total resistance	55
Table 4.5: Values of sinkage and trim with different Froude number	56
Table 4.6: Shallow water resistance coefficients at various ship speeds	62
Table 4.7: Sinkage and Trim values for medium deep, shallow and very shallow water at various ship speeds	64
Table 4.8: Squat calculation data	65
Table 4.9: Status of Inland Waterways of Bangladesh	66
Table 4.10: Minimum depth of the shallow water regions in Dhaka-Chittagong waterway	71
Table 4.11: Description of various colours in Hydrographic charts	71

Abstract

There are very shallow water regions in Dhaka-Chittagong route of Bangladesh where inland vessels having draft 3.8 meter or more can not operate at its design speed even on high-tide all through the dry season. This thesis work presents hydrodynamic analysis of a 158 TEU container ship by a 3D numerical simulation using SHIPFLOW software to find out resistance, sinkage, trim and squat and suggests how to operate the vessel in very shallow water regions.

To validate the computational results, a benchmark KRISO Container Ship (KCS) hull is used. Moreover, the flow around a 158 TEU container ship is simulated in deep water at different Froude numbers and the computed results are compared with experimental results for validation.

Then, the flow around 158 TEU container ship is simulated in medium deep, shallow and very shallow water at different Froude numbers to obtain the resistance, sinkage, trim and squat values. The present squat obtained (subtracting deep water sinkage from shallow water sinkage) is checked with the maximum standard squat value. It is seen that the present squat is less than the maximum squat.

Finally, from the calculated values of sinkage and trim, the dynamic aft draft of the ship is predicted for those finite depths of water and it is seen that the aft draft increases for the sinkage and trim effect. The navigable route of the container ship is Dhaka-Chittagong waterway which is the inland waterway of Bangladesh. After checking the hydrographic chart of this waterway, three zones were found where the water depth is less than the dynamic aft draft of the ship. If the ship will run in low-tide time in these three zones the bottom part of the ship structure may be damaged for the grounding effect. As a result, in these dangerous zones, how the ship can operate successfully to avoid grounding is shown in this thesis by reducing her speed at a prescribed limit and waiting for high-tide.

Nomenclature

Acronyms

Symbol	Description
<i>ADB</i>	Asian Development Bank
<i>ATTC</i>	American Towing Tank Conference
<i>BC</i>	Boundary Condition
<i>BIWTA</i>	Bangladesh Inland Water Transport Authority
<i>CAD</i>	Computer Aided Design
<i>CFD</i>	Computational Fluid Dynamics
<i>CPA</i>	Chittagong Port Authority
<i>CPCT</i>	Chittagong Port Container Terminal
<i>DC</i>	Dhaka-Chittagong
<i>DNS</i>	Direct Numerical Simulation
<i>DTMB</i>	David Taylor Model Basin
<i>DWT</i>	Deadweight Tonnage
<i>EFD</i>	Experimental Fluid Dynamics
<i>FVM</i>	Finite Volume Method
<i>ICD</i>	Inland Container Depot
<i>ITTC</i>	International Towing Tank Conference
<i>KCS</i>	KRISO Container Ship
<i>KVLCC</i>	KRISO Very Large Crude Carrier
<i>LAD</i>	Least Available Depth
<i>LES</i>	Large Eddy Simulation
<i>LCF</i>	Longitudinal Center of Flotation
<i>NMRI</i>	National Maritime Research Institute
<i>PICT</i>	Pangaon Inland Container Terminal
<i>RANSE</i>	Reynolds Averaged Navier-Stokes Equation
<i>RANS</i>	Reynolds Averaged Navier-Stokes
<i>RE</i>	Richardson Extrapolation
<i>RMG</i>	Ready-Made Garments
<i>SST</i>	Shear-Stress Transport

<i>TEU</i>	Twenty-foot Equivalent Unit
<i>V & V</i>	Verification and Validation

Roman Symbols

Symbol	Description
C_b	Block coefficient
C_P	Pressure coefficient
C_F	Frictional resistance coefficient
C_f	skin fraction
C_T	Total resistance coefficient
C_V	Viscous resistance coefficient
C_W	Wave resistance coefficient
F_n	Froude number
g	Gravitational constant
h	Water depth
L	length of the ship
N_H	number of panels on the hull surface
n	unit normal vector on the surface
P	Pressure
Re	Reynolds number
R_W	Wave resistance
R_T	Total resistance
R_F	Frictional resistance
S	Wetted surface area of the ship
S_{ij}	Strain rate
ΔS	Area of a panel on the hull surface
T	Ship's draft
U	uniform velocity in the positive x-direction
U_{SN}	Numerical Uncertainty
U_G	Discretization Uncertainty
U_I	Iterative Uncertainty

U_{val}	Validation Uncertainty
u, v, w	Velocity components in x-, y- and z- directions
V	Velocity of ship
V_k	Ship speed in knot

Greek Symbols

Symbol	Description
δ	Squat
μ	Dynamic Viscosity
ρ	Density
Φ	Total Velocity Potential
ϕ	Perturbation velocity potential due to uniform flow
τ	Shear Stress
ν	Kinematic Viscosity
δ	Boundary Layer Thickness
Ω_{ij}	Vorticity

Chapter 1

Introduction

1.1 Background

A container ship can be loaded and unloaded in a few hours compared to days in a traditional cargo vessel. Besides cutting labor costs, this has reduced shipping times between ports to a great extent. It has also resulted in less breakage due to less handling; also, there is less danger of cargo shifting during a voyage. As containers are sealed and only opened at the destination, pilferage and theft levels have been greatly reduced. As a result, container ships are constantly becoming larger in size and are required to carry more loads and travel at faster speeds. It means they have to achieve the required speed with as minimum fuel consumption as possible. In this century the main purpose of shipbuilding industries is to design the fuel-efficient and less pollutant ships which will ultimately reduce the cost of transportation without harming the environment. To design a more fuel-efficient ship, the naval architects or ship designers need to predict the amount of power required. The power requirement of ships in turn depends on how much resistance they face to overcome the seaway. So, prediction of resistance in early design stage is very important for ship designers. In this thesis at first the resistance, sinkage, trim and squat of 158 TEU container ship is predicted in deep water also in shallow inland waterway of Bangladesh.

Bangladesh has one of the largest inland waterway networks in the world which connects almost all the country's major cities, towns, and commercial centers, occupying about 11 % of the country. About 700 natural rivers & tributaries with an overall 24,000 km- long network are crisscrossing the country. Only about 5,970 km is navigable by mechanized vessels during monsoon period, which shrinks to about 3,970 km during dry period making navigation for mechanized vessels above 500 DWT difficult (Mahmud et al., 2006). An Asian Development Bank (ADB) report states, Bangladesh can raise its foreign trade by 20 percent if the inland water transport logistics systems are made efficient and competitive.

These days, both Chittagong and Mongla ports receive huge number of containers because of increased activities mainly in the ready-made garments (RMG) sector of Bangladesh. Chittagong port handles about 76% of the country's 10 million tons of annual foreign trade of which 85% is carried through the Dhaka-Chittagong (DC) economic corridor. The DC corridor is mainly dominated by road service and the DC highway is already congested with heavy

traffic and to release the pressure, the highway is being converted into a four-lane one (Habib, 2016). The total fleet of on road motorized vehicles has increased significantly. The growth of truck has increased about 11.2%. Road network from Dhaka to Chittagong is 278 km. Goods movement of these areas is mainly dependent on trucking and it is around 80% of total goods (Chowdhury et al., 2002). This costly container movement through Dhaka-Chittagong highway is growing faster than the investment and maintenance capacity available, for the road system. Other problems are:

- 1) The fare is the key item of road transportation. Presently there are some rules in maintaining the fare policy. In practice these are not followed. Negotiation is done. The cost varies with different situation like weather, political instability etc.
- 2) As both passengers and cargo carrying vehicles move on the same road, congestion is ultimate result. As a result, delay occurs.
- 3) The possibility of accidents and losing of goods is much more on the highway.
- 4) Environmental pollution is another factor that occurs more by highway vehicles.
- 5) During rainy or flood season, roads become unfit and unsafe for use.
- 6) This mode of transport is unsuitable and costly for transporting cheap and bulky goods over long distances.

The Inland Container Depot (ICD), Dhaka, is near Kamalapur Railway Station. The existing rail road distance between Dhaka-Chittagong is 320.79 km. Annually 8,000 TEU's were transported by Bangladesh Railway, which is remarkably shown negative growth (-22%) in 2009 (Ahmed, 2012) and the trend continuing due to multiple reasons but primarily for:

- 1) The number of container trains is insufficient on the Dhaka-Chittagong route. Bangladesh needs more container trains in order to increase the mobility of container goods.
- 2) Transportation of containers through Dhaka-Chittagong railway suffers greatly for the infrequency of departure time of trains.
- 3) After unloading from ships container aimed to be carried by train are kept at G-shade of Chittagong port. There is long queue for railway space at the Port. As containers

arrived in Chittagong from Singapore within 3 days only, but it takes 15-20 days to reach in Dhaka from Chittagong through railway.

- 4) Also, there is day time restriction on cargo movement in Kamalapur ICD.

Water transport, in contrast to the Roadway and Railway freight transport, does not have congestion problems. Bangladesh Inland Water Transport Authority (BIWTA) and the Chittagong Port Authority (CPA) jointly built the first inland container terminal of Bangladesh at Pangaon, south Keraniganj, Dhaka by the side of the Buriganga river. The Pangaon Inland Container Terminal (PICT) is expected to play a positive role in the country's economic development by opening up a new horizon in the transportation of exported and imported goods through waterways. The project aims to help ease the pressure of cargo movement on the Dhaka-Chittagong highway and railway corridors. The PICT has a storage capacity of 3,500 TEU of containers and can handle 116,000 TEU containers annually (PICT, 2018). The distance of the river route from Chittagong Port Container Terminal (CPCT) to PICT is approximately 157 nautical miles. The draft of the river is around 3.5-4.5 meter except some area of Sandwip but at high tide vessel ranging from 3.5-4.0 meter draft can move easily. Presently in this route Bulk cargo, petroleum & other cargo are transported through small vessels.

1.2 Motivation

From the background, it is seen the Roadway and Railway freight transport is directly related to the congestion problem on Dhaka-Chittagong corridor. Impacts of traffic congestion includes: accidents, increased energy consumption, environmental damage, increased commuting times, and greater social tension. Water transport, in contrast, does not have congestion problems. Again, water transport has little impact on densely populated areas: shallow-draft vessels operate in mid-river, well away from shore, and because of the large tonnage moved at one time which is infrequent (Habib, 2016). According to a survey made by the Chinese experts; the energy consumption ratio of highway, railway and waterway transport is 14:1.8:1 (Ahmed, 2012). Now it is necessary to reduce the pressure of cargo movement on the Dhaka-Chittagong highway and railway corridors by increasing the waterway transport.

Many researches were done on shallow water or finite depth of water in different regions of the world, but in the shallow inland waterway of Bangladesh (from PICT to CPCT), no research is

done yet. So, the recent scenario for the month of February, 2018 of the Dhaka-Chittagong waterway is reviewed in this Master's thesis for a 158 TEU container ship of draft 3.8 meter by using the hydrographic chart. As the container ship is one type of high-speed vessel and the speed of the ship is directly proportional with its income (Figure 1.1), the speed limitation for this container ship in very shallow water region is should be checked to avoid grounding, keeping in mind the financial factor. In DC waterway there are three very shallow water places named (i) Bhasanchar near Sandwip, (ii) Chairman Ghat near Hatia and (iii) Ilisha near Bhola where the available water depth is less than the draft of the ship. If the ship will run in low-tide time in these three zones the bottom part of the ship structure may be damaged for the grounding effect. The ship must wait for high-tide to pass those shallow water regions and obviously by reducing her speed to a prescribed limit.

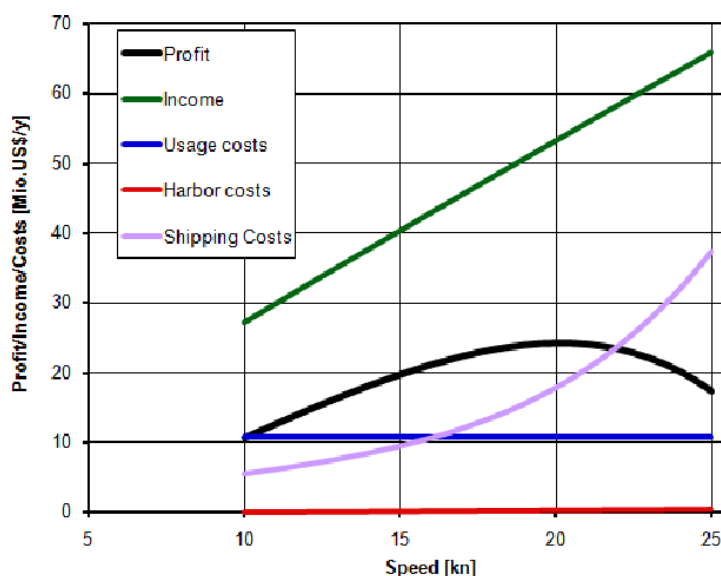


Figure 1.1: Income, Costs, and Profit as functions of vessel speed (Dagkinis. 2015)

Determination of the hydrodynamic performance such as resistance, sinkage and trim of ship has always been biggest concern at all stages of a design both for ship designers and ship yards. In this century, the main goal of shipbuilding industries is to design ships with more fuel efficiency and less pollutant and green-house gas emission which will ultimately reduce the cost of transportation without harming the environment. To design a more fuel-efficient ship, the ship designers need to predict the amount of power required. The power requirement of ships in turn depends on how much resistance they have to overcome in a seaway. In order to achieve these tasks, the features of the flow around the ship hull must be well-understood and

measured accurately in a way that designers can try many hulls and propulsion arrangements without spending too much time, effort and resources.

1.3 Literature Review

Recently, due to the increased computer's capacity as well as the reduced time spent on running the practical calculation of the shallow water effect on ship's hydrodynamic performance, the resistance, sinkage, trim, squat and other hydrodynamic performance seems to be a very interesting topic. The main focus of Previous studies was deep water resistance, sinkage and trim. Nowadays, the shallow water resistance, sinkage and trim became the subject of many investigations.

In the field of ship hydrodynamics, the first theoretical solution for the problem of wave resistance was given by Michell (1898) for a thin ship moving on the surface of an inviscid fluid. Later on, Kelvin (1905) established the fundamental theory of ship waves. Since then many theoretical studies in ship hydrodynamics have been undertaken. Havelock (1908) studied the effects of shallow water on the wave resistance and wave pattern for a point pressure impulse traveling over a free surface. Peng (2001) presented a numerical method based on Michell's theory for the resistance in calm water.

Bartesaghi (2008) investigated the resistance and wave pattern of a Wigley hull using RANS equation. The pressure, viscous and total resistance of the hull were computed and compared with experimental data in their report. The difference between CFD and experimental data were about 1%. Their study showed that the numerical calculation based on RANSE can compute sufficiently accurate results of hull resistance for the purpose of design process. Jones (2010) applied FLUENT code to solve the RANS Equations to compute the total ship resistance of a Naval Destroyer (David Taylor Model Basin model, DTMB 5415). Moctar et al. (2010) used numerical solutions of RANSE using Comet and OpenFOAM to measure the resistance and motion of a Panamax Container Ship (KCS, KRISO Container Ship; developed by Korean Ship Research Institute now KORDI), a Tanker (KVLCC2, KRISO Very Large Crude Carrier) and a Destroyer (DTMB 5415). Guo et al. (2013) studied the ship resistance and flow field of KVLCC2 (KRISO Very Large Crude Carrier) both experimentally and numerically. Saha and Miazee (2017) numerically calculated the resistance of a container ship.

Suzuki (1979) developed the Neumann-Kelvin problem as a method of calculating the effect of sinkage and trim on the wave resistance of a ship. Yasukawa (1993) predicted the wave-making resistance considering the effect of sinkage and trim by the Rankine source method. The importance of the trim and sinkage of a ship are well indicated by Subramani et al. (2000). The other researchers who have made important contributions in the field of wave-making resistance of ship taking into account the effects of sinkage and trim are Tuck (1967), Bessho (1992), Gourlay (2001), Azcueta (2002) etc. Later on, Tarafder (2006) extended Morino's panel method for the calculation of wave-making resistance of ships with special reference to sinkage and trim.

The solution of problems involving determination of resistances using CFD analysis is now becoming tractable due to enhanced accessibility to high performance computing. Determination of the resistance characteristics of ships/vessels is one of the most important topics in Naval Architecture, Offshore and Ocean Engineering.

Today, several CFD software play an important role on the design of the ship hull forms. CFD has been used for the analysis of ship resistances, seakeeping, maneuvering and investigating the variation in resistance encountered due to changes in the ship hull resulting from variation in its parameters.

1.4 Objectives

Even though many numerical codes were used for the prediction of ship resistance, almost all of them were developed for general purpose fluid flow problems. Therefore, in this thesis an attempt is made to involve the SHIPFLOW software developed for dedicated naval hydrodynamics purpose to solve viscous flow around a ship hull. A detailed numerical investigation will be carried out in this thesis to utilize the CFD techniques for prediction of ship resistance in different Froude numbers. The major objectives of this thesis are as follows:

- To determine the Hydrodynamic Performance such as resistance, sinkage and trim of a container ship at different Froude number and at different depth of water by using a CFD modeling software SHIPFLOW.
- To validate the results of total resistance by using the KCS ship hull.
- To show the wave pattern and wave profile at various speed in deep water as well as shallow water.
- To determine the effect of shallow water on Resistance, Sinkage and Trim.

- To determine the Squat effect in case of shallow water.
- To validate the computational results with the experimental results.
- To determine the maximum speed by which the container ship can run in the restricted water depth to avoid grounding in the Dhaka-Chittagong waterway during high-tide.

1.5 Outline of the Methodology

In this thesis, the hydrodynamic performance mainly the resistance of ship will be predicted for two different hull forms by a commercial CFD software SHIPFLOW. First one is KRISO Container Ship (KCS) hull which will be used to validate the resistance results with experimental results for various grid densities. Second one is a 158 TEU container ship, for which the resistance, sinkage and trim values will be computed for both in deep and shallow water.

The geometry of the ship hull will be represented by a single block structured grid. In SHIPFLOW the simulation will be completed by giving all the required values those represents the fluid properties. For turbulence modeling, $k-\omega$ SST model without wall functions will be used by the RANS solver (Naz, 2017). Finite Volume Method (FVM) will be used to discretize the governing equations.

Verification and Validation (V&V) studies for resistance coefficients will be carried out using ITTC (1999) recommended procedure. For the accurate and reliable prediction of hydrodynamic behavior of ships, this V&V analysis will lead to ensure the applicability of the numerical codes.

By collecting the hydrographic charts and tide tables from BIWTA a detailed investigation of the Dhaka-Chittagong waterway will be performed as a part of shallow water analysis. In the very shallow water regions the maximum speed by which the ship can pass will be checked as the speed will affects the sinkage and trim in very shallow water.

Chapter 2

Theory and Mathematical Formulation

2.1 Definition of Ship Resistance, Sinkage and Trim

2.1.1 Ship resistance is defined as the force required to tow the ship in water at a constant velocity (Figure 2.1). A body in water which is stationary with respect to water, experiences only hydrostatic pressure. Hydrostatic pressure always acts to oppose the weight of the body. If the body is in motion, then there are also hydrodynamic pressures that act on the body.

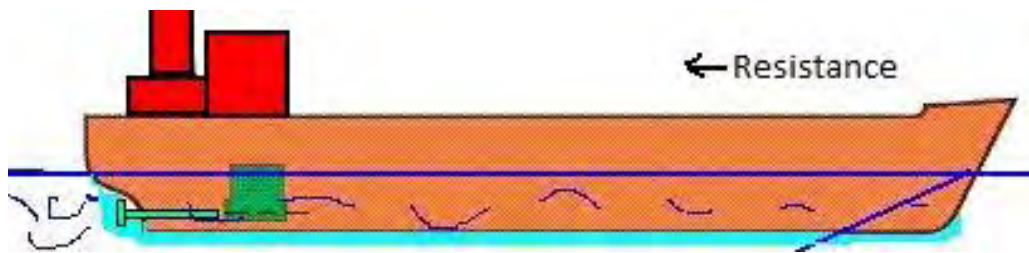


Figure 2.1: Definition of Ship Resistance

The resistance of a ship at a given speed is the fluid force acting on a ship in such a way as to oppose its motion. The resistance will be equal to the component of the fluid forces acting parallel to the axis of motion of the ship. Figure 2.2 shows the components of resistance, where the abscissa is a Froude number given by

$$F_n = \frac{V}{\sqrt{gL}} \quad 2.1$$

and the ordinate is the resistance coefficient defined by

$$C = \frac{R}{\rho V^2 S} \quad 2.2$$

Where V is the speed, L is the length of the body, g is the acceleration due to gravity, ρ is the mass density and S is the wetted surface of the body.

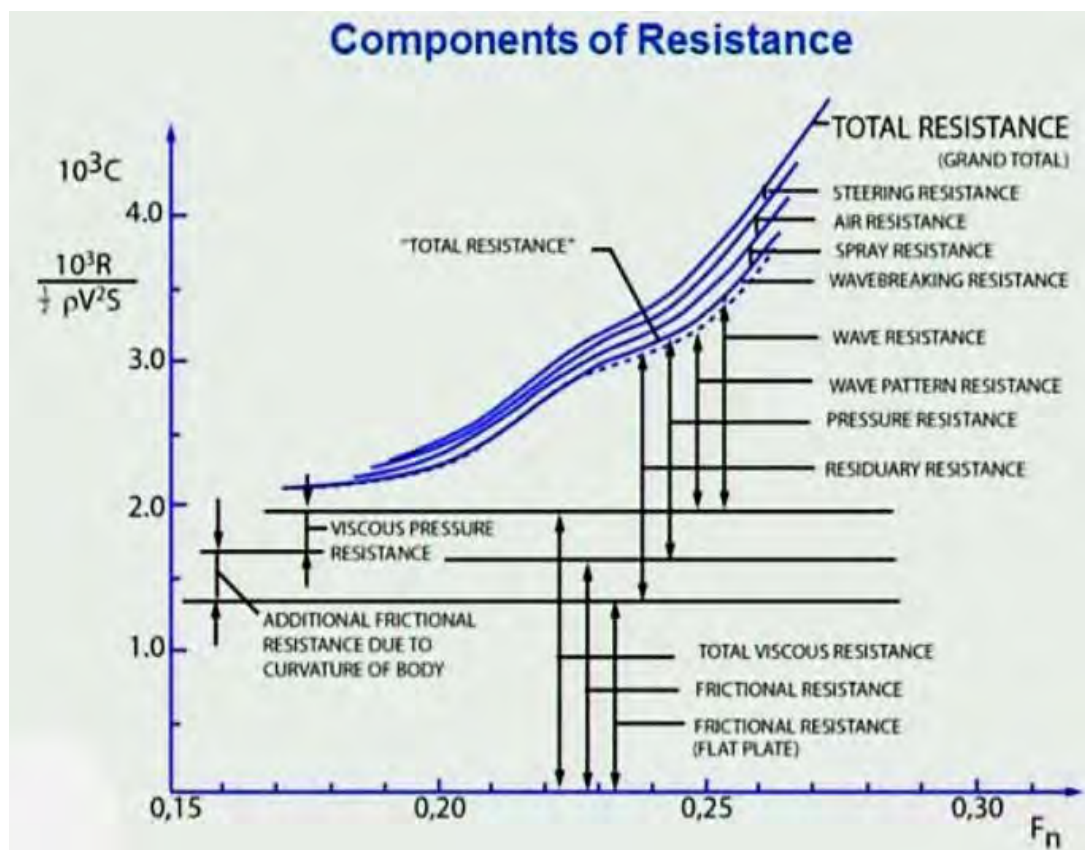


Figure 2.2: Components of resistance of ships

In Figure 2.2, the specific resistance of a ship is given as function of Froude number F_n , and some of the possible components are marked. The components can be described briefly as follows, using the ITTC definitions where possible.

Frictional Resistance, R_F : The frictional resistance is the component of resistance obtained by integrating the tangential stresses over the wetted surface of the ship in the direction of motion.

The relative velocity at the interface between the hull surface and the water is zero and increases with distance out from the hull surface. This is because of skin friction, which is the force due to the interaction between the hull surface and water. A boundary layer is created along the entire hull which grows downstream. The flow in the most forward part of the boundary layer is laminar, without fluctuations, and eventually the flow will get unstable and become turbulent, containing eddies (vortices) (Figure 2.3). The thickness of the boundary layer is defined as the distance from the hull surface to the point where the velocity is 99% of the undisturbed flow velocity. The rapid variation of velocity in the normal direction causes higher

shear stresses in the boundary layer. The frictional resistance, or flat plate friction, is generated by the integral of the shear stresses over the wetted surface of the hull (Bertram, 2000).

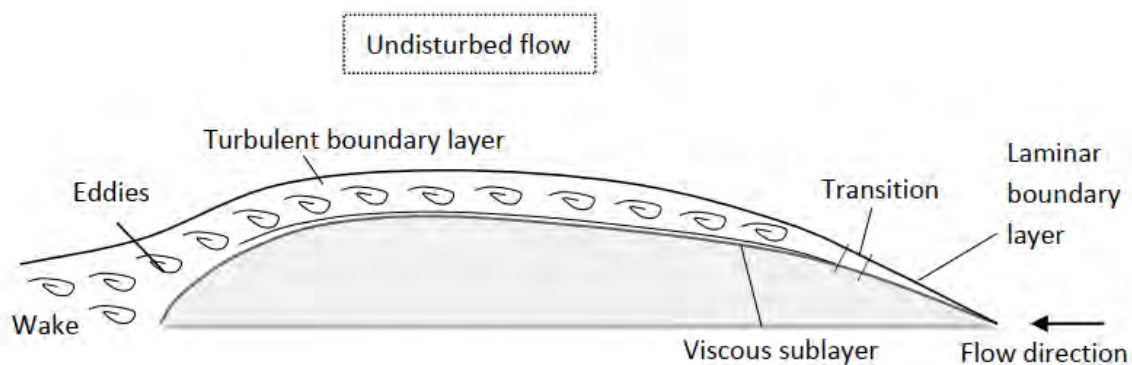


Figure 2.3: Boundary layer along the hull

Residuary Resistance, R_R : The residuary resistance is a quantity obtained by subtracting from the total resistance of a hull, a calculated frictional resistance obtained by any specific formulation. In general, the greater part of the residuary resistance of merchant ships will be wave making resistance.

Viscous Resistance, R_V : The viscous resistance is the component of resistance associated with the energy expended due viscous effects.

Pressure Resistance, R_P : The pressure resistance is the component of resistance obtained by integrating the normal stresses over the surface of a body in the direction of motion.

Viscous Pressure Resistance, R_{PV} : The viscous pressure resistance is the component of resistance obtained by integrating the component of the normal stresses due to viscosity and turbulence. This quantity cannot be directly measured except for a fully submerged body, where it is equal to the pressure resistance.

Wavemaking Resistance, R_W : The wavemaking resistance is the component of resistance associated with the energy expended generating gravity waves.

Wavepattern Resistance, R_{WP} : The resistance component deduced from measurements of wave elevations remote from the ship or model, where it is assumed that the subsurface velocity field and, hence, the momentum of the fluid can be related to the wave pattern by means of a so called linearized theory. The resistance so deduced does not include wave breaking resistance.

Wavebreaking Resistance, R_{WB} : The wavebreaking resistance is a resistance component associated with the breakdown of the ship bow waves.

Spray Resistance, R_S : The spray resistance is the component of resistance associated with the energy expended generating spray.

To with these resistance components some additional resistances, R_A , should be added:

Appendage Resistance: This is the resistance of shaft bossing, shaft brackets, and shafts; bilge keels; rudders; etc. When using physical models, the appendages are often fitted to the model and the appendage resistances are then included in the measured resistance. Normally bilge keels are not fitted. If the hull has no appendages fitted, the resistance is called the bare hull resistance.

Roughness Resistance: This is the resistance due to the roughness, for instance, owing to collision and fouling on the ship hull.

Air Resistance: This is the resistance component experienced by the above water part of the main hull and the superstructures owing to the motion of the ship through the air.

Steering Resistance: To maintain a straight-line path it is in general necessary to use a rudder for corrections. The use of the rudder results in an extra resistance component called steering resistance (Harvald, 1983).

From Figure 2.2, it is seen that the major portions of the total resistance are Frictional resistance, Viscous resistance and Wave resistance. So, in this thesis these three parts of the resistance components are calculated using SHIPFLOW software.

2.1.2 Sinkage: As the speed of the ship increases, the ship increases her draft so that the drafts forward and aft are increased by the same amount when moving through the water is called **parallel sinkage**. Longitudinal Center of Flotation (LCF) is the geometric center point of the ship's waterline plane. The ship trims about this point. This point may be forward or aft of the amidships depending on the ship's hull shape at the waterline. When weight is removed/added from/to a ship at LCF, the forward and aft drafts will change by the same amount. This amount is called the parallel sinkage (Figure 2.4).

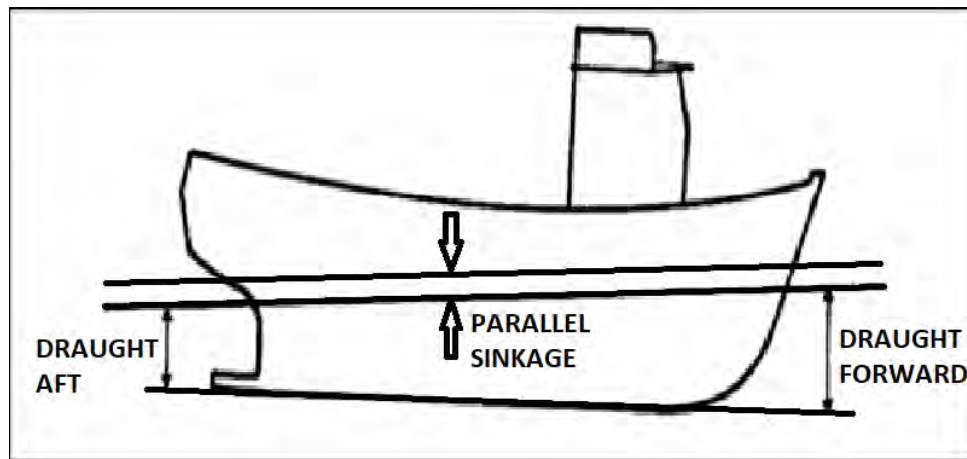


Figure 2.4: Definition of Sinkage and Trim

2.1.3 Trim: Trim may be considered as the longitudinal equivalent of list. Trim is also known as ‘longitudinal stability’. It is in effect transverse stability turned through 90° . Instead of trim being measured in degrees it is measured as the difference between the drafts forward and aft. If difference is zero then the ship is on even keel. If forward draft is greater than aft draft, the vessel is trimming by the bow. If aft draft is greater than the forward draft, the vessel is trimming by the stern (Barrass, 1999).

2.1.4 Shallow Water: A ship’s behavior in general, and her manoeuvrability in particular, depends on the water depth, h of the navigation area. According to the ratio of the water depth, h to the ship’s draft T , a rather arbitrary distinction can be made between (PIANC, 1992)

- Deep water $h/T > 3.0$
- Medium deep water $1.5 < h/T < 3.0$
- Shallow water $1.2 < h/T < 1.5$
- Very shallow water $h/T < 1.2$

The effect of depth restrictions in ship’s hydrodynamic performance can be noticed in medium deep water, is very significant in shallow water, and dominates in very shallow water (Vantorre, 2003).

2.2 Different Methods for the Prediction of Ship's Resistance

There are mainly four different methods to predict the resistance of a ship such, these are described below:

2.2.1 Empirical Methods

The empirical methods are the simplest and fastest methods among them which can be used only at the earliest design stage, when main dimensions and hull coefficients often vary due to lack of accuracy. Such methods are of two different types: systematic series and statistical formulas based on unsystematic data. The first comprehensive series of systematic tests was carried out in the Experimental Model Basin in Washington during the first years of the 20th century, by Admiral Taylor. The series is known as the Taylor standard series and has been used extensively over the years (Larsson, 2010). To obtain results for more modern ships, the Society of Naval Architects, in cooperation with the American Towing Tank Conference (ATTC), initiated a new series in 1948. The results of this new series were presented by Todd (1963) in a comprehensive report. A statistical formula for resistance based on unsystematic data was made by Doust (1959). They used results from tests of 150 fishing vessels and tried to express the total resistance at a given speed-length ratio as a function of six different shape parameters.

Only certain parameters of ships in general such as length, breadth, draft, displacement are considered in this approach. This method is not suitable for the varying shape of the ships that are of similar dimensions and types. But the frictional resistance, which is one of the principal components of total ship resistance, depends significantly upon the shape of the hull and wake generated by propeller. So, undoubtedly, empirical formulas for ship resistance do not necessarily give an accurate result to the ship designers (Naz, 2017).

2.2.2 Use of the Methods

The three different methods for determining resistance are used at different stages of the ship design process. At the very early basic design stage, the main parameters of the hull are often varied and the design space explored with respect to length, beam, draft, block coefficient, and longitudinal position of the center of buoyancy. Because the entire design of the ship depends on these parameters, time is often short, and a reasonable estimate is required rapidly. Because the shape variation is very much linked to computer-aided design (CAD), most CAD packages

for ship design contain a module for predicting ship resistance, in most cases based on the Holtrop (1978) method.

During the past couple of decades, the numerical methods have made their way into design offices. Thus, having a good idea of the hull main dimensions, they may be further optimized using these methods. More important, however, is the possibility of optimizing the local shape of the hull, not only the main parameters. Forebody optimization using potential flow methods is now a standard procedure used by most ship designers. Particular features to look at are the size and shape of the bulb and the radius of the fore shoulder. The purpose is normally to minimize wave resistance (Valdenazzi et al., 2003).

Very recently, afterbody optimization has started to appear in ship design offices. Because the effect of the boundary layer is much larger at the stern than at the bow, viscous flow methods are required. Boundary layer theory is too approximate for computing the wake behind the hull, so more advanced methods are required. At present, the only alternative is the RANS technique. Even though the computational effort is considerably larger than for potential flow methods, several alternatives may be evaluated in one day, which is good enough. Recently, the effect of the rudder has also been included. Normally, the purpose is not to minimize resistance, but delivered power, and this calls for some method to estimate the interaction between the hull and the propeller. Some designers do that by experience, but methods are available for computing the effect (Han, 2008).

Note that it is not only delivered power that is of interest; noise and vibrations caused by the propeller in the uneven wake should also be considered. Although most optimizations so far are carried out manually by systematically varying the hull shape, formal optimization methods may be applied as well. Hence, this procedure can't give an accurate result and definitely increases the time required to estimate or predict the resistance as the calculation involves lot of steps.

2.2.3 Physical Experiments: Model Testing

One of the best ways to predict the resistance is by model tests in a towing tank. In this method a small model of the actual ship is built and tested in a long basin in calm water or waves to estimate the ship hull resistance as shown in Figure 2.5. The model resistance is then converted to actual ship hull resistance by Froude's Law (Froude, 1810-1879) or other methods.



Figure 2.5: Towing tank at Gdansk University of Technology, Poland

Using model testing facility for the prediction of calm water and wave resistance of ships is very time consuming and expensive. The models have to be carefully built, so that the ratios of principal dimensions are not distorted and the shape of the model hull correctly represents the shape of the actual hull. Building models hence takes up a lot of time and the material cost is also high. Again, if the designers wish to compare several alternative choices, the models of each design option have to be built and tested in the towing tank accordingly. This procedure significantly increases the time required to estimate or predict the resistance and power which ultimately slows down the entire ship design process. Also, the cost associated with building each model separately is added up to the building cost thus making the construction of a ship less economical. Hence, model testing has some disadvantages to the ship designers (Shabnam, 2015).

2.2.4 Numerical Methods: Computational Fluid Dynamics

Computational Fluid Dynamics (CFD) has been a revolution in the world of engineering and the rapid growth of computer capacities during the past decades has opened new horizons for ship hydrodynamics. CFD is very efficient because it allows exploration of new engineering frontiers in the most economical way. As a result, CFD analysis has become crucial in the design phase of big structures, like ships. Hydrodynamic aspects play an important role in the quality of a ship. Dominant criteria for the hull form design of many ships are the resistance and powering performance. The most dominant application of CFD is the prediction of

resistance (64%), as seen from Figure 2.6. In industry, University and Model basin other applications such as self-propulsion, propulsors, maneuvering, seakeeping, and ocean engineering are also of great interest with about 40% (ITTC, 2011).

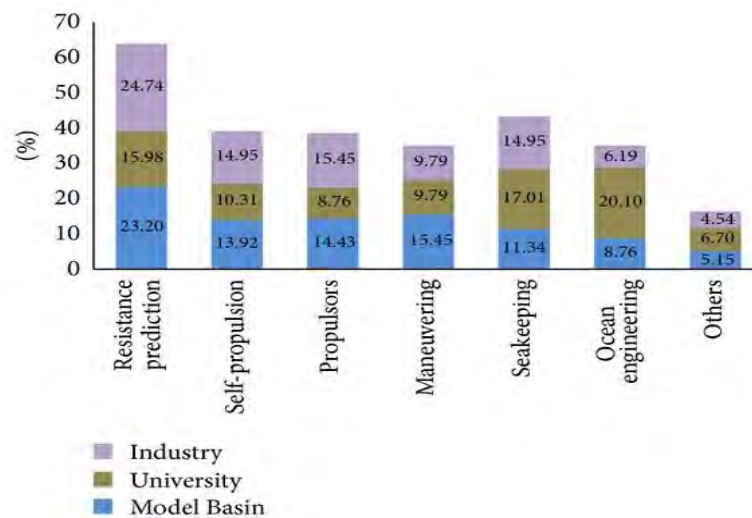


Figure 2.6: Applications of CFD in Marine Hydrodynamics (ITTC, 2011)

The development of CFD technique has made it possible to numerically model the flow around ship hull. Over the last few decades, RANS based numerical approaches are widely used in ship design (Purnamasari et al., 2017).

CFD involves solving the governing equations of fluid flow with a numerical approach. The benefits of CFD compared to traditional model tests are many, some are listed below:

- ❖ Simulation cost is relatively very low compared to physical experiments.
- ❖ CFD simulations can be carried out faster than physical experiments.
- ❖ Changes to the original design can be made quickly.
- ❖ Comprehensive data can be extracted from CFD, whereas a physical test case can only provide data from a limited number of locations. In addition, there is no testing apparatus interacting with the flow.
- ❖ Greater control of the set-up of the experiment. Conditions which would be difficult or impossible to achieve in a towing tank can be easily created in numerical artificial tank.

The field of ship hydrodynamics mostly involves formulating and solving non-linear problems. Due to improvement of solution algorithms and computational infrastructure, it is now possible to simulate even non-linear viscous flows by CFD techniques. Due to this reason, CFD has

become an essential tool in the field of marine hydrodynamics. The value of CFD in ship design process can be broken down into three aspects such as:

- 1) Firstly, CFD simulations can add time benefits to the ship design process. The shipbuilding industry works in a very tight schedule. CFD plays a special role in this context, as an investigation of new hull performance, numerical pre-optimization can save time-consuming iterations in model tests and thus reduce total time. Early use also reduces development risks for new ships. This is especially important for unconventional ships where design cannot be based on previously constructed basis ships.
- 2) In addition to time, another important strength of CFD are cost benefits. Firstly, the time savings will directly cut down on costs. Before conducting model tests, CFD simulations can be act as tools for narrowing down design choices. In addition, the expensive modifications at late stages of ship design projects can be avoided as different designs can quickly be reviewed with CFD. Thus, CFD will lower the financial risk of the whole ship design project.
- 3) The third aspect associated with CFD is quality. Although towing tank tests are considered reliable, CFD allows the investigation of the flow in much greater detail than experiments. CFD can indicate where and how a design could be improved, and it also allows for rapid optimization of hull designs (Shabnam, 2015).

However, the main advantage of CFD comes from its ability to fulfill both Froude and Reynolds similarities meaning that model-scale results and full-scale results can be directly calculated while providing a great deal of detail about the flow. The absolute accuracy of CFD is still under concern and final decisions about the predictions of resistance and propulsive factors are still made by model tests.

So, in this thesis the resistance, sinkage and trim of the container ship is calculated by the CFD modelling software SHIPFLOW and then the results is compared with the experimental model test results.

2.3 Numerical Methods for Prediction of Ship Resistance, Sinkage and Trim using SHIPFLOW

In this section the basic governing equations of fluid flow such as the continuity equation, Bernoulli's equation and the Navier-Stokes equations are discussed. In SHIPFLOW, the flow domain around the ship hull is divided into three regions, Figure 2.7, and a computational method is developed for each region. The first region covers the entire hull and a part of its surrounding free-surface. A free-surface potential-flow method of Rankine-source type is used. The second region is a thin layer at the hull surface and a boundary layer method of the momentum integral type is used. The momentum integral equations are solved along streamlines traced from the potential flow solution. Finally, the third region includes the aft part of the hull and extends about half a ship length downstream of the hull. A Navier-Stokes method of the RANS type and a wall-law is used. The reason for the division of the flow field into zones is that the computational time may be reduced considerably compared to the global approach where the Navier-Stokes method is used in the entire computational domain (Larsson, 1996).

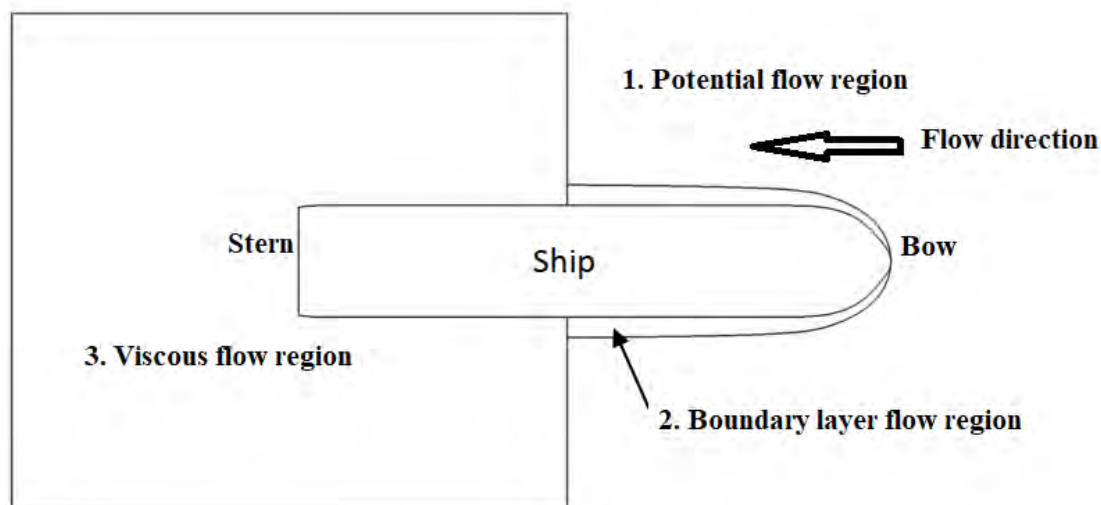


Figure 2.7: Flow region

2.3.1 Potential Flow Region

A flow that is irrotational, inviscid and incompressible is called potential flow. If irrotational flow is assumed, $\nabla \times V = 0$, the components of the velocity vector are no longer independent of each other and a velocity potential ϕ exist as described by Equation 2.3.

$$\nabla\phi \equiv \left(\frac{\partial\phi}{\partial x}, \frac{\partial\phi}{\partial y}, \frac{\partial\phi}{\partial z} \right) = V \equiv (u, v, w) \quad 2.3$$

$$\nabla \cdot V \equiv \frac{\partial u}{\partial x} + \frac{\partial v}{\partial y} + \frac{\partial w}{\partial z} = 0 \quad 2.4$$

Equation 2.3 together with the continuity equation, Equation 2.4, yield Laplace's equation for the potential flow, Equation 2.5, which is the equation that potential flow methods are based upon. (Larsson, 2004)

$$\frac{\partial u}{\partial x} + \frac{\partial v}{\partial y} + \frac{\partial w}{\partial z} = 0 \Rightarrow \frac{\partial^2\phi}{\partial x^2} + \frac{\partial^2\phi}{\partial y^2} + \frac{\partial^2\phi}{\partial z^2} \equiv \nabla^2\phi = 0 \quad 2.5$$

When the flow involves a free surface, the Bernoulli equation, Equation 2.6, provides a relation between the flow velocity, V , and the elevation of the free surface, z , according to Equation 2.7. (White, 2008)

$$\frac{\partial\phi}{\partial t} + \frac{p}{\rho} + \frac{1}{2}V^2 + gz = \text{constant} \quad 2.6$$

$$V^2 = |\nabla\phi|^2 = \text{constant} - 2gz \quad 2.7$$

After calculating the fluid velocity $\nabla\phi$ at the control points on the hull surface the pressure coefficients can be evaluated as

$$C_p = 1 - \left(\frac{\nabla\phi}{U} \right)^2 \quad 2.8$$

Now including the waterline integral the wave resistance coefficient can be obtained as

$$C_w = - \frac{\sum_{i=1}^{N_H} C_p n_x \Delta S}{\sum_{i=1}^{N_H} \Delta S} \quad 2.9$$

Where ΔS denotes the area of a panel on the hull surface, L is the waterline length of the ship, u is the uniform velocity in the positive x -direction and N_H is number of panels on the hull surface. (Tarafder, 2006)

Now the wave resistance,

$$R_W = C_w \times \frac{1}{2} \rho S V^2 \quad 2.10$$

One advantage with potential flow methods compared to methods based on Navier-Stokes equations, is that Laplace's equation is linear. Elementary solutions of the equation may thus be added together to complex solutions. Complex flows can be solved by using a large number of simple solutions called singularities that together yields a solution for the flow. The

singularities may be sources (inflow of fluid), sinks (outflow of fluid) dipoles or vortices. The potential flow is solved with a panel method. The surface of the ship and the water surface are divided into flat, ideally square, panels commonly with a constant source strength (referred to as meshing). This means that the only unknown parameter for each panel is the source strength. An equation corresponding to the boundary condition is applied to one point on each panel, the collocation point, which gives N points with N equations and N unknown source strengths. From this system of equations, it is then possible to calculate the velocity at every point in the flow and get the potential flow around the hull.

Potential flow methods can be either linear or nonlinear for the free surface. Linear methods apply the boundary conditions on an undisturbed free surface and then on linear terms for the unknowns are dismissed. For nonlinear methods the boundary conditions are applied to a free surface using waves generated from the previous solution in the next iteration. Nonlinear methods are considered more accurate but are also more time consuming.

Since potential flow is an irrotational flow and viscosity is neglected, so some disadvantages are given below. In regions with high vorticity, for example wakes and boundary layers, potential flow methods will not give reasonable results. Unfortunately, this also means that the solution provided by potential flow methods is erroneous even outside the boundary layer. This error is usually small for the forebody and middle section but can be significant for the stern flow where viscous effects strongly influence the flow. (Bertram, 2000).

2.3.2 Boundary layer Flow Region

The boundary layer around the ship consists of three different regions: laminar, transitional and turbulent. It is important to determine the location and extent of the different regions in order to make a correct analytical prediction of the ship performance where the laminar and transitional boundary layer may occupy a large part of the hull.

The coordinate system adopted in the boundary layer calculation is an orthogonal curvilinear coordinate system. The parametric curves $z=\text{constant}$ and $x=\text{constant}$ on the ship surface are chosen to coincide with the potential flow streamlines and the equipotential lines respectively. The y -axis is locally normal to the hull surface. From the output of the potential flow computation the direction cosines of the velocity and also of the streamlines at a large number

of points on the hull surface are known. By numerical integration, streamline may then be traced section by section along the hull. No equipotential lines have to be traced.

Because of the bending of the x - and z - axes the corresponding coordinates are stretched in a non-uniform manner. The stretching is taken into account by the matrices h_1 and h_3 which are functions of x and z respectively. The curvatures K_{13} of the x -axis and K_{31} of the z -axis are connected to the metrics via the relations

$$K_{13} = \frac{1}{h_1 h_3} \frac{\partial h_1}{\partial z} \quad 2.11$$

$$K_{31} = \frac{1}{h_1 h_3} \frac{\partial h_3}{\partial x} \quad 2.12$$

In the derivation of the momentum integral equations, following variables appear

$$\delta_1 = \int_0^\infty \left(1 - \frac{u}{u_e}\right) dy \quad 2.13$$

$$\delta_2 = - \int_0^\infty \frac{w}{u_e} dy \quad 2.14$$

$$\theta_{11} = \int_0^\infty \frac{u}{u_e} \left(1 - \frac{u}{u_e}\right) dy \quad 2.15$$

$$\theta_{12} = \int_0^\infty \frac{w}{u_e} \left(1 - \frac{u}{u_e}\right) dy \quad 2.16$$

$$\theta_{21} = - \int_0^\infty \frac{uw}{u_e^2} dy \quad 2.17$$

$$\theta_{22} = - \int_0^\infty \frac{w^2}{u_e^2} dy \quad 2.18$$

which characterize the boundary layer in an average sense. $\bar{v} = (u, v, w)$ is the velocity vector. It should be interpreted as the mean velocity vector in the case of a turbulent boundary layer. Its magnitude is equal to u_e at the boundary layer edge. Another vector which will appear in the integral boundary layer equations is the wall shear stress vector defined by,

$$\tau_{wx} = \rho \left(v \frac{\partial u}{\partial y} - \overline{u'v'} \right) \quad 2.19$$

$$\tau_{wz} = \rho \left(v \frac{\partial w}{\partial y} - \overline{v'w'} \right) \quad 2.20$$

The primed quantities are the fluctuations of the velocity component and vanish in the case of a laminar boundary layer. Under the assumption of “small cross-flow”, the governing equations of the three-dimensional laminar boundary layer can be written as

$$(h_3\theta_{11})^2 = \frac{4}{9} \frac{v}{u_e^6} \int_0^s h_3^2 u_e^5 ds \quad 2.21$$

$$\frac{d\theta_{21}}{ds} = \frac{\tau_{wz}}{\rho u_e^2} - 2\theta_{21} \left(\frac{1}{u_e} \frac{du_e}{ds} + K_{31} \right) + K_{13}\theta_{11}(1 + H_{12}) + K_{13}H_2\delta_2 \quad 2.22$$

where δ is the boundary layer thickness, s is the arc length along the x -axis, and

$$H_{12} = \frac{\delta_1}{\theta_{11}} \quad 2.23$$

$$H_2 = \frac{\theta_{22}}{\delta_2} \quad 2.24$$

Solutions are obtained along a number of streamlines. On each streamline the instability of the laminar boundary layer is examined and the transition is predicted according to various empirical criteria. The governing equations of the three-dimensional turbulent boundary layer can be written as

$$\begin{aligned} \frac{1}{h_1} \frac{\partial \theta_{11}}{\partial x} + \frac{1}{h_3} \frac{\partial \theta_{12}}{\partial z} + \frac{1}{h_1 u_e} \frac{\partial u_e}{\partial x} (2\theta_{11} + \delta_1) + K_{13}(\theta_{12} + \theta_{21}) + K_{31}(\theta_{11} - \theta_{22}) + \\ \frac{1}{h_3 u_e} \frac{\partial u_e}{\partial z} (\theta_{21} + \theta_{12}) = \frac{\tau_{wz}}{\rho u_e^2} \end{aligned} \quad 2.25$$

$$\begin{aligned} \frac{1}{h_1} \frac{\partial \theta_{21}}{\partial x} + \frac{1}{h_3} \frac{\partial \theta_{22}}{\partial z} + \frac{2}{h_1 u_e} \frac{\partial u_e}{\partial x} \theta_{21} + \frac{2}{h_3 u_e} \frac{\partial u_e}{\partial z} \theta_{22} - K_{13}(\theta_{11} + \delta_1 - \theta_{22}) \\ + 2K_{31}\theta_{21} = \frac{\tau_{wz}}{\rho u_e^2} \end{aligned} \quad 2.26$$

In the above equations the following relations are introduced

$$\beta_w = \arctan \frac{\tau_{wz}}{\tau_{wx}} \quad 2.27$$

$$\frac{\tau_{wx}}{\rho u_e^2} = \frac{C_{fx}}{2} \quad 2.28$$

$$\frac{\tau_{wz}}{\rho u_e^2} = \frac{C_{fx}}{2} \tan \beta_w \quad 2.29$$

$$C_1 = \frac{1}{h_3} \frac{\partial \theta_{12}}{\partial z} \quad 2.30$$

$$C_2 = \frac{1}{h_3} \frac{\partial \theta_{22}}{\partial z} \quad 2.31$$

C_1 and C_2 are crosswise derivatives calculated after taking one step along each streamline. Repeating the step several times, each time holding C_1 and C_2 constant, they will converge and

a fully 3-D solution is obtained. The partial derivatives of the above equations may then be written in the ordinary form and solved along each streamline. It yields

$$\frac{d\theta_{11}}{ds} = \frac{C_{fx}}{2} - \frac{\theta_{11}}{u_e} \frac{du_e}{ds} (2 + H_{12}) - K_{31}(\theta_{11} - \theta_{22}) - C_1 \quad 2.32$$

$$\frac{d\theta_{21}}{ds} = \frac{C_{fx}}{2} tg\beta_w - 2\theta_{21} \left(\frac{1}{u_e} \frac{du_e}{ds} + K_{31} \right) + K_{13}\theta_{11}(1 + H_{12}) + K_{13}\theta_{22} - C_2 \quad 2.33$$

To close the system of equations an auxiliary equation which is the entrainment equation due to Head (H), the skin fraction (C_f) and velocity profile relations are employed.

2.3.3 Viscous Flow Region, RANS

In viscous flow region, there are different types of methods to compute the turbulent flow depending on the approximation or modeling the turbulence. Direct Numerical Simulation (DNS) method is based on the instantaneous continuity and Navier–Stokes equations and "develops a transient solution on a sufficiently fine spatial mesh with sufficiently small time steps to resolve even the smallest turbulent eddies and the fastest fluctuations." (Versteeg, 2007). This conditions for ship hydrodynamics however are extremely expensive in terms of computational power since full scale ships are mostly order of 100 m on the other hand smallest scale eddies are down to 0.1 mm. Large Eddy Simulation (LES) resolves the large-scale turbulent motions in order to model the small-scale eddies using sub-grid scale models. Reynolds Averaged Navier-Stokes (RANS) method solves the mean flow by time-averaging the Navier-Stokes equation and models the turbulence. Due to the limited computational resources, the RANS method is the most widely used CFD technique in practice.

The Navier-Stokes equations can be solved numerically by resolving all scales. Turbulent flows would require extremely dense grids to resolve the smallest turbulent length scales.

The continuity equation states that mass is conserved

$$\frac{1}{\rho} \frac{\partial \rho}{\partial t} + \frac{\partial U_i}{\partial x_i} = 0 \quad 2.34$$

Only incompressible flow is considered. That means that the changes in density is negligible. Then the continuity equation can be written

$$\frac{\partial U_i}{\partial x_i} = 0 \quad 2.35$$

The Navier-Stokes equations of motion can be written in the following form

$$\rho \frac{\partial U_i}{\partial t} + \rho \frac{\partial (U_j U_i)}{\partial x_j} = \rho R_i + \frac{\partial \sigma_{ij}}{\partial x_j} \quad 2.36$$

where σ_{ij} is the total stress and for a Newtonian fluid it can be written

$$\sigma_{ij} = -P \delta_{ij} + 2\mu(S_{ij} - \frac{1}{3}S_{kk}\delta_{ij}) \quad 2.37$$

where S_{ij} is the strain-rate defined as

$$S_{ij} = \frac{1}{2} \left(\frac{\partial U_i}{\partial x_j} + \frac{\partial U_j}{\partial x_i} \right) \quad 2.38$$

S_{kk} is zero for incompressible flow

$$S_{kk} = \frac{1}{2} \left(\frac{\partial U_k}{\partial x_k} + \frac{\partial U_k}{\partial x_k} \right) = \frac{\partial U_k}{\partial x_k} = 0 \quad 2.39$$

The Reynolds-averaged Navier-Stokes equations can be derived by splitting the instant velocity components, U_i , in time mean velocity, u_i , and time fluctuating velocity, u_i'' ,

$$U_i = \bar{U}_i + u_i'' \equiv u_i + u_i'' \quad 2.40$$

and the instant pressure, P , in time mean pressure, p , and time fluctuating pressure, p'' ,

$$P = \bar{P} + p'' \equiv p + p'' \quad 2.41$$

The time mean of a variable is defined as

$$\bar{\phi} = \lim_{T \rightarrow \infty} \frac{1}{2T} \int_{-T}^T \phi dt \quad 2.42$$

The following rules of averaging apply for any two turbulent quantities ϕ_1 and ϕ_2

$$\begin{aligned} \phi_1 &= \bar{\phi}_1 + \phi_1'' & \overline{\phi_1''} &= 0 & \overline{\overline{\phi_1}} &= \bar{\phi}_1 \\ \overline{\phi_1 \phi_2} &= \bar{\phi}_1 \bar{\phi}_2 & \overline{\phi_1'' \phi_2} &= 0 & \frac{\partial \bar{\phi}_1}{\partial s} &= \frac{\partial \phi_1}{\partial s} \\ \overline{\phi_1 + \phi_2} &= \bar{\phi}_1 + \bar{\phi}_2 & \overline{\phi_1 \phi_2} &= \bar{\phi}_1 \bar{\phi}_2 + \overline{\phi_1'' \phi_2''} \end{aligned} \quad 2.43$$

Taking the time average of the continuity equation gives

$$\frac{\partial \bar{U}_i}{\partial x_i} = \frac{\partial \bar{U}_i}{\partial x_i} = \frac{\partial u_i}{\partial x_i} = 0 \quad 2.44$$

Subtracting Equation 2.45 from Equation 2.36 gives that also the time fluctuating velocity fulfills the incompressible continuity equation

$$\frac{\partial u_i''}{\partial x_i} = 0 \quad 2.45$$

Then taking the time average of the Navier-Stokes equations (first moving all terms to the left-hand side)

$$\begin{aligned} & \overline{\rho \frac{\partial U_i}{\partial t} + \rho \frac{\partial (U_j U_i)}{\partial x_j} - \rho R_i + \frac{\partial P}{\partial x_i} - \frac{\partial}{\partial x_j} \left(\mu \left(\frac{\partial U_i}{\partial x_j} + \frac{\partial U_j}{\partial x_i} \right) \right)} = \cdot \\ & = \rho \frac{\partial \bar{U}_i}{\partial t} + \rho \frac{\partial (\bar{U}_j \bar{U}_i)}{\partial x_j} - \rho \bar{R}_i + \frac{\partial \bar{P}}{\partial x_i} - \frac{\partial}{\partial x_j} \left(\mu \left(\frac{\partial \bar{U}_i}{\partial x_j} + \frac{\partial \bar{U}_j}{\partial x_i} \right) \right) = \quad 2.46 \\ & = \rho \frac{\partial u_i}{\partial t} + \rho \frac{\partial (u_j u_i + \overline{u_j'' u_i''})}{\partial x_j} - \rho \bar{R}_i + \frac{\partial p}{\partial x_i} - \frac{\partial}{\partial x_j} \left(\mu \left(\frac{\partial u_i}{\partial x_j} + \frac{\partial u_j}{\partial x_i} \right) \right) \cdot \end{aligned}$$

Hence, the time averaged continuity equation and Navier-Stokes equations for incompressible flow can be written (Flowtech Int., XCHAP Theoretical Manual, 2010)

$$\frac{\partial u_i}{\partial x_i} = 0 \quad 2.47$$

$$\frac{\partial u_i}{\partial t} + \frac{\partial (u_j u_i + \overline{u_j'' u_i''})}{\partial x_j} = \bar{R}_i + \frac{1}{\rho} \frac{\partial p}{\partial x_i} + \frac{\partial}{\partial x_j} \left(\nu \left(\frac{\partial u_i}{\partial x_j} + \frac{\partial u_j}{\partial x_i} \right) \right) \quad 2.48$$

Where

$$\nu = \frac{\mu}{\rho} \quad 2.49$$

2.3.3.1 Turbulence Modeling

Turbulence model is used as a computational procedure to close the system of mean flow equations. It is unnecessary to resolve the details of the turbulent fluctuations. Turbulence models allow the calculation of the mean flow without first calculating the full time-dependent flow field. Turbulence models to close the Reynolds equations can be divided originally into three groups in general. First models which (directly) use the Boussinesq assumption. Most models currently employed in engineering are this type. Experimental evidence indicates this valid in many circumstances. Second are models using the effect of closure to the Reynolds equation without this assumption.

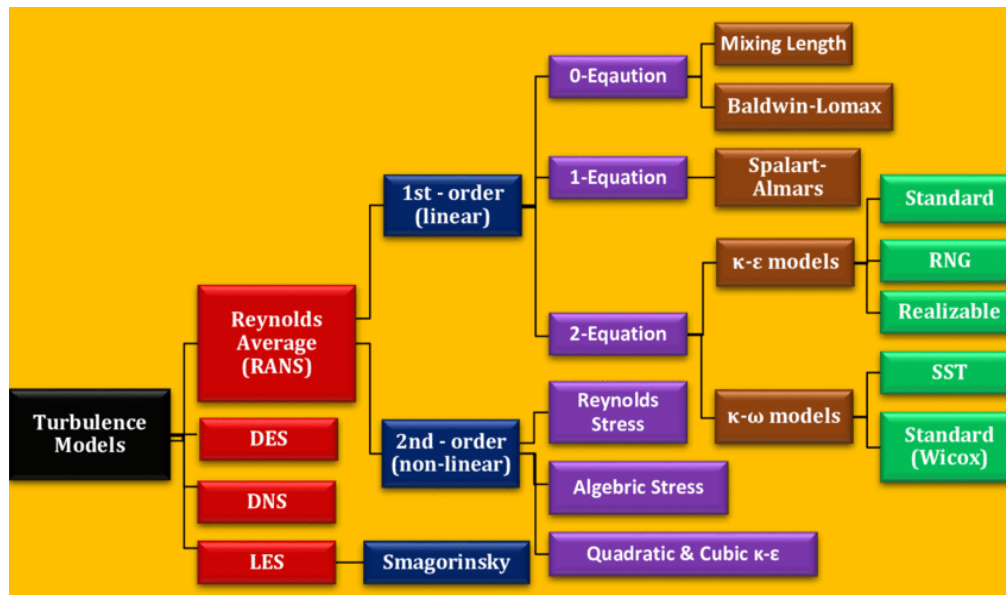


Figure 2.8: Hierarchy of Turbulence Models (Sadrehaghghi, 2018)

The third category is defined as those that are not based entirely on the Reynolds equation. These are (Figure 2.8) some of models mentioned here and by no means is it exclusive. An ideal model should be with minimum amount of complexity while capturing the essence of the relevant physics. The number of equations indicates the number of additional Partial Differential Equations that are being solved.

2.3.3.2 Selection of Turbulence Modeling

The important fact is that no single turbulence model is completely accepted as being best for all classes of problems. The choice of turbulence model will depend on considerations such as the physics encompassed in the flow, the established practice for a specific class of problem, the level of accuracy required, the available computational resources, and the amount of time available for the simulation. For a turbulence model to be useful it must have wide applicability, be accurate, simple, and economical to run. In this thesis $k-\omega$ Shear-Stress Transport (SST) model will be used for modeling the turbulence flow.

2.3.3.3 Shear-Stress Transport (SST) $k-\omega$ model

This model was developed by Menter (1993) to effectively blend the robust and accurate formulation of the $k-\omega$ model in the near-wall region with the free-stream independence of

the $k - \epsilon$ model in the far field. To achieve this, the $k - \epsilon$ model is converted into a $k - \omega$ formulation.

SST $k - \omega$ model is similar to the standard $k - \omega$ model, but includes the following refinements:

- The standard $k - \omega$ model and the transformed $k - \epsilon$ model are both multiplied by a blending function and both models are added together. The blending function is designed to be one in the near wall region, which activates the standard $k - \omega$ model, and zero away from the surface, which activates the transformed $k - \epsilon$ model.
- The SST model incorporates a damped cross-diffusion derivative term in the ω equation.
- The definition of the turbulent viscosity is modified to account for the transport of the turbulent shear stress.
- The modeling constants are different.

These features make the SST $k - \omega$ model more accurate and reliable for a wider class of flows (e.g., adverse pressure gradient flows, airfoils, transonic shock waves) than the standard $k - \omega$ model (Naz, 2017). The relationship between ω and ϵ is

$$\omega = \frac{\epsilon}{0.09k} \quad 2.50$$

The SST $k - \omega$ model is based on Bradshaw's assumption that the principal shear-stress is proportional to the turbulent kinetic energy, which is introduced into the definition of the eddy-viscosity. The $k - \epsilon$ models overpredict the turbulent shear stress in boundary layers under adverse pressure gradient. The previous $k - \omega$ models give somewhat more realistic solutions for such flows, but the improvement is only partial. With the $k - \omega$ SST model a significant improvement is reached. The $k - \omega$ SST model also has the advantage of being insensitive to the free stream ω value.

In the $k - \omega$ SST model the $k - \omega$ model is used near the wall and a $k - \epsilon$ model, transformed to resemble a $k - \omega$ model, is used outside of this region. The different sets of coefficients and the additional cross-diffusion term from the transformed $k - \epsilon$ model are combined by blending or switching functions F_i in an intermediate region.

The equations for k and ω in the SST model can be written

$$\frac{\partial k}{\partial t} + \frac{\partial(u_j k)}{\partial x_j} = -\overline{u_i'' u_j''} \frac{\partial u_i}{\partial x_j} - \beta^* k \omega + \frac{\partial}{\partial x_j} \left((v + \sigma_k v_T) \frac{\partial k}{\partial x_j} \right) \quad 2.51$$

$$\frac{\partial \omega}{\partial t} + \frac{\partial(u_j \omega)}{\partial x_j} = -\frac{\gamma}{v_T} \overline{u_i'' u_j''} \frac{\partial u_i}{\partial x_j} - \beta^* \omega^2 + \frac{\partial}{\partial x_j} \left((v + \sigma_\omega v_T) \frac{\partial \omega}{\partial x_j} \right) + 2\sigma_\omega \omega^2 \frac{1-F_1}{\omega} \frac{\partial k}{\partial x_j} \frac{\partial \omega}{\partial x_j} \quad 2.52$$

F_1 is the switching function for handling the change between the ω and ϵ -equations. The blending of the ω and ϵ -equations takes place in the wake region of the boundary layer and is governed by the switching function

$$F_1 = \tanh(\Gamma^4) \quad 2.53$$

Where

$$\Gamma = \min\left(\max\left(\frac{\sqrt{k}}{\beta^* \omega d}, \frac{500v}{\omega d^2}\right); \frac{4\rho\sigma_\omega k}{CD_{k\omega} d^2}\right) \quad 2.54$$

In this equation d is the normal distance from the wall and

$$CD_{k\omega} = \max\left(\frac{2\rho\sigma_\omega}{\omega} \frac{\partial k}{\partial x_j} \frac{\partial \omega}{\partial x_j}; 10^{-20}\right) \quad 2.55$$

The eddy viscosity μ_T is defined as

$$v_T = \frac{a_1 k}{\max(a_1 \omega; |\Omega_{ij}| F_2 F_3)} \quad 2.56$$

Ω_{ij} is the vorticity

$$\Omega_{ij} = 1/2 \left(\frac{\partial u_i}{\partial x_j} - \frac{\partial u_j}{\partial x_i} \right) \quad 2.57$$

Where $|\Omega_{ij}| = \sqrt{2\Omega_{ij}\Omega_{ij}}$. The constant $a_1 = 0.31$. The switching function F_2 is defined as

$$F_2 = \tanh(\Gamma_2^2) \quad 2.58$$

where

$$\Gamma_2 = \max\left(\frac{2\sqrt{k}}{\beta^* \omega d}, \frac{500v}{\omega d^2}\right) \quad 2.59$$

Function F_3 is defined as

$$F_3 = 1 - \tanh\left[\left(\frac{150v}{\omega d^2}\right)^4\right] \quad 2.60$$

Let ϕ_1 represent any constant in the original $k - \omega$ model, ϕ_2 the corresponding constant in the $k - \epsilon$ model and ϕ the constant in the SST model (Flowtech, 2010). Then the relation between them is

$$\phi = F_1\phi_1 + (1 - F_1)\phi_2 \quad 2.61$$

Table 2.1: Coefficients in turbulence model.

ϕ	1	2
$\sigma_{k\phi}$	0.85	1.0
$\sigma_{\omega\phi}$	0.5	0.856
β_ϕ	0.075	0.0828

The constants are summarized in the Table 2.1. The coefficients κ and β^* have constant values of 0.41 and 0.09, and γ is calculated from

$$\gamma = \frac{\beta}{\beta^*} - \frac{\sigma_\omega \kappa^2}{\sqrt{\beta^*}} \quad 2.62$$

2.3.3.4 Wall Functions vs. Near-Wall Model

Traditionally, there are two approaches to modeling the near-wall region. In one approach, the viscosity-affected inner region (viscous sublayer and buffer layer) is not resolved. Instead, semi-empirical formulas called “wall functions” are used to bridge the viscosity-affected region between the wall and the fully-turbulent region. The use of wall functions obviates the need to modify the turbulence models to account for the presence of the wall.

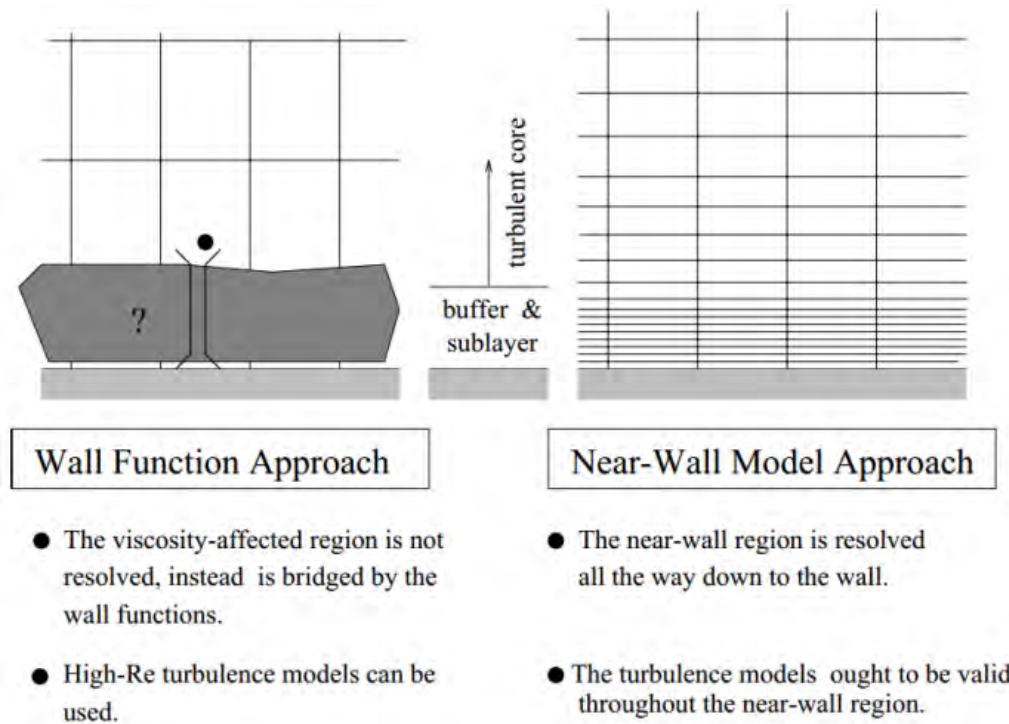


Figure 2.9: Wall functions vs. near-wall model

In another approach, the turbulence models are modified to enable the viscosity-affected region to be resolved with a mesh all the way to the wall, including the viscous sublayer. This approach is known as "near-wall modeling approach". These two approaches are depicted schematically in Figure 2.9.

In SST $k-\omega$ model, the flow is resolved up to the wall. Therefore near-wall model approach is used instead of wall function for the treatment of boundary layer region.

2.4 SHIPFLOW CFD Software

The CFD software used for the investigation in this thesis is called SHIPFLOW which is a powerful suite of CFD tools developed by FLOWTECH International AB with close cooperation of Shipping and Marine Technology Department at Chalmers University of Technology and SSPA Sweden AB which provides high-tech consulting services such as ship design, maritime operation, port, and coastal development services worldwide and owned by the Foundation Chalmers University of Technology.

The code is specially optimized for ship hydrodynamics and all outputs of resistance and propulsion are presented in the way of Naval Architects. SHIPFLOW is built up from a number of modules each briefly described in chapters 2.3.1 to 2.3.5 below (Flowtech, 2010).

2.4.1 XMESH

XMESH is a panel generator for the potential flow module XPAN. XMESH can be executed as a separate program to check the panelization of the body and free-surface before the potential flow computation is executed. The XMESH module is also executed during the potential flow computation when sinkage/trim or non-linear iterations are performed and the panelization is updated in each iteration. XMESH generates the panels used for a sink-disk representation of a propeller in the potential flow. Off-body points can also be generated using the XMESH module. Off-body points are used in potential flow computations when the result is to be displayed at points in the flow field outside the hull surface.

2.4.2 XPAN

XPAN is the flow solver for the potential flow around three dimensional bodies based on a surface singularity panel method. A wide range of problems may be analyzed. These include

- Flows with or without a free surface
- Ship flows with or without a transom stern
- Ship flows with or without sinkage and trim
- Multiple ship speeds
- Multiple onset flow directions
- Influence of the propeller
- Lifting surfaces
- Shallow water
- Ship in a canal

With the following options

- First or higher order panel method
- Linear or non-linear free surface boundary condition
- Neumann-Kelvin, double-model or single-model solution as base flow
- Symmetry feature
- Initial ship position specification
- Velocity and pressure computations at specified off-body points

Using the XPAN program, the following features of the flow around the hull may be computed

- Wave resistance from pressure integration and from transverse wave cuts
- Wave pattern
- Wave profile along the waterline
- Wave profile along longitudinal and transverse wave cuts
- Far-field waves in deep water
- Potential streamlines (traced in XBOUND)
- Pressure contours
- Velocity vectors
- Sinkage and trim
- Lift and induced drag

XPAN creates a data base file, id_XPDB, used by XBOUND, XGRID and XCHAP. The data base file contains all the results from the potential flow computation that are needed for the execution of XBOUND and XCHAP (zonal approach).

2.4.3 XBOUND

XBOUND is a program for thin turbulent boundary layer computations. The momentum integral equations for boundary layers are solved along streamlines traced from a potential flow computation. XBOUND is also capable of computing the laminar boundary layer and the transition to the turbulent boundary layer for simpler cases with a well-defined stagnation point or line. The computations can be carried out for a smooth surface or for a specified surface roughness.

The following boundary layer quantities can be computed in XBOUND:

- Boundary layer thickness
- Displacement thickness
- Momentum thickness
- Shape factor
- Cross-flow angle
- Skin friction coefficient
- Transition between laminar and turbulent flow
- Limiting streamlines

The friction is integrated over a specified region of the hull. XBOUND creates a data base file, `id_XBDB`, used by XCHAP. The data base file contains all the results from the boundary layer computation needed for the execution of XCHAP.

2.4.4 XGRID

XGRID generates the grid used for the viscous computations in XCHAP

- around a ship or submarine hull
- with constant x-surfaces
- with proper concentration close to the hull surface regardless of humps and hollows.
- where the position of the parametric edges leaving the keel/water line can be specified to avoid singularity problems in the XCHAP module.
- with a concentration of x-planes in the stern region where it is needed the most.
- with a strong concentration of points close to the singularity lines (the parametric edges between the continuation of the hull surface, the wake plane, and the adjacent parametric surfaces)
- which includes sinkage and trim
- create a transom grid for XCHAP
- mirror grid for unsymmetrical cases
- handle twin skeg hulls
- adopt horizontal plane to a prescribed free surface from XPAN

Appendages however are not possible to handle with XGRID.

2.4.5 XCHAP

XCHAP is a finite volume code that solves the Reynolds Averaged Navier-Stokes equations. It uses several turbulence models (*EASM*, *k- ω BSL*, *k- ω SST*). The solver can be used in a zonal or a global approach. The solver can handle overlapping grids. Several parametrised models of appendices are available in the system, e.g. rudder, shafts, brackets and vortex generators. Grids can also be imported from external grid generators. There are also two actuator disk models available, a simple force model and a lifting line model. The flow can be computed with a double model or with a prescribed free-surface from XPAN.

The following quantities are computed

- Velocity field
- Pressure

- Turbulent kinetic energy and specific turbulent kinetic energy
- Local skin friction coefficient
- Friction and pressure resistance coefficients for the hull part covered by the grid
- Total resistance and its components using the results from XPAN, XBOUND and XCHAP.

XCHAP can use the grid provided by XGRID. Inflow boundary conditions are generated from results provided by XPAN and XBOUND when the zonal approach is used. XCHAP can also use block structured grids generated in an external grid generator. These grids can be either the entire hull so that no XGRID grid is needed or appendage grids that are added to XGRID grid (Flowtech, 2010).

The total resistance can be computed by combining the results from XPAN, XBOUND and XCHAP.

2.4.6 Co-ordinate system in SHIPFLOW

The Cartesian coordinate system (x, y, z) is defined as origin is located in the undisturbed free surface at fore perpendicular (F.P) of the hull so that the undisturbed incident flow with a constant speed U appears to be a streaming in the positive- x direction where y -axis extends to the starboard side and z -axis upwards as shown in Figure 2.10.

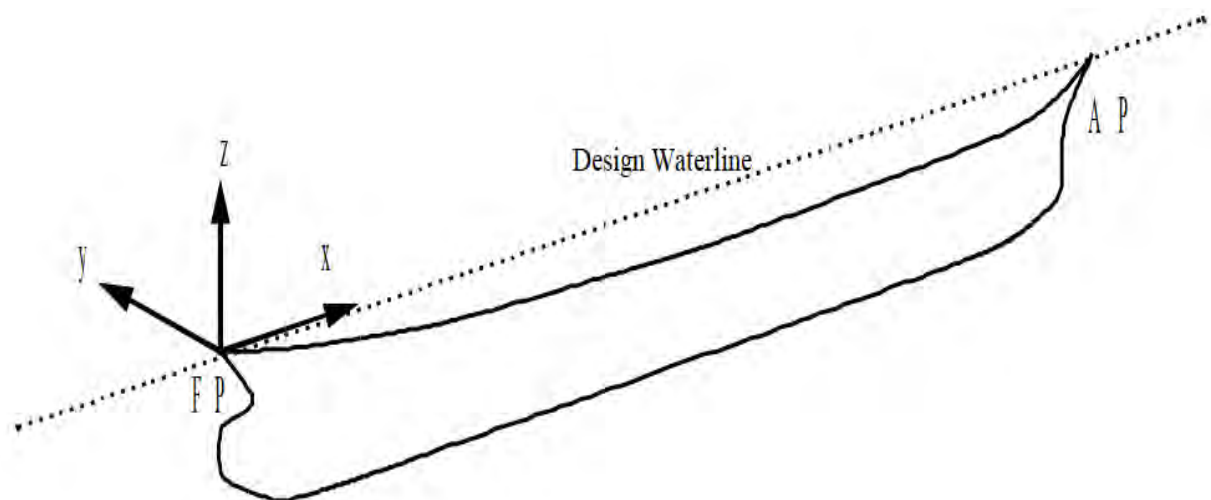


Figure 2.10: Cartesian coordinate system in SHIPFLOW

2.4.7 Initial and Boundary Conditions

In order to solve the partial differential equations, boundary conditions are defined in the computational domain. Two layers of ghost cells are used in XCHAP. Two basic boundary conditions are used: Dirichlet and Neumann. The first specifies the value of a solution at the domain boundaries and the latter specifies values of the derivative normal to the surface of a solution. These are used then according to the physical properties of different types of boundaries that define a computational problem.

Inlet: At the inlet it is assumed that the flow is undisturbed. Constant values are prescribed for the velocity as well as the turbulent quantities. The void fraction is also described with the Dirichlet BC, but the fraction varies at the inlet face. It gets values equal to 1 in the water and 0 in the air. The pressure gradient in the longitudinal direction is set to zero.

Outlet: A simplification is made that the boundary is far downstream, which means that the flow is fully developed and that the waves are entirely damped. Therefore, it is acceptable to use the Neumann BC for the velocity, void fraction and turbulent quantities. For the current surface capturing method implementation, the Neumann BC is also used for the pressure.

Slip: The physical boundaries-such as top, bottom and side faces of the domain are assumed solid walls and create an enclosed space in which the hull is placed. No flow through such a boundary is ensured – the normal velocity component is zero – and the flow is free to slip along the boundaries – the normal velocity gradient is zero. The Neumann BC is used for the pressure, void fraction and turbulent quantities. The same conditions are used at the symmetry plane. The slip condition is a good approximation for the symmetry plane and also the outer boundary if the computational domain is large compared to the ship dimensions. A modified slip condition is applied to a part of the top boundary. The Dirichlet BC is used for the pressure in order to solve the equations (Orych, 2013).

No slip: At the hull surface the velocity is zero i.e. no flow through the boundary is possible and the fluid sticks to the surface. The Neumann BC is used for the pressure and void fraction. Figure 2.11 illustrates the boundary conditions for a typical flow domain.

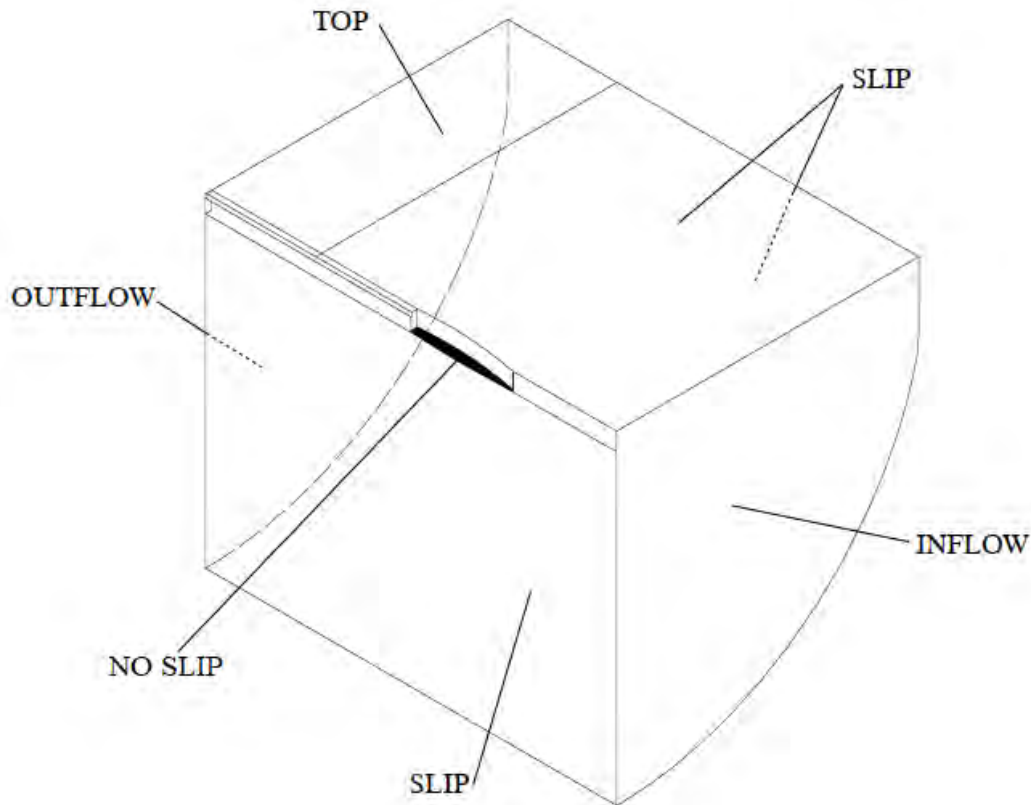
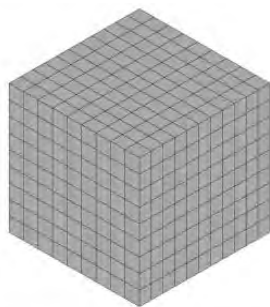


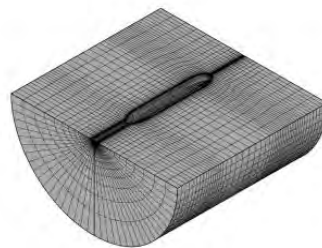
Figure 2.11: boundary conditions for a typical flow domain

2.4.8 Grid

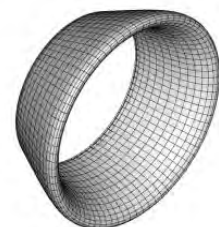
Finite volume method requires grid cells in order to discretize the partial differential equations and approximate algebraic equations. In XCHAP module only structured grids are used. A simple geometry such as bare hull can be represented by a single block structured grid while more complex geometries such as hull with appendixes can be expressed by the multi-block structured grid and overlapping grid. Three grid topologies used in XCHAP are H-H, H-O and O-O types. Figure 2.12 represents examples of grids with very coarse grid densities for clarity. Although it is possible to import grids from externally generated structured grids.



(a) H-H grid topology



(b) H-O grid topology



(c) O-O grid topology

Figure 2.12: Examples of grid topologies

2.4.9 Overlapping grids

Overlapping grids were introduced to XCHAP in order to compute the flow around more complicated geometries (rudders, shafts, brackets, or fins) than a single block of structured grids. Overlapping grid technique is powerful because it mostly offers the generality of unstructured grids while most of the advantages of structured grids is retained. One more advantage of overlapping grids is that they are not depending on the use of structured component grids even though all component grids are structured in SHIPFLOW. It is very useful in ship hydrodynamics because it allows to create a library of ready-made grids for standard shapes such as rudders, struts, fins, possibly parametrized so that they can be customized (Regnström, 2008). Another important application of overlapping grids is the refinements on the single block of structured grids. Often stern region of the ship is expected to have denser grids than other regions. In order to refine the grid only at the desired region such as stern, overlapping grids works with high accuracy and cost effective (Korkmaz, 2015).

2.5 Verification and Validation (V&V)

Verification is the process of determining that a model implementation accurately represents the developer's conceptual description of the model and the solution to the model. Roache coined the phrase 'solving the equations right'. This process quantifies the errors. Thus, Verification is the process of determining the match between the CFD results and the conceptual model of the fluid flow to quantify errors.

Validation is the process of determining the degree to which a model is an accurate representation of the real world from the perspective of the intended uses of the model. Roache called this 'solving the right equations'. This process quantifies the uncertainty. Thus, Validation is the process of determining the match between the CFD results and the real flow problem to quantify uncertainty (Versteeg, 2007).

The procedure of numerical simulation starts with building the conceptual model. At this stage physical phenomena behind the specified problem is identified. A conceptual mathematical model, which consists of sets of differential or integral equations, is formed. In order to solve these equations numerically, they have to be discretized first and then solved by numerical methods. Iterative approach is used by most of the numerical methods. When convergence criterion is satisfied, iterative solver stops and the solution is supposed to be calculated. However, as shown in Figure 1.13 each step introduces error to the solution. Modelling errors

occur due to assumptions needed to construct the conceptual model and approximations in equations such as linearization or usage of empirical data. Numerical errors are discretization errors, convergence errors and roundoff errors which is introduced due to internal representation of numbers. Depending on the type of problem, numerical method can be based on potential/inviscid flow theory, viscous flow theory or even a combination of potential and viscous flow (Korkmaz, 2015).

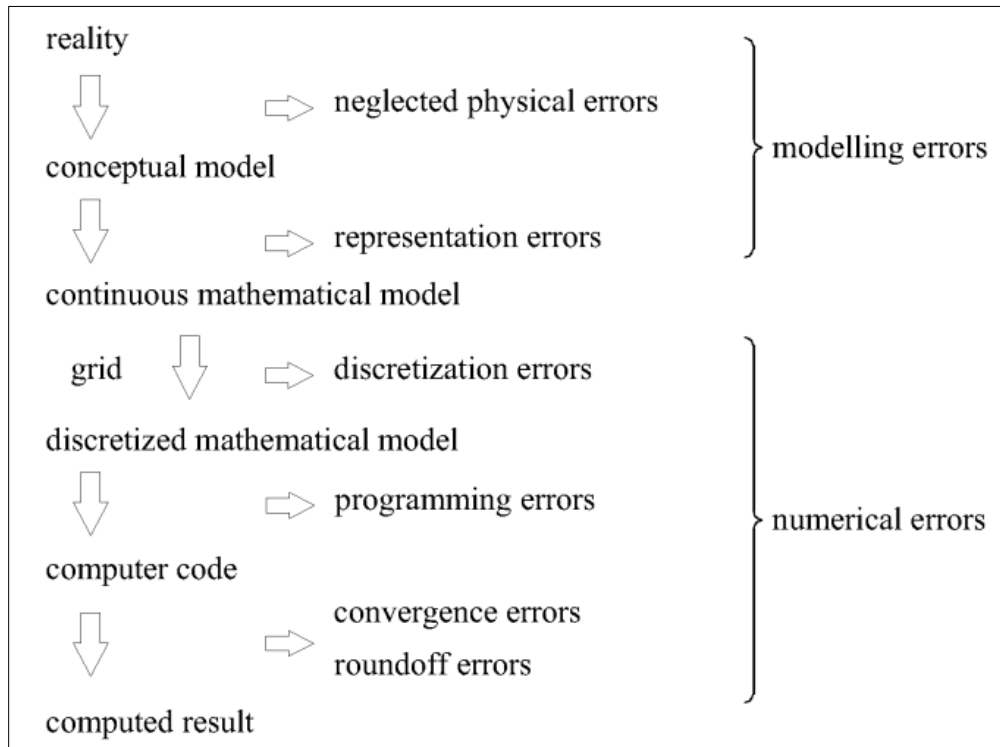


Figure 2.13: Sources of errors in computed results

It is a well-known fact from the literature that assessing accuracy just by comparing the EFD results with the CFD results is not sufficient. However formal V&V methods has the capacity of determining the numerical errors and modelling errors.

2.5.1 Verification

Governing equations of ship hydrodynamics have non-linear nature that can be solved through iterative methods. This approach brings an inevitable error when the flow is complex such as flow around the ship. In this thesis, the flow around ship hull has been determined using SHIPFLOW CFD code. V&V of the results is done according to the ITTC recommended procedures and guidelines ITTC (1999).

The convergence ratio R_G is defined as:

$$R_G = \frac{\varepsilon_{21}}{\varepsilon_{32}} \quad 2.63$$

Where $\varepsilon_{21} = S_2 - S_1$, $\varepsilon_{32} = S_3 - S_2$ give the change of solutions between the medium-fine and coarse-medium grids.

The first order Richardson Extrapolation estimate,

$$\delta_{REG}^* = \frac{\varepsilon_{21}}{r_G^{P_G-1}} \quad 2.64$$

order of accuracy,

$$P_G = \frac{\ln\left(\frac{\varepsilon_{32}}{\varepsilon_{21}}\right)}{\ln(r_G)} \quad 2.65$$

and correction factor,

$$C_G = \frac{r_G^{P_G-1}}{r_G^{P_{Gest}-1}} \quad 2.66$$

where $P_{Gest} = P_{th} = 2$ is used. Uncertainty and error estimates are made considering C_G as sufficiently less than or greater than 1 and lacking confidence and C_G as close to 1 and having confidence,

The Discretization uncertainty,

$$U_G = |C_G \delta_{REG}^*| + |(1 - C_G) \delta_{REG}^*| \quad 2.67$$

Assuming that round-off error is negligible, the numerical uncertainty becomes:

$$U_{SN} = \sqrt{U_I^2 + U_G^2} \quad 2.68$$

where U_G is the discretization uncertainty and U_I is the iterative uncertainty. If discretization uncertainty is much bigger than iterative uncertainty, then U_I can be ignored.

Therefore,
$$U_{SN} = \sqrt{U_I^2 + U_G^2} \approx U_G \quad 2.69$$

2.5.2 Validation

Validation process is a tool for assessing the errors or uncertainties of a numerical computation in a more fundamental way. A simplified version of the validation procedure adopted here is ITTC recommended procedures and guidelines ITTC (1999). In this simplified procedure, two parameters, validation comparison error and validation uncertainty are introduced. Comparison error is defined as:

$$E = D - S \quad 2.70$$

where S is the simulated solution and D is experimental data. The validation uncertainty is defined as:

$$U_{val}^2 = U_{SN}^2 + U_{input}^2 + U_D^2 \quad 2.71$$

where U_{SN} is the numerical uncertainty, U_{input} is the input parameter uncertainty and U_D represents the data uncertainty in experiment. For a strong model concept, U_{input} can be ignored ($U_{input}=0$) and U_{val} becomes:

$$U_{val}^2 = U_{SN}^2 + U_D^2 \quad 2.72$$

Therefore,
$$U_{val} = \sqrt{U_{SN}^2 + U_D^2} \quad 2.73$$

When two uncertainties, validation comparison error and validation uncertainty are determined, validation result can be checked as:

- ❖ if $|E| > U_{val}$, the simulation results are not validated.
- ❖ if $|E| \leq U_{val}$, the simulation results are validated.

Chapter 3

Geometry and Condition

In this thesis, two container ships have been chosen to carry out the computations. The first one is KRISO Container Ship (KCS) which is a well-known benchmark ship hull with a bulbous bow for the researchers in the field of ship hydrodynamics. It was developed by the Korea Research Institute for Ships and Ocean Engineering (KRISO) where towing tank experiments were carried out to obtain resistance, mean flow data and free surface waves. This KCS hull is used to check the simulation result. As KCS hull is a standard hull, the V&V is done by this hull. The second one is a local 158 TEU container ship without bulbous bow. The hull geometry, principal particulars and the conditions for simulation of these two container ships are given in this chapter.

3.1 Geometry and Principal Particulars

In this section the hull geometry and principal particulars for both of the container ships are given.

3.1.1 Case model-1: KRISO Container Ship (KCS) Hull

The geometry of KCS both in iges and offset format can be seen in Figure 3.1 and Figure 3.2 respectively.

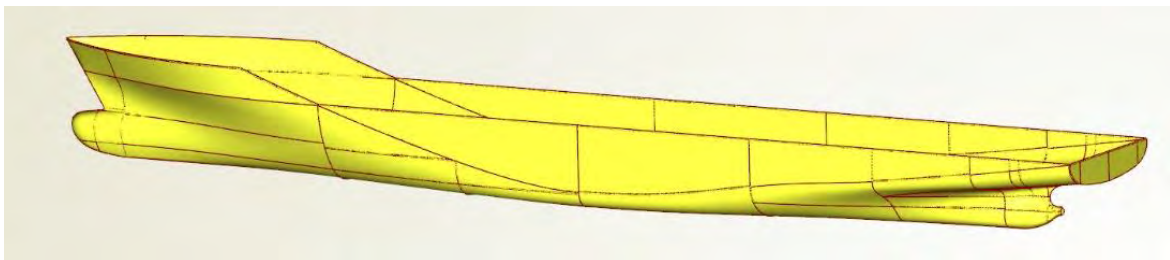
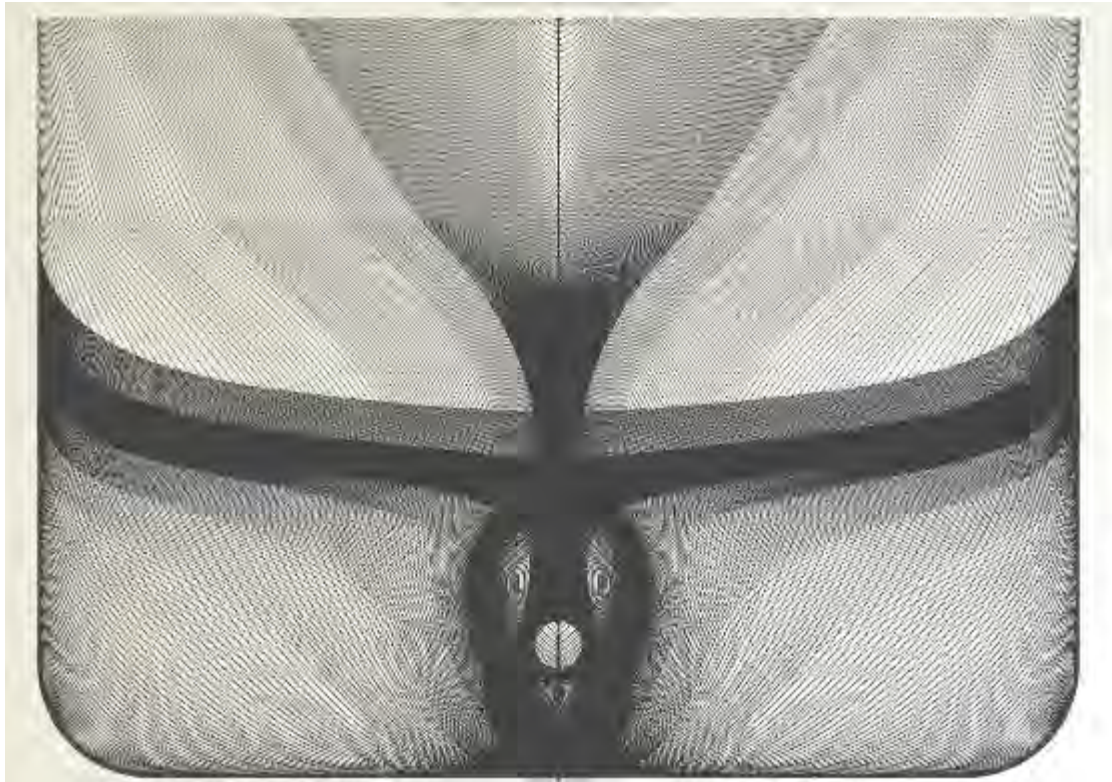
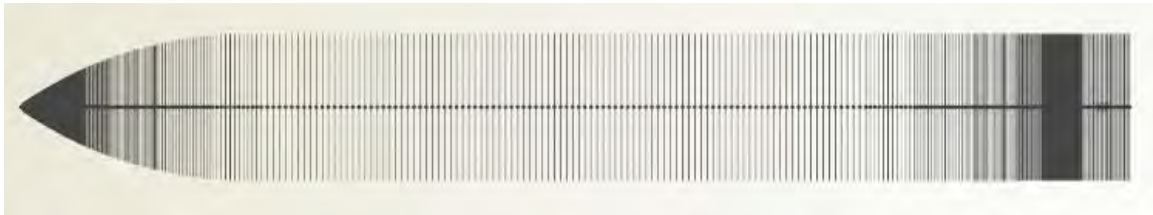


Figure 3.1: Geometry of KCS hull



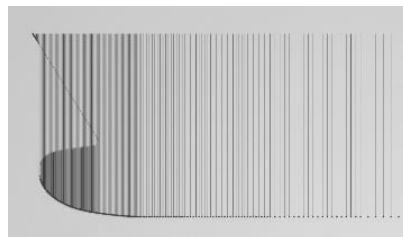
(a) Body Plan



(b) Top view



(c) Profile view



(d) Enlarged forward part of profile view

Figure 3.2: Lines plan of KCS hull

The principal particulars in full and model scale for the KCS hull is given in the Table 3.1.

Table 3.1: Principal particulars for KCS hull

Main Particulars	Prototype	Model (NMRI, 2015)
Length Over All (LOA)	232.5 m	7.3577 m
Length between perpendiculars (LBP)	230.0 m	7.2786 m
Breadth Overall	32.2 m	1.019 m
Draft	10.8 m	0.3418 m
Depth	19.0 m	0.6013 m
Block Coefficient	0.6505	0.6505
Displacement	52030 m ³	1.6490 m ³
Design Speed	24 knots (12.3467 m/s)	2.196 m/s
Froude Number	0.260	0.26

3.1.2 Case model-2: 158 TEU Container Ship Hull

The geometry of 158 TEU container ship hull both in iges and offset format can be seen in Figure 3.3 and Figure 3.4 respectively.

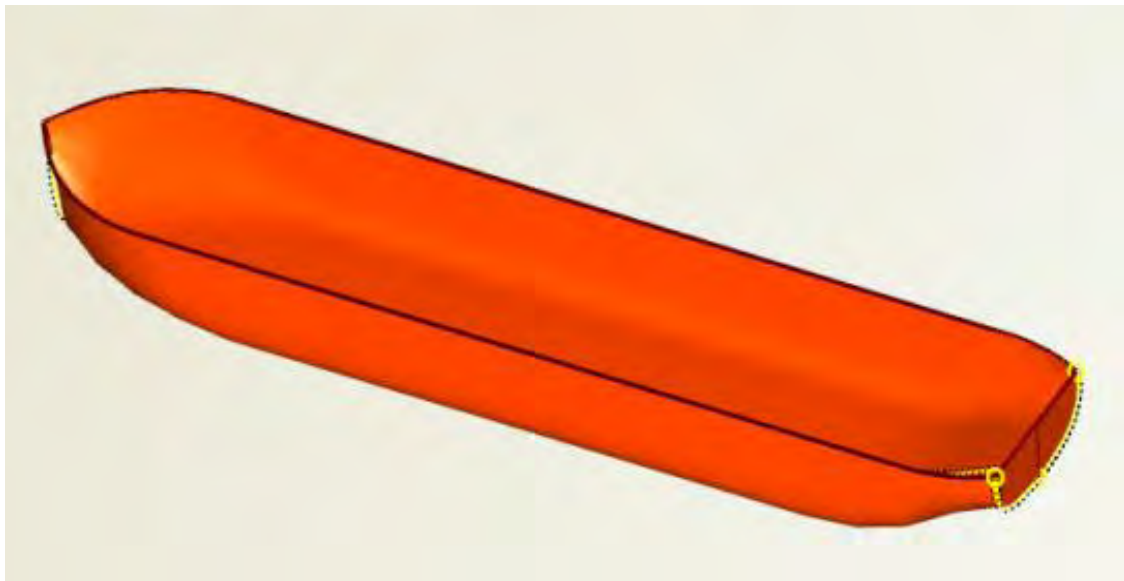


Figure 3.3: Geometry of 158 TEU container ship hull

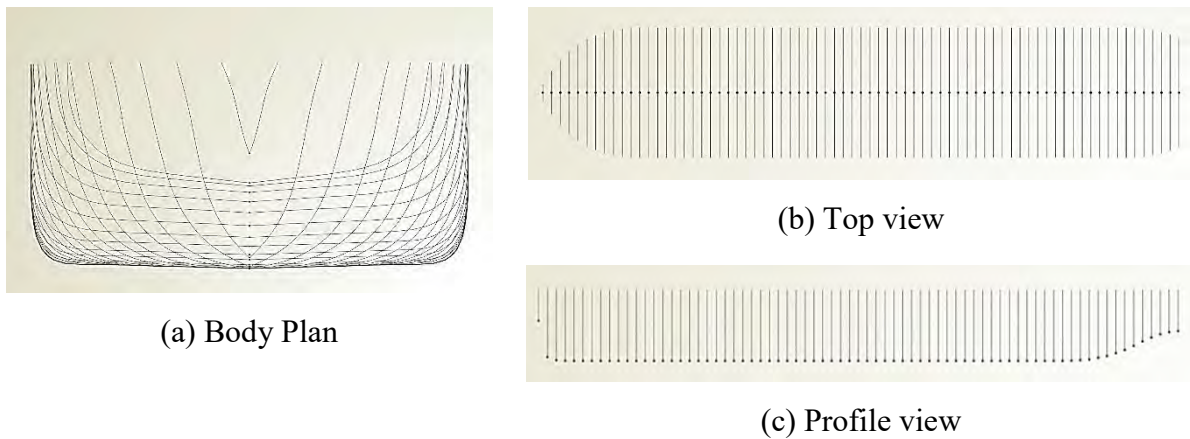


Figure 3.4: Lines plan of 158 TEU container ship

The principal particulars in full and model scale for the 158 TEU container ship hull is given in the Table 3.2.

Table 3.2: Principal particulars for 158 TEU Container ship

Main Particulars	Prototype	Model
Length Over All (LOA)	76.00 m	4.750 m
Length between perpendiculars (LBP)	72.87 m	4.554 m
Breadth Overall	15.00 m	0.938 m
Draft	3.80 m	0.238 m
Depth	7.00 m	0.438 m
Block Coefficient	0.843	0.843
Displacement	3501 m ³	0.857 m ³
Design Speed	10 knots (5.1444 m/s)	1.286 m/s
Froude Number	0.192	0.192

3.2 Conditions

Some conditions must be adopted in order to get the corresponding results in prescribed format both in model tests experiment and simulation of the SHIPFLOW software. These conditions are described below:

3.2.1 Conditions for Model Test Experiment

KCS model: The Korea Research Institute for Ships and Ocean Engineering (KRISO) performed towing tank experiments to obtain resistance, mean flow data and free surface waves. Self-propulsion tests were carried out at the Ship Research Institute (now NMRI) in Tokyo and are reported in the Proceedings of the CFD Workshop Tokyo in 2005 (NMRI, 2015). The conditions are given in Table 3.3.

Table 3.3: Conditions for Resistance, Sinkage and Trim test of KCS model

Wave	Calm
Condition	Towing
Froude Number, F_n	0.26
Reynolds Number, R_e	1.26×10^7
Speed	2.196 m/s
kinematic viscosity, ν	$1.27 \times 10^{-6} \text{ m}^2/\text{s}$
Density, ρ	999.5 kg/m^3
Rudder	With
Propeller	Without
Validation Variables	Resistance, Sinkage and Trim
EFD provider	NMRI

158 TEU Container Ship model: The model was made by reinforced fiberglass material (FRP) with geometric scale ratio 1:16. The scale of the model is determined based on the hydrodynamic considerations. The model was ballasted to represent the loaded condition. Model towing test were conducted in the speed range to cover the design speed. Results were obtained by extrapolation based on ITTC 78 prediction method using Froude's law of scaling. The model loaded draft is 0.2375 meter and the design speed Froude number is 0.192. The procedure followed is the ITTC 78 prediction method. The tank dimensions were 82.0 m \times 3.2 m \times 2.5 m (water depth) and the maximum towing carriage speed was 5 m/s. The towing

carriage was fully automatic speed control with closed-loop feedback control system for the synchronized drive motors of its four wheels.

3.2.2 Conditions for Simulation in SHIPFLOW

For completing the simulation correctly, the following parameters of SHIPFLOW software should be given in the proper way. In case of 158 TEU container ship at 10 knot speed, following parameters are given those are shown in Table 3.4.

Table 3.4: Parameters for completing the simulation in SHIPFLOW

Parameters	Symbol	Description	Value
Ship Speed	f_n	Froude Number	0.192
Fluid Flow Properties	R_n	Reynolds Number	4.32×10^8
	Fsflow	Free surface flow	N/A
Ship Length	L_{PP}	Length Between Perpendicular	72.87 m
Ship Type	Shiptype	Type of ship hull	Mono
Ship Hull	H1gr	Name of an offset group that describes the main hull	Hull
Coordinate Direction	Xaxdir	The x-axis of the computational coordinate system is pointing from the bow towards the stern. XAXDIR must be set to -1.0 if the x-axis of the offset coordinate system is pointing in the opposite direction.	-1
	Ysign	YSIGN is used to specify if the y-coordinate of the offset points is input using positive (ysign=1.0) or negative (ysign=-1.0) values.	+1
	Xori	Specifies the location of the origin of the computational coordinate system in the offset coordinate system. The origin is normally specified at the fore perpendicular.	72.87
	Zori		3.8
Special for shallow water simulation			
	BC	Boundary Condition	Linear
	Model	Condition of model (free or fixed)	free

3.2.3 Boundary Conditions in SHIPFLOW

Figure 3.5 illustrates the boundary conditions for flow domain of KCS hull. As stated in section 2.4.7, here the green colored surface indicates outflow and the opposite surface is inflow, no slip at the hull surface where the velocity is zero, i.e., no flow through the boundary and the remaining surfaces represent the slip condition.

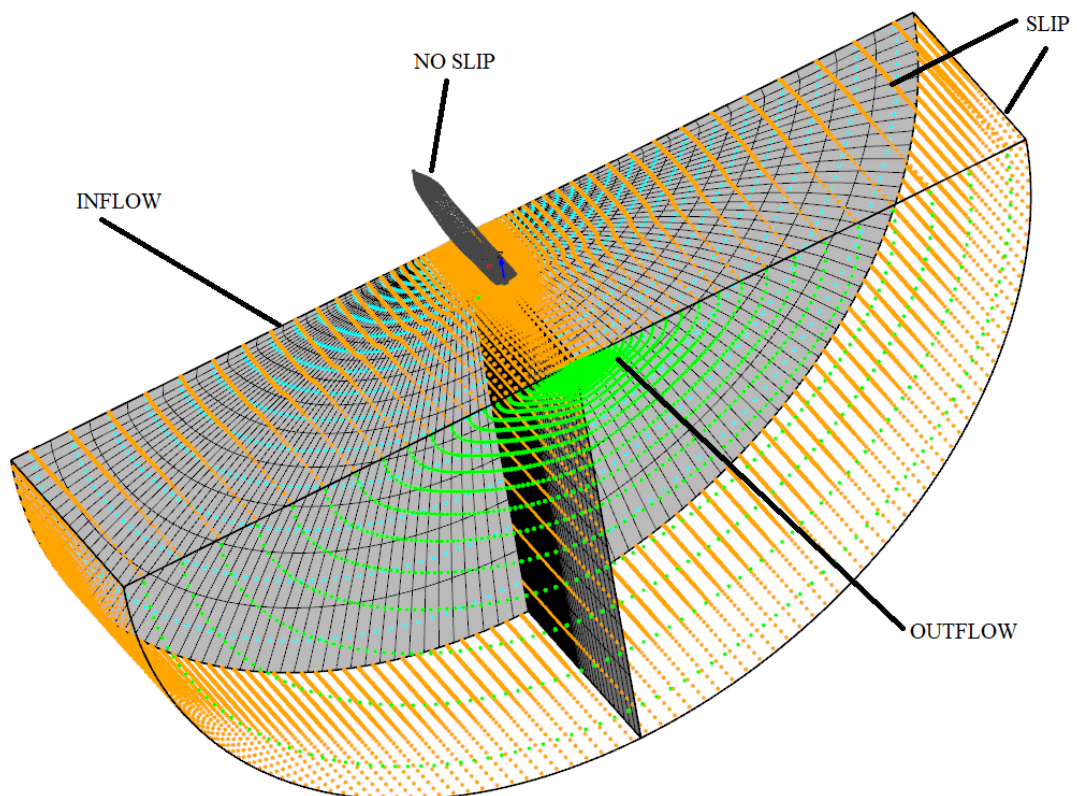


Figure 3.5: Boundary conditions for KCS hull

Chapter 4

Results and Discussions

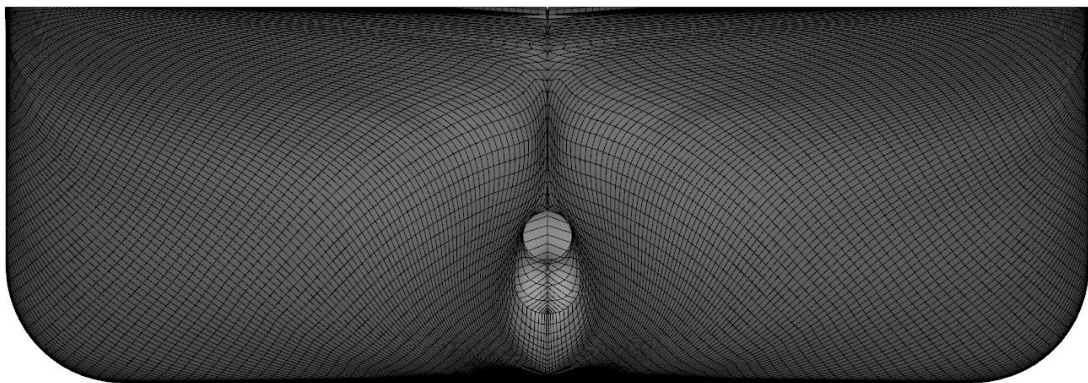
The results of the thesis work are presented in this chapter. At first, to check the validation of the SHIPFLOW software, the resistance result of a standard model KCS hull is evaluated and then the comparison with the experimental result is shown. Secondly, the results of the deep-water resistance, sinkage and trim of the 158 TEU container ship have been presented and then comparison with the experimental results is shown. Thirdly, the shallow water resistance, sinkage and trim have been presented, also the squat obtained is checked with the maximum standard squat value. Finally, the maximum speed is determined by which the container ship can run in the restricted water depth to avoid grounding in the Dhaka-Chittagong waterway of Bangladesh during high-tide.

4.1 Case Study 1: KRISO Container Ship (KCS) Hull

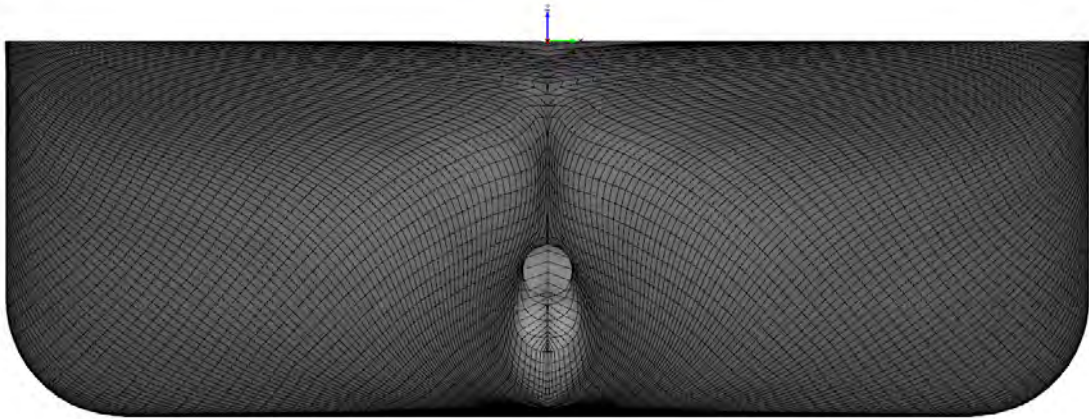
Verification and Validation of the total resistance is performed according to the procedures stated in section 2.5. The grid size variable h_i is calculated according to Equation 4.1. The examined grids are ordered from finest to coarsest which means that the grid which contains most cells will have a h_i value of one (Orych, 2013).

$$\frac{h_i}{h_1} = \sqrt[3]{\frac{(\text{Number of cells})_1}{(\text{Number of cells})_i}} \quad (4.1)$$

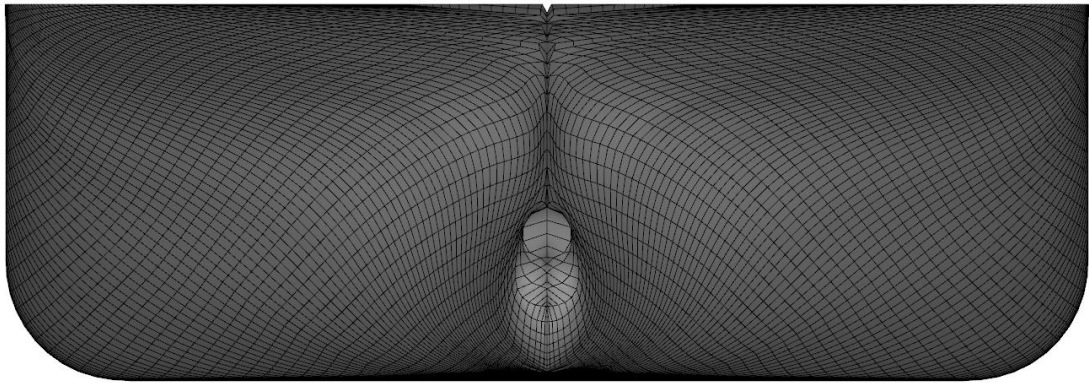
A sequence of four geometrically similar grids is generated for the grid dependence study. The four sets of grids for KCS hull are shown in Figure 4.1.



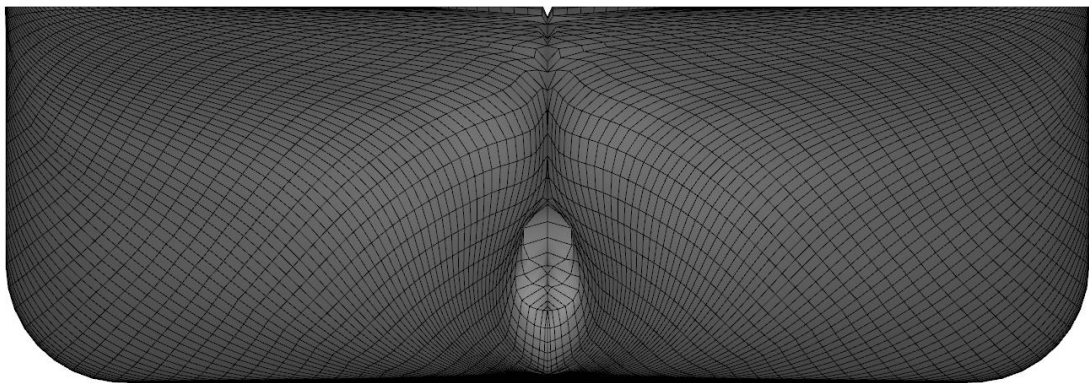
(a) Fine



(b) Medium



(c) Coarse



(d) Vcoarse

Figure 4.1: Four sets of grids for KCS hull: (a) Fine, (b) Medium, (c) Coarse, (d) Vcoarse

The number of cells varies from 0.286 to 1.218 million, values are given in Table 4.1 with the grid size variable h_i .

Table 4.1: Grid sequence for the KCS hull

Grid	Cells $\times 10^6$	h_i / h_1 ($i=1,2,3,4$)
Grid 1 (Fine)	1.218	1.000
Grid 2 (Medium)	0.744	1.179
Grid 3 (Coarse)	0.446	1.398
Grid 4 (Vcoarse)	0.286	1.621

For three different grid densities from fine (S_1) to coarse (S_3) as shown in Table 4.2 for KCS hull. For determining validation errors numerical solutions are evaluated against experimental data. EFD result and data uncertainty are provided for Total resistance coefficient (C_T) and $U_D\%D$ is reported as 1% (NMRI, 2015).

Table 4.2: V&V study of KCS hull for $R_e = 1.26 \times 10^7$ and $F_n = 0.260$

Parameter	EFD (D)	Grid 1 (S_1)	Grid 2 (S_2)	Grid 3 (S_3)
$C_T \times 10^3$	3.65	3.68	3.74	3.82
E%D		-0.822	-1.918	-4.658

4.1.1 Verification & Validation for KCS Hull

From section 2.4 the convergence ratio R_G is

$$R_G = \frac{\varepsilon_{21}}{\varepsilon_{32}} = \frac{0.06 \times 10^{-3}}{0.08 \times 10^{-3}} = 0.75$$

Where $\varepsilon_{21} = S_2 - S_1 = 0.06 \times 10^{-3}$, $\varepsilon_{32} = S_3 - S_2 = 0.08 \times 10^{-3}$ give the change of solutions between the medium-fine and coarse-medium grids.

The first order Richardson Extrapolation estimate, $\delta_{REG}^* = \frac{\varepsilon_{21}}{r_G^{P_G-1}} = \frac{0.06 \times 10^{-3}}{(\sqrt{2})^{0.83-1}} = 0.18 \times 10^{-3}$

order of accuracy, $P_G = \frac{\ln\left(\frac{\varepsilon_{32}}{\varepsilon_{21}}\right)}{\ln(r_G)} = \frac{\ln\left(\frac{0.08 \times 10^{-3}}{0.06 \times 10^{-3}}\right)}{\ln(\sqrt{2})} = 0.83$

and correction factor, $C_G = \frac{r_G^{P_G} - 1}{r_G^{P_{Gest} - 1}} = \frac{(\sqrt{2})^{0.83} - 1}{(\sqrt{2})^2 - 1} = 0.33$

where $P_{Gest} = P_{th} = 2$ is used.

The Discretization uncertainty, $U_G = |C_G \delta_{REG}^*| + |(1 - C_G) \delta_{REG}^*| = 0.18 \times 10^{-3}$

Assuming that round-off error is negligible, the numerical uncertainty becomes:

$$U_{SN} = \sqrt{U_I^2 + U_G^2}$$

where U_G is the discretization uncertainty and U_I is the iterative uncertainty. Discretization uncertainty is much bigger than iterative uncertainty, so U_I can be ignored.

Therefore, $U_{SN} = 0.18 \times 10^{-3} = \sqrt{U_I^2 + U_G^2} \approx U_G = 4.93\%D$

Comparison error is

$$E = D - S = 3.65 \times 10^{-3} - 3.68 \times 10^{-3} = -0.03 \times 10^{-3} = -0.822\%D$$

Therefore $|E| = 0.822\%D$.

where S is the simulated solution for Grid 1 and D is experimental data. The validation uncertainty is defined as:

$$U_{val}^2 = U_{SN}^2 + U_{input}^2 + U_D^2$$

where U_{SN} is the numerical uncertainty, U_{input} is the input parameter uncertainty and U_D represents the data uncertainty in experiment. For this model, U_{input} can be ignored ($U_{input} = 0$) and U_{val} becomes:

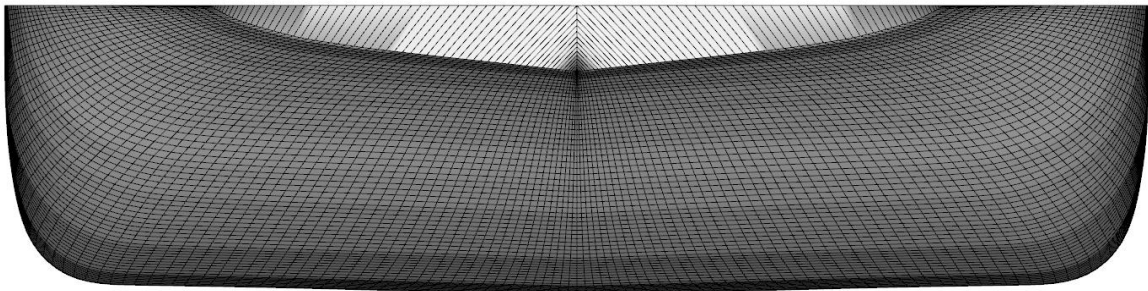
$$U_{val}^2 = U_{SN}^2 + U_D^2$$

Therefore, $U_{val} = \sqrt{U_{SN}^2 + U_D^2}$
 $= \sqrt{(0.18 \times 10^{-3})^2 + (0.0365 \times 10^{-3})^2} = 0.184 \times 10^{-3} = 5.04\%D$

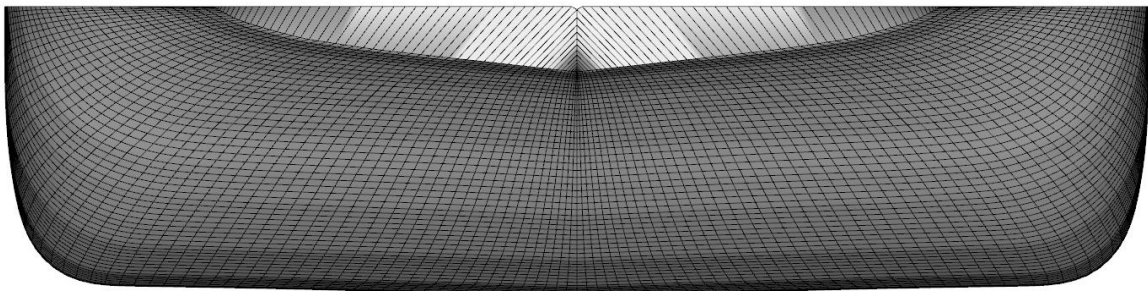
As $|E| < U_{val}$, this indicates the simulation results are valid.

4.2 Case Study 2: 158 TEU Container Ship Hull

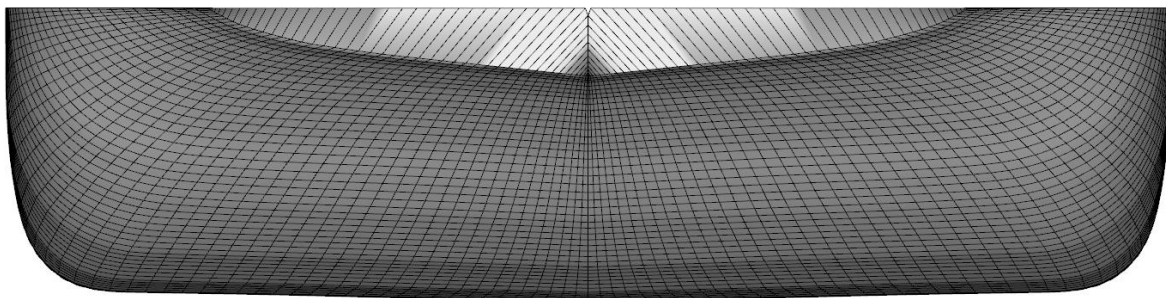
For this container ship, the four sets of grids of the hull are shown in Figure 4.2.



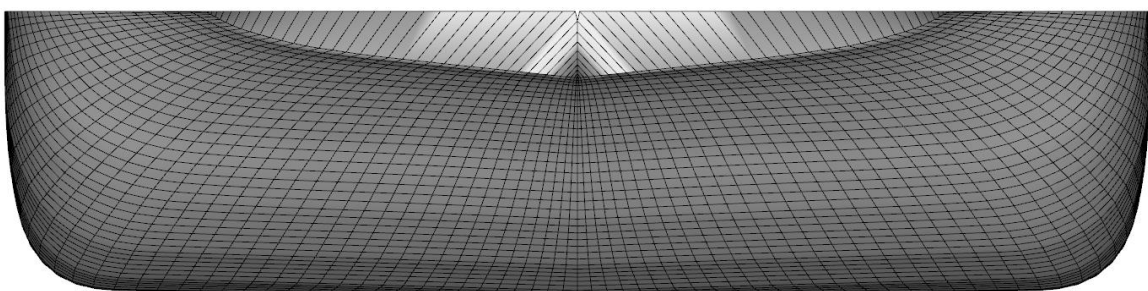
(a) Fine



(b) Medium



(c) Coarse



(d) Vcoarse

Figure 4.2: Four sets of grids for 158 TEU container ship hull: (a) Fine, (b) Medium, (c) Coarse, (d) Vcoarse

At first, the deep-water resistance, sinkage and trim was calculated by the CFD software SHIPFLOW. Then the calculated resistance result was compared with the model test experiment results. In case of shallow water, the value of squat is evaluated with the resistance, sinkage and trim result. These are discussed in the sections below:

4.2.1 Deep Water Resistance, Sinkage and Trim

4.2.1.1 Calculation of Resistance

In order to check the pattern of the graph of Wave Resistance Coefficient (C_W) and Frictional Resistance Coefficient (C_F) simulation is done from ship speed 5 knots to the hull speed 21 knots.

$$\text{Hull Speed, } V_{hull} = 2.43 \times \sqrt{L_{WL}} = 2.43 \times \sqrt{76} = 21.184 \approx 21 \text{ knots}$$

Where, V_{hull} is the hull speed of the vessel in knots and L_{WL} is the length of the waterline in meters.

Results are given in Table 4.3 and the curve is plotted in the Figure 4.3. It is seen that the shape of the graph follows the standard pattern.

Table 4.3: Deep Water Resistance Coefficients at various ship speeds

Ship Speed, V (knots)	Froude Number, F_n	Reynolds Number, $R_n \times 10^{-8}$	Wave Resistance Coefficient, $C_W \times 10^3$	Frictional Resistance Coefficient, $C_F \times 10^3$
5	0.096	2.159	0.002	1.791
6	0.115	2.590	0.032	1.742
7	0.135	3.022	0.129	1.701
8	0.154	3.454	1.581	1.671
9	0.173	3.885	1.285	1.642
10	0.192	4.317	1.100	1.601
11	0.212	4.749	3.416	1.587
12	0.231	5.180	6.399	1.567
13	0.250	5.612	9.415	1.550
14	0.269	6.044	7.982	1.532
15	0.289	6.476	10.373	1.519
16	0.308	6.907	14.087	1.508
17	0.327	7.339	14.775	1.494
18	0.346	7.771	13.685	1.482
19	0.366	8.202	12.777	1.470
20	0.385	8.634	11.978	1.458
21	0.404	9.066	11.476	1.450

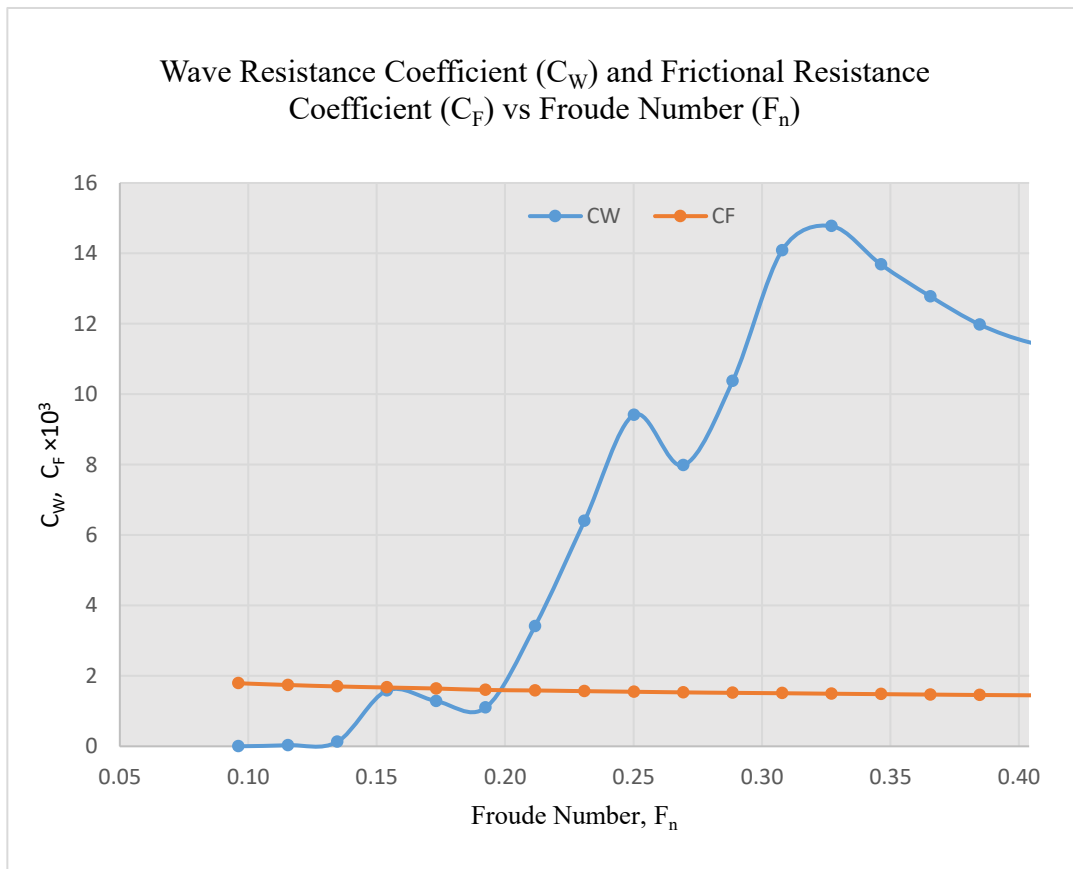


Figure 4.3: Resistance coefficients (C_W , C_F) at varying Froude numbers

The computed values of all resistance coefficients are tabulated in Table 4.3. Here it is seen that the Viscous resistance coefficient (C_V) which is the combination of Frictional resistance coefficient (C_F) and Viscous Pressure resistance coefficient (C_{PV}) decreases with the increase of Froude number (F_n). The Wave resistance coefficient (C_W) also decreases with the increase of Froude number. Though the value of total resistance (R_T) increases with the increase of Froude number but the total resistance coefficient (C_T) decreases smoothly. As this scenario is only for the short range of Froude number from 0.154 to 0.192, the total range of Froude number from 0.096 to 0.404 can be seen from Figure 4.3.

Table 4.4: Computed and experimental values of total resistance

Ship Speed	Froude Number	Resistance Coefficient Computed by SHIPFLOW					Experimental results	
V (Knots)	F_n	$C_{F3} \times 10^3$	$C_{PV3} \times 10^3$	$C_F + C_{PV} = C_Y \times 10^3$	$C_{W3} \times 10^3$	$C_V + C_W = C_T \times 10^3$	Total Resistance	
							R_T (kN)	R_T (kN)
8	0.154	1.671	0.611	2.282	1.581	3.862	48.2	49.7
8.5	0.164	1.653	0.610	2.264	1.393	3.657	51.5	54.4
9	0.173	1.642	0.609	2.252	1.285	3.537	55.9	62.6
9.5	0.183	1.626	0.606	2.233	1.201	3.434	60.4	74.7
10	0.192	1.601	0.605	2.206	1.100	3.306	64.5	83.9

Figure 4.4 shows the comparison of total resistance (R_T) between the computed value of SHIPFLOW and the experimental results. Therefore, it is observed that the difference between the computed values and the experimental values increases with the increase of speed. It is shown that in the lower Froude number the agreement is good but the difference is high in higher Froude number.

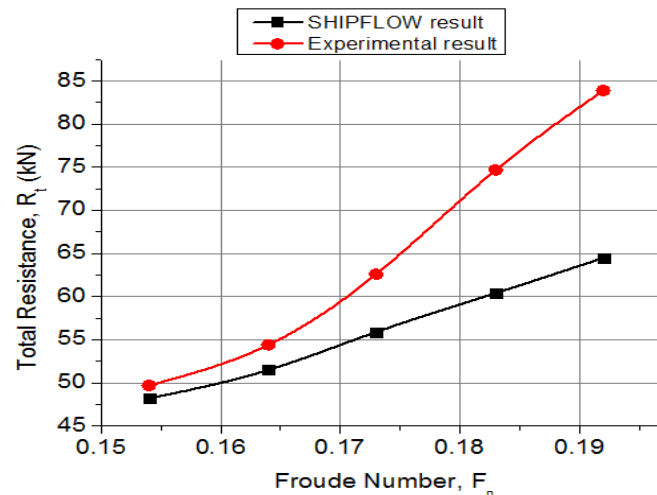


Figure 4.4: Prediction of resistance in SHIPFLOW and Towing Tank

4.2.1.2 Calculation of Sinkage and Trim

Table 4.5 shows the changes of Sinkage and Trim at center of flotation with changes of speed. Negative sinkage indicates downwards directions from free surface and negative trim indicates anticlockwise directions or trim by stern. It is seen that for the ship speed range from 8 knots to 10 knots the values of sinkage and trim increases with the increase of Froude number.

Table 4.5: Values of sinkage and trim with different Froude number

Speed (Knots)	Froude Number	Sinkage (m)	Trim (Degree)
8	0.154	-0.0722142	-0.095
8.5	0.164	-0.0823431	-0.112
9	0.173	-0.0918162	-0.130
9.5	0.183	-0.1034754	-0.150
10	0.192	-0.1136772	-0.173

Results regarding sinkage and trim are presented in Figure 4.5. From this Figure, it is seen that the sinkage is less than 5% of the draft and the absolute trim angle remains small ($<1^{\circ}$).

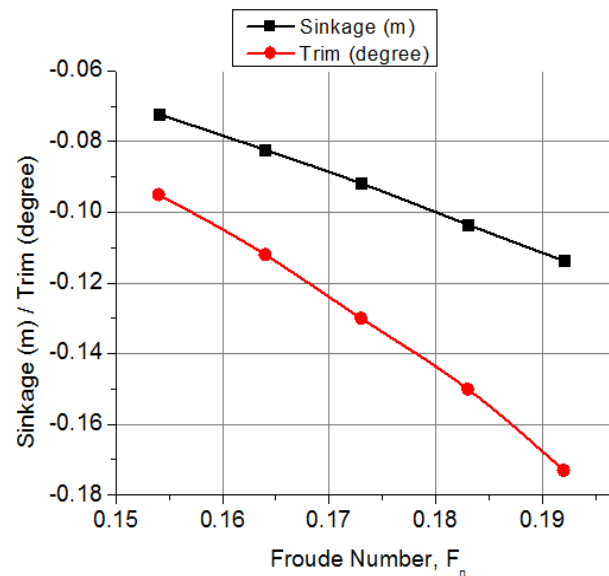


Figure 4.5: Sinkage and trim variation with Froude numbers

Figure 4.6 represents the Kelvin wave pattern (wave contours) and wave profiles for the design speed 10 knots at Froude number 0.192. The remaining wave contours and wave profiles for ship speeds 9.5, 9, 8.5 and 8 knots are shown in Figures 4.7, 4.8, 4.9 and 4.10 respectively. The values of WaveHeight those are shown in color map are non-dimensionalized by length between perpendicular of the ship. The variation in the wave pattern as the wave propagates away from the hull can be observed. The resolution of the free surface reduces significantly and the wave cuts along the length of the ship increases with speed. The wave height increases with the increase of ship speed.

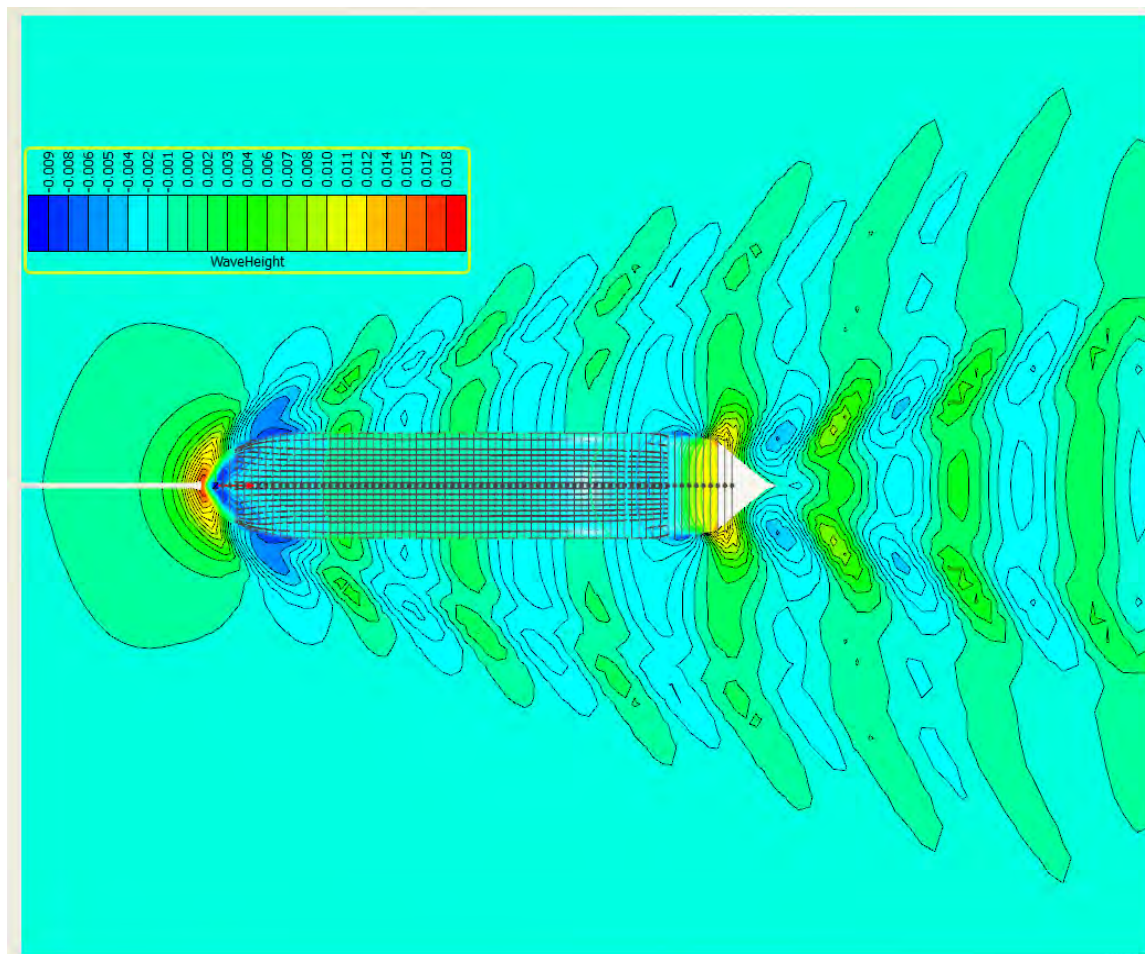


Figure 4.6 (a): Kelvin wave pattern at the speed of 10 knots

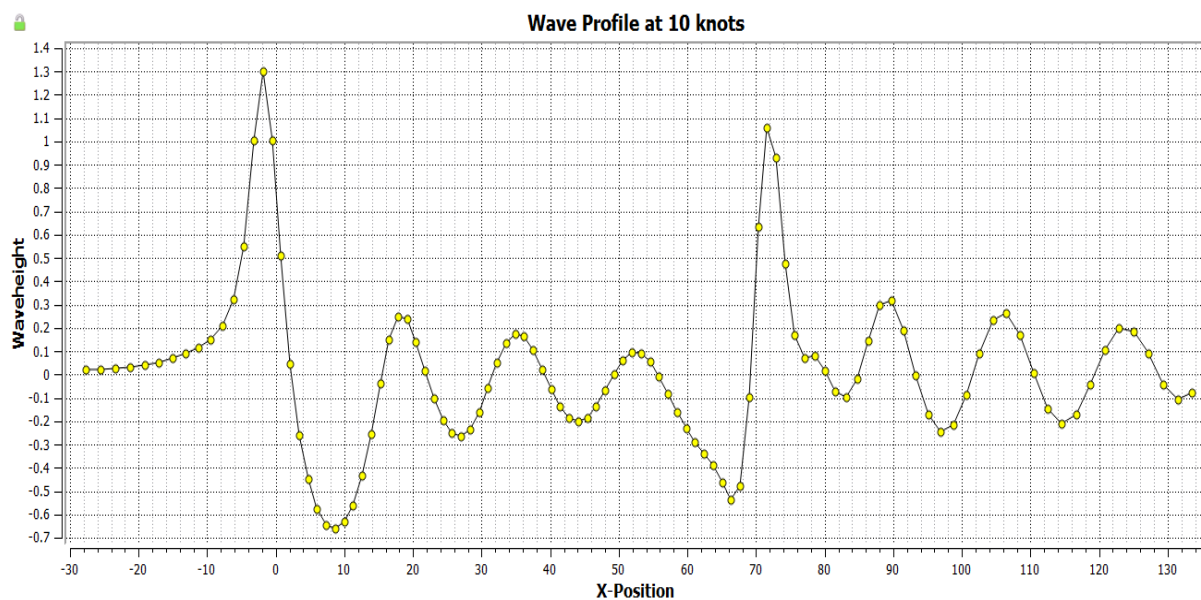


Figure 4.6 (b): Wave profile at the speed of 10 knots (units are meter)

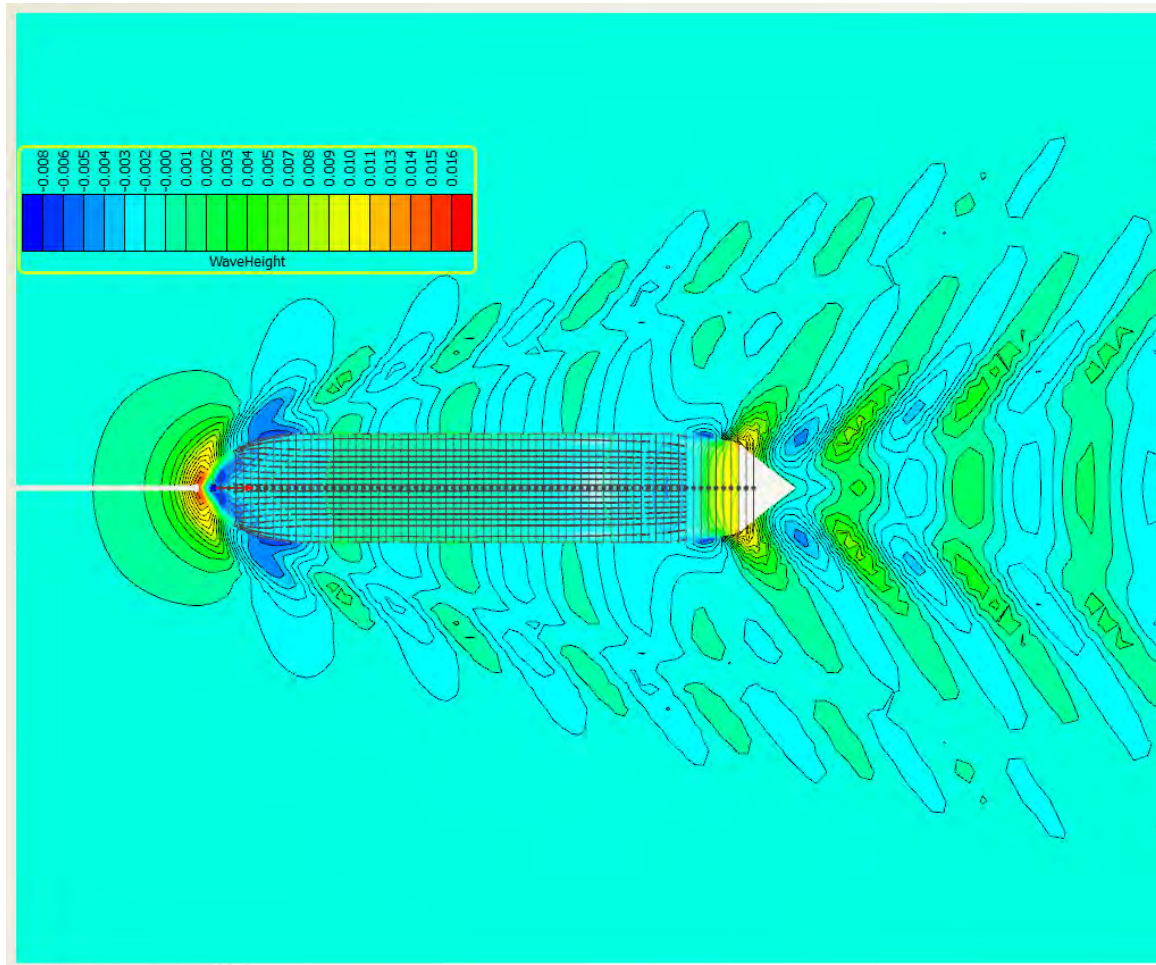


Figure 4.7 (a): Kelvin wave pattern at the speed of 9.5 knots

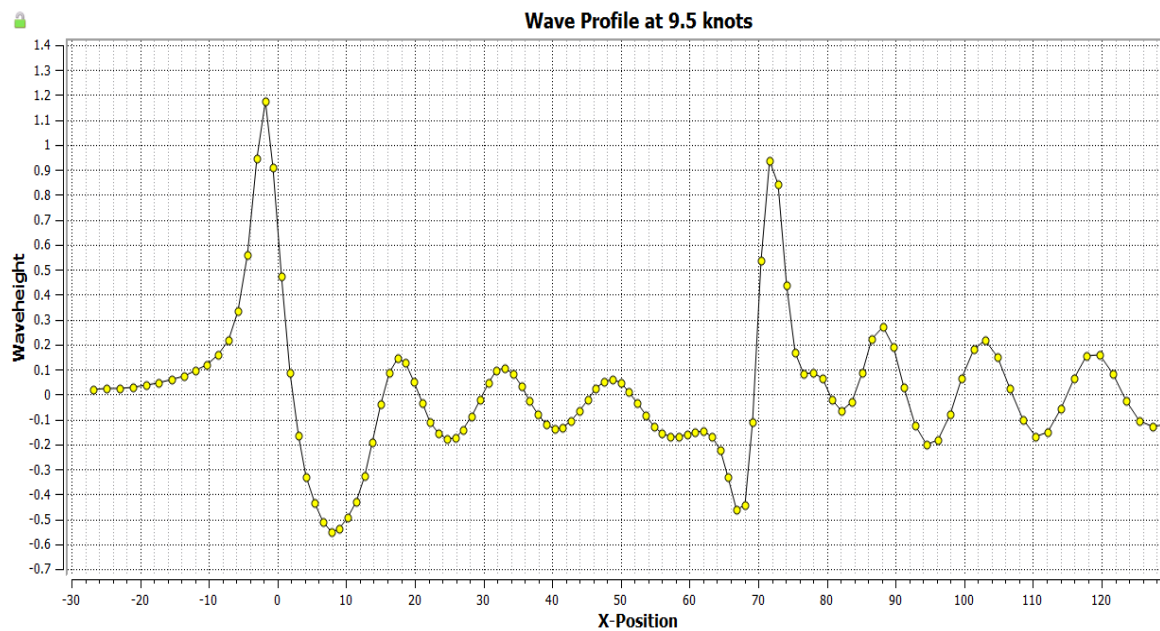


Figure 4.7 (b): Wave profile at the speed of 9.5 knots (units are meter)

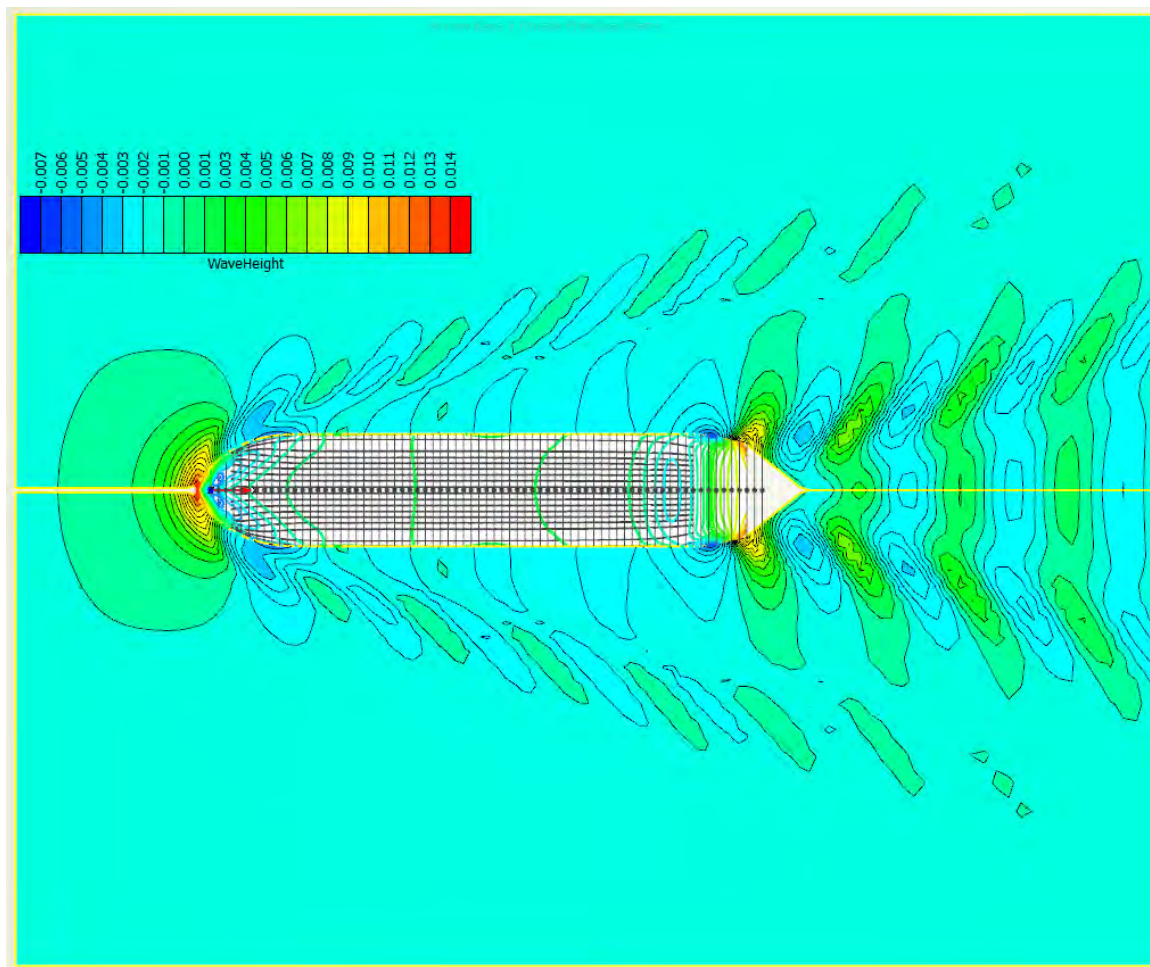


Figure 4.8 (a): Kelvin wave pattern at the speed of 9 knots

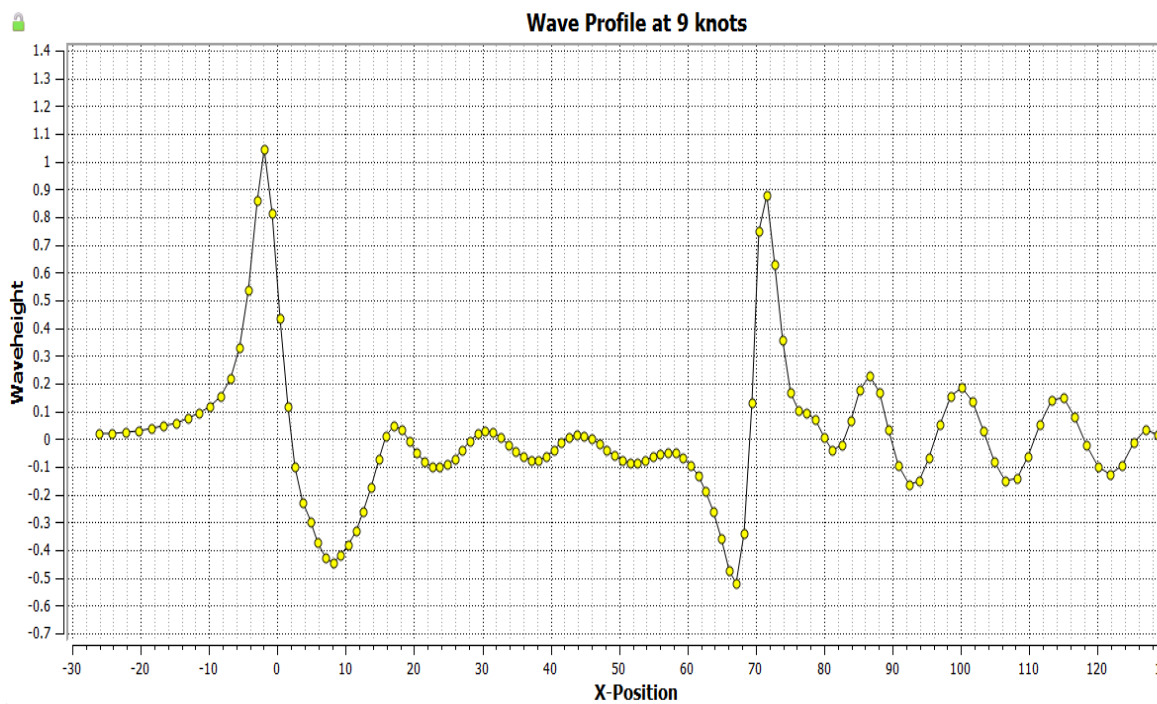


Figure 4.8 (b): Wave profile at the speed of 9 knots (units are meter)

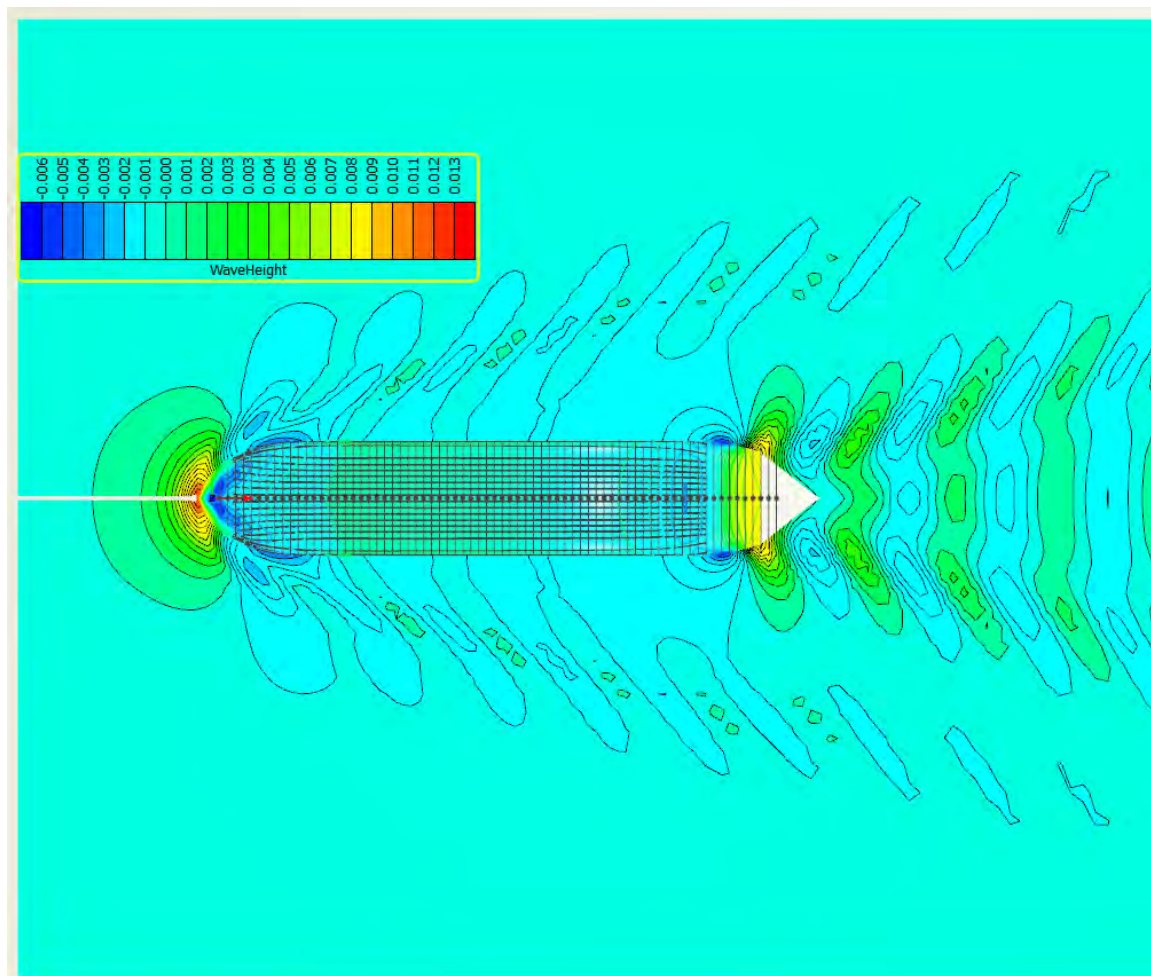


Figure 4.9 (a): Kelvin wave pattern at the speed of 8.5 knots

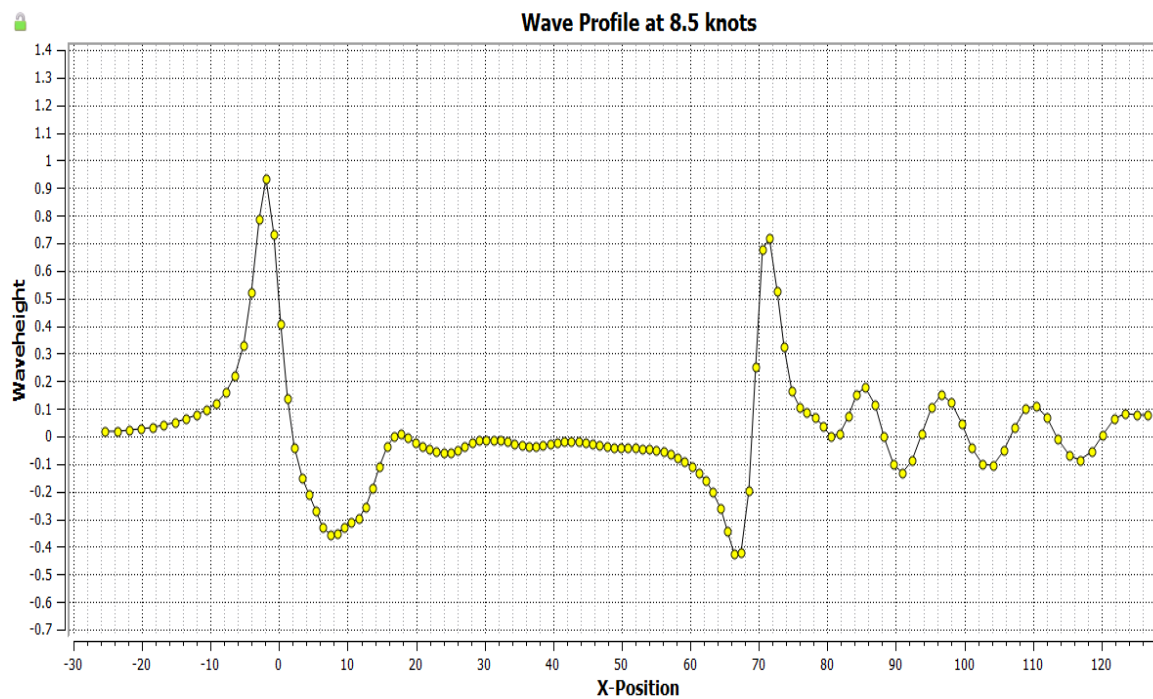


Figure 4.9 (b): Wave profile at the speed of 8.5 knots (units are meter)

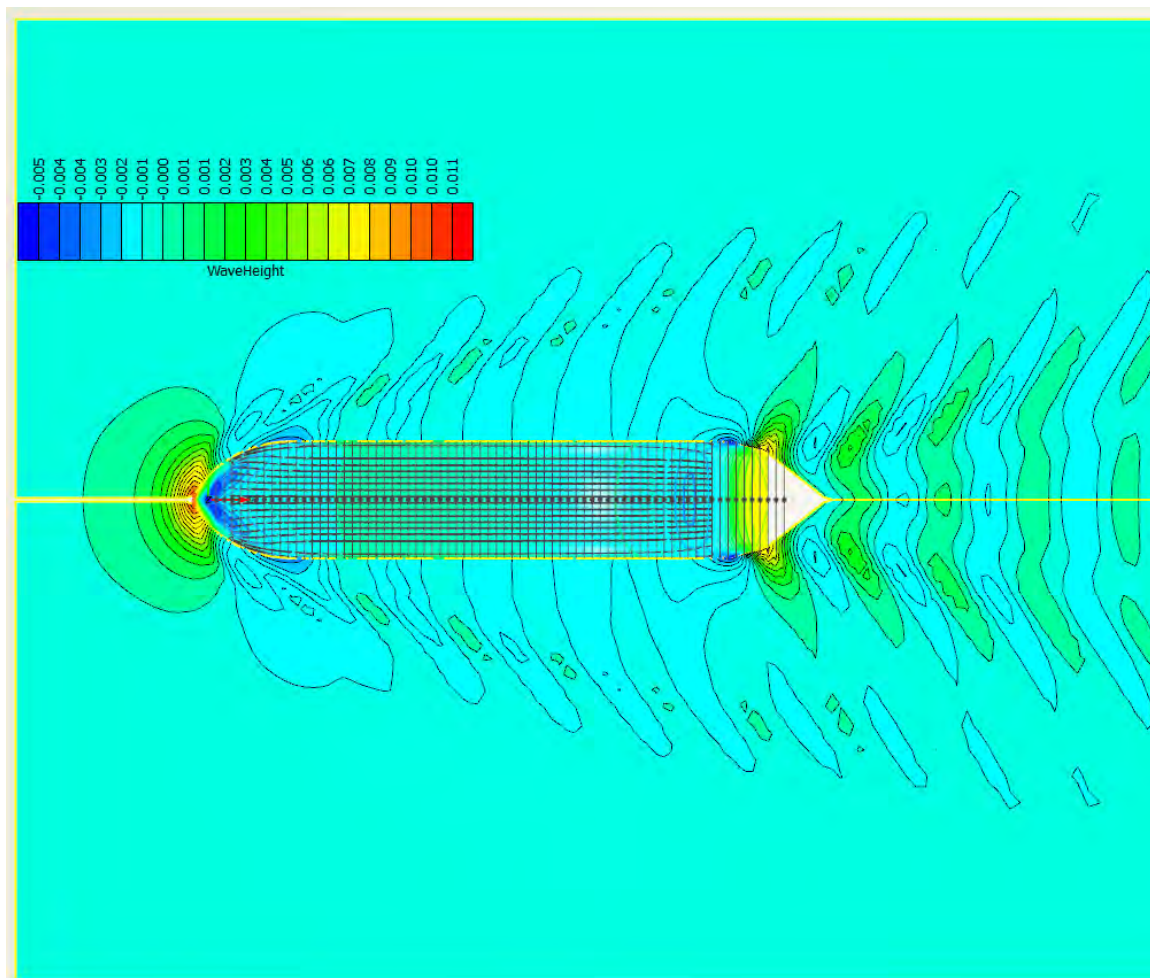


Figure 4.10 (a): Kelvin wave pattern at the speed of 8 knots

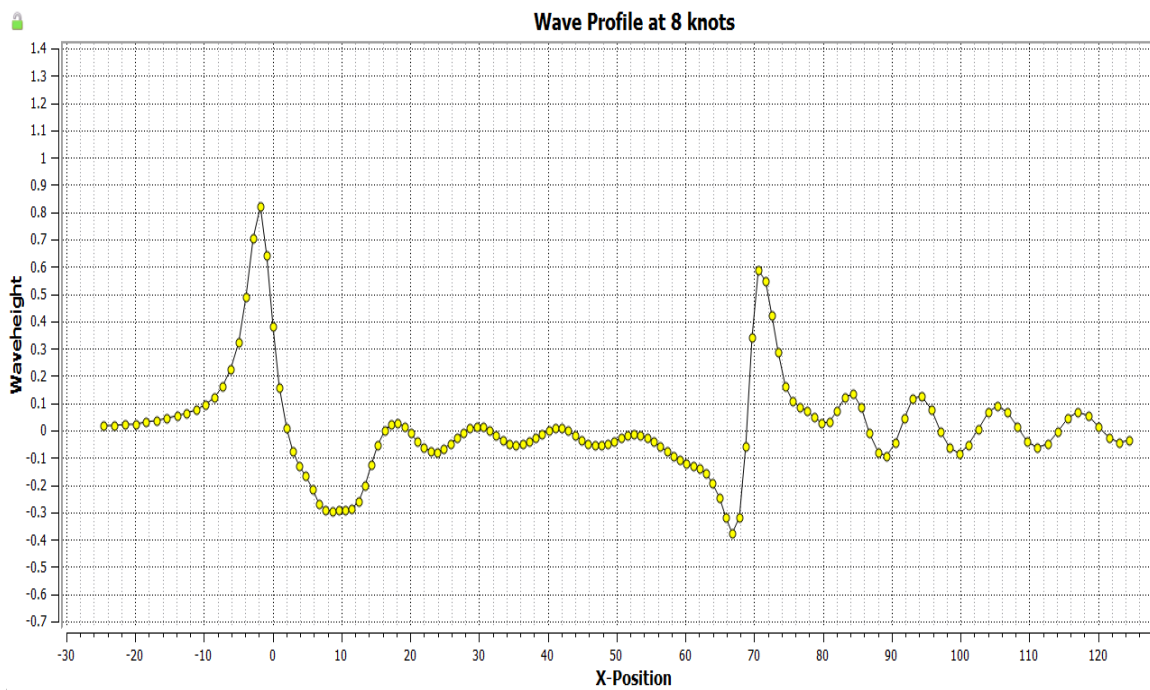


Figure 4.10 (b): Wave profile at the speed of 8 knots (units are meter)

4.2.2 Shallow Water Resistance, Sinkage and Trim

A brief description about shallow water is given in section 2.1.4. Shallow water affects the performance of the ship and decreases the efficiency from economic and hydrodynamic point of view. Operations in shallow water is different from open and deep water, sometimes very dangerous if the effects are not understood properly by the Naval Architects at design stage and Mariners during operation. Bangladesh being riverine country, one of her major transport and communication medium is shipping. The ship owners always want to reduce the fuel consumption to maximize the profit and want to get the best possible output from the installed engine. It is a well-known phenomenon that due to the effects of shallow water, a ship faces different types of problems, such as, increased resistance, squat, grounding, problem in manoeuvring etc.

4.2.2.1 Resistance: According to PIANC (1992) the very shallow, Shallow and medium deep-water resistance is calculated by SHIPFLOW, and the values of the resistance coefficients are given in Table 4.6.

Table 4.6: Shallow Water Resistance Coefficients at various ship speeds

Depth of water, h (m)	Ship Speed (Knot)	Froude Number, Fn	Reynolds number, Rn $\times 10^{-8}$	Resistance Coefficients				Total Resistance, R _T (kN)
				Frictional, C _F $\times 10^3$	Viscous, C _V $\times 10^3$	Wave, C _W $\times 10^3$	Total, C _T $\times 10^3$	
4.56 (Very shallow h/T=1.19)	6	0.116	2.59	2.02	2.48	0.07	2.55	18.04
	7	0.135	3.02	2.01	2.37	0.09	2.46	23.61
	8	0.154	3.45	2.01	2.84	0.22	3.05	38.32
5.69 (Shallow, h/T=1.49)	7	0.135	3.02	1.91	2.51	0.05	2.56	24.58
	8	0.154	3.45	1.90	2.62	0.06	2.68	33.63
	9	0.173	3.89	1.89	2.11	0.20	2.31	36.78
	10	0.192	4.32	1.88	2.66	0.23	2.89	56.65
	11	0.211	4.75	1.89	2.69	6.25	8.94	212.27
	12	0.230	5.18	2.34	4.03	12.38	16.40	463.41
11.39 (Medium deep h/T=2.99)	8	0.154	3.45	1.75	2.39	0.36	2.75	34.57
	9	0.173	3.89	1.73	2.37	1.00	3.37	53.50
	10	0.192	4.32	1.71	2.35	2.35	4.70	92.27
	11	0.211	4.75	1.69	2.35	2.51	4.86	115.37
	12	0.230	5.18	1.68	2.38	6.91	9.29	262.53
	13	0.250	5.61	1.69	2.43	8.43	10.87	360.48
	14	0.269	6.04	1.68	2.45	8.15	10.60	407.68
	15	0.288	6.47	1.72	2.81	15.34	18.15	801.34
	16	0.307	6.91	1.77	3.26	20.80	24.06	1208.64
	17	0.326	7.34	1.76	3.21	18.45	21.66	1228.33

For medium deep water the values of resistance coefficients are plotted in the following Figure 4.11. From this figure, it can be seen that the wave resistance coefficient and total resistance coefficient are increases with the increase of ship speed but the frictional resistance component decreases with the increase of ship speed in between the Froude number range from 0.15 to 0.32.

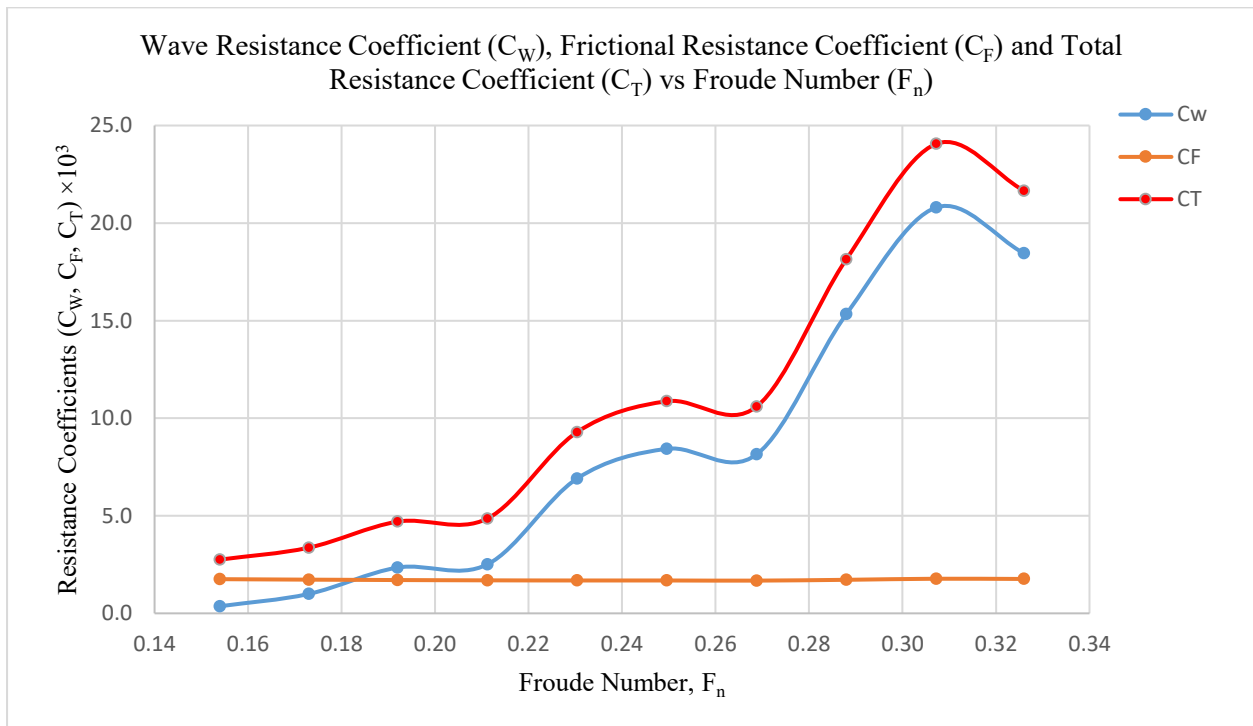


Figure 4.11: Resistance coefficients (C_w , C_f , C_T) at varying Froude numbers for medium deep water

4.2.2.2 Sinkage and Trim: The sinkage and trim values for medium deep, shallow and very shallow water are given in Table 4.7. Figure 4.12 represents the values of Sinkage and Trim at different Froude number for medium deep water. It can be said from Figure 4.6 that the values of sinkage and trim remain constant from Froude number 0.15 to 0.26, but in the range of Froude number 0.26 to 0.33 the sinkage increases where the trim by bow occurs. It is noted that negative sinkage indicates downwards directions from free surface of the ship and positive trim indicates clockwise directions or trim by bow.

Table 4.7: Sinkage and Trim values for medium deep, shallow and very shallow water at various ship speeds

Height, h (m)	Speed, V (Knot)	Froude Number, F_n	Reynolds Number, $R_n \times 10^{-8}$	Sinkage at aft draft (m)	Trim by stern (m)	Even-keel Draft (m)	Aft Draft with sinkage (m)	Aft Draft with sinkage and Trim (m)
11.39 (Medium deep $h/T=2.99$)	8	0.154	3.45	-0.0587	-0.115	3.8	3.859	3.916
	9	0.173	3.89	-0.0713	-0.153	3.8	3.871	3.948
	10	0.192	4.32	-0.0801	-0.196	3.8	3.880	3.978
	11	0.211	4.75	-0.0962	-0.244	3.8	3.896	4.018
	12	0.230	5.18	-0.1704	-0.193	3.8	3.970	4.067
	13	0.250	5.61	-0.2542	-0.149	3.8	4.054	4.129
	14	0.269	6.04	-0.3124	-0.158	3.8	4.112	4.192
	15	0.288	6.47	-0.7813	0.417	3.8	4.581	4.373
	16	0.307	6.91	-1.2628	1.030	3.8	5.063	4.548
	17	0.326	7.34	-1.2633	0.875	3.8	5.063	4.626
5.69 (Shallow, $h/T=1.49$)	7	0.135	3.02	-0.1827	-0.091	3.8	3.983	4.028
	8	0.154	3.45	-0.2518	-0.137	3.8	4.052	4.120
	9	0.173	3.89	-0.3367	-0.225	3.8	4.137	4.249
	10	0.192	4.32	-0.4497	-0.378	3.8	4.250	4.439
	11	0.211	4.75	-0.6124	-0.717	3.8	4.412	4.771
4.56 (Very shallow $h/T=1.19$)	6	0.116	2.59	-0.1872	-0.041	3.8	3.987	4.008
	7	0.135	3.02	-0.2752	-0.065	3.8	4.075	4.107
	8	0.154	3.45	-0.4034	-0.105	3.8	4.203	4.256
	9	0.173	3.89	-0.7350	-0.709	3.8	4.535	4.890

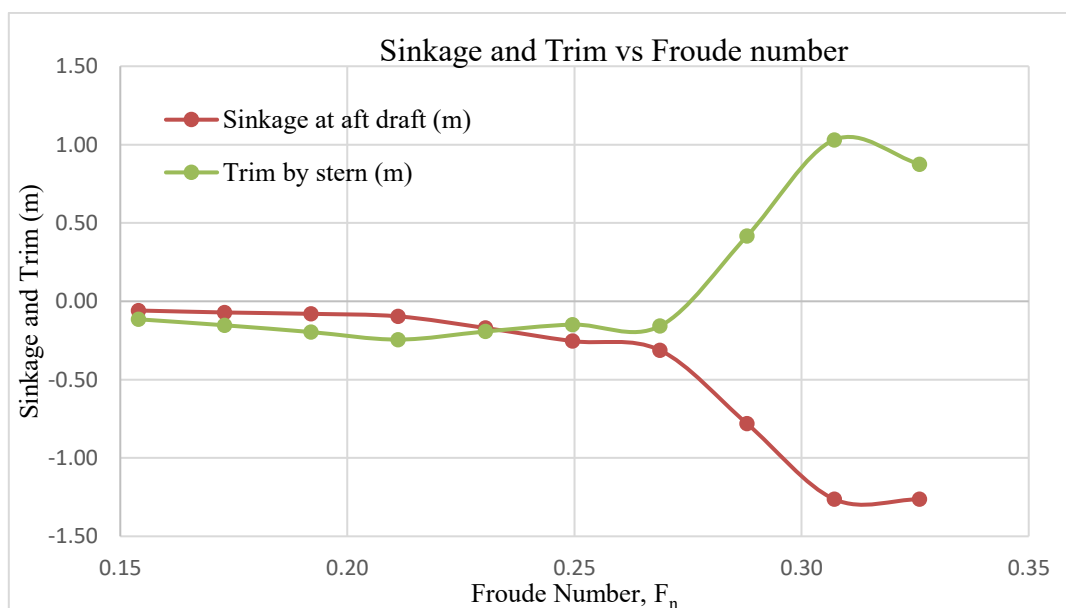


Figure 4.12: Sinkage and Trim at different Froude number for medium deep water

4.2.3 Squat Calculation

When a ship proceeds through water, she pushes water ahead of her. In order not to leave a "hole" in the water, this volume of water pushed ahead of the ship must return down the sides and under the keel of the ship. The streamlines of return flow are speeded up under the ship. This causes drop in pressure according to the Bernoulli's theorem, resulting in the ship dropping vertically in the water. As well as dropping vertically, the ship trims fore and aft. The overall decrease in the underkeel clearance fore or aft is called **ship squat**. **Squat** is the decrease in underkeel clearance caused by the forward motion of a ship in shallow water (Svetak, 2001). In this thesis, for 158 container ship, the shallow water sinkage and the deep water sinkage is calculated by the SHIPFLOW software. The values of squat are determined by subtracting the deep water sinkage values from shallow water sinkage. For validation of squat, the present squat is compared with the maximum squat. Where

$$\text{Maximum Squat, } \delta_{max} = \frac{C_B \times V_k^2}{100} \text{ metres (Barrass, Ship Squat, 1999)}$$

The comparison of the present value of squat with the maximum value of squat is given in the Table 4.8 and plotted in Figure 4.13. It is seen that the present value of squat is lower than the maximum standard value given by Barrass (Ship Squat, 1999).

Table 4.8: Squat calculation data

Water depth, h (m)	Ship Speed, V_k (knot)	Block Coefficient, C_B	Maximum Squat, (m)	Shallow Water Sinkage, (m)	Deep Water Sinkage, (m)	Present Squat, (m)
5.6999999 (Shallow, $h/T=1.49999$)	7	0.843	0.41307	0.1827	0.0432	0.1395
	8	0.843	0.53952	0.2518	0.0722	0.1796
	9	0.843	0.68283	0.3367	0.0918	0.2449
	10	0.843	0.84300	0.4497	0.1137	0.3360
	11	0.843	1.02003	0.6124	0.1365	0.4759



Figure 4.13: Squat at different ship speeds

4.3 Case Study 3: Investigation of the Dhaka Chittagong Route for the Container Ship

According to Bangladesh Inland Water Transport Authority (BIWTA), Bangladesh has about 24,000 km. of rivers, streams and canals that together cover about 7% of the country's surface. Most part of the country is linked by a complex network of waterways which reaches its extensive size in the monsoon period. Out of 24,000 km. of rivers, streams and canals only about 5,995 km. is navigable by mechanized vessels during monsoon period which shrinks to about 3,865km. during dry period (BIWTA, 2018). The waterways of Bangladesh have been classified into four categories depending on Least Available Depth (LAD) ranging from 3.66 m to 1.52m that is given in Table 4.9.

Table 4.9: Status of Inland Waterways of Bangladesh

Name of Route	Minimum Depth	Length of Route and Percentage	Minimum Vertical Clearance	Minimum Horizontal Clearance
Class- I	3.66 m	683 kilometers (11.39%)	18.30 m	76.22 m
Class- II	2.13 m	1027 kilometers (17.13%)	12.20 m	76.22 m
Class -III	1.52 m	1885 kilometers (31.44%)	7.62 m	30.48 m
Class -IV	Less than 1.52 m	2400 kilometers (40.04%)	5.00 m	20.00 m
Total		5995 kilometers (100%)		

The inland waterways of Bangladesh can be seen from Figure 4.14. In this figure, the red coloured rectangle carries the magenta coloured line that indicates the DC waterway and it is enlarged for clear view in Figure 4.15. In this figure it is seen that the magenta coloured line for DC waterway starts from Dhaka and ends to Chittagong via Chandpur, Ilishaghat, Bhola, Hatia channel and Sandwip channel. The route of the 158 TEU container ship from Pangaon inland container terminal, Dhaka to Chittagong port container terminal is clearly seen from Figure 4.16, which is Class-I route, where the minimum depth of water is 3.66m (from Table 4.9).

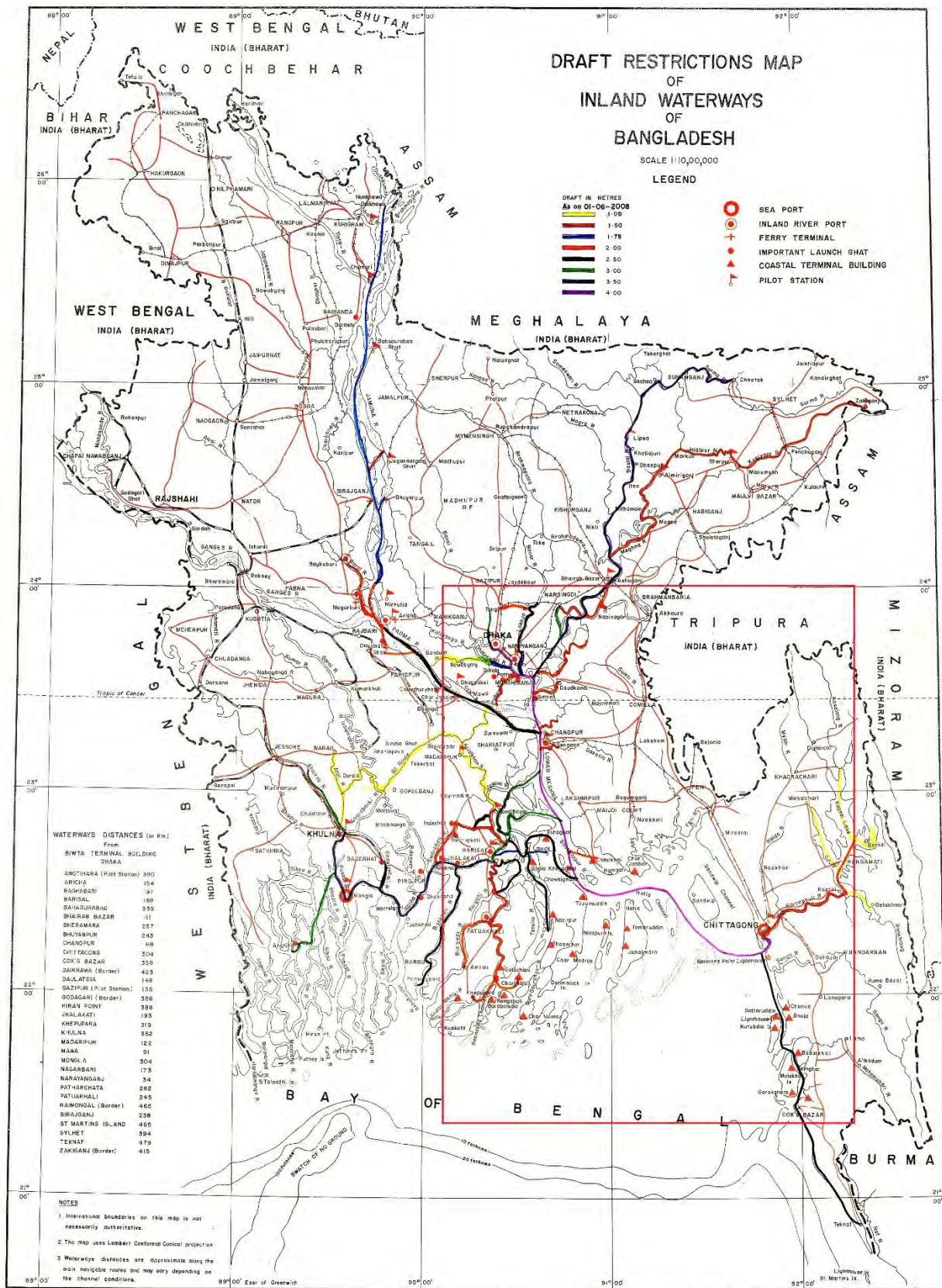


Figure 4.14: The map for inland waterways of Bangladesh

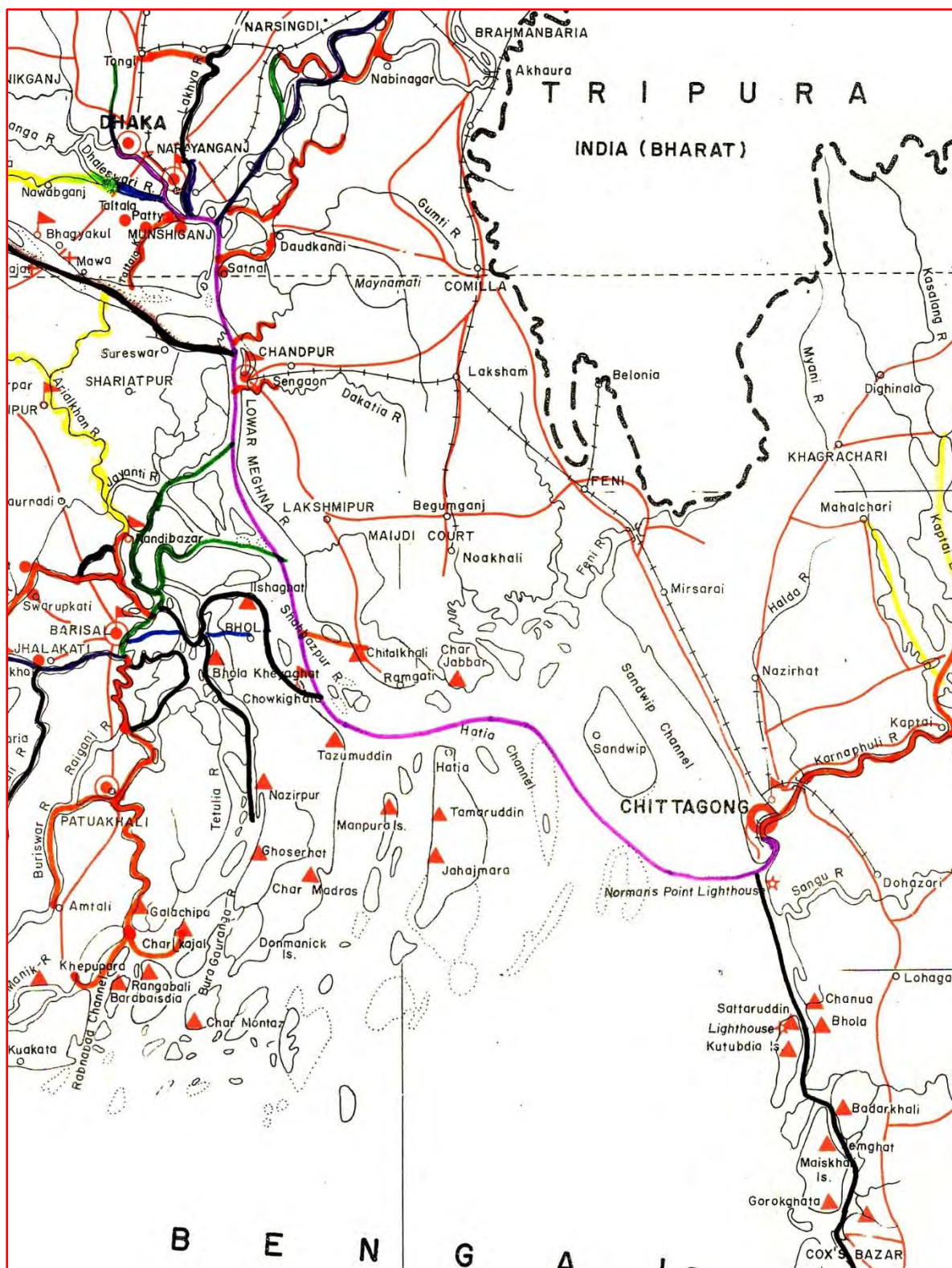


Figure 4.15: Dhaka to Chittagong waterway (magenta colored line)

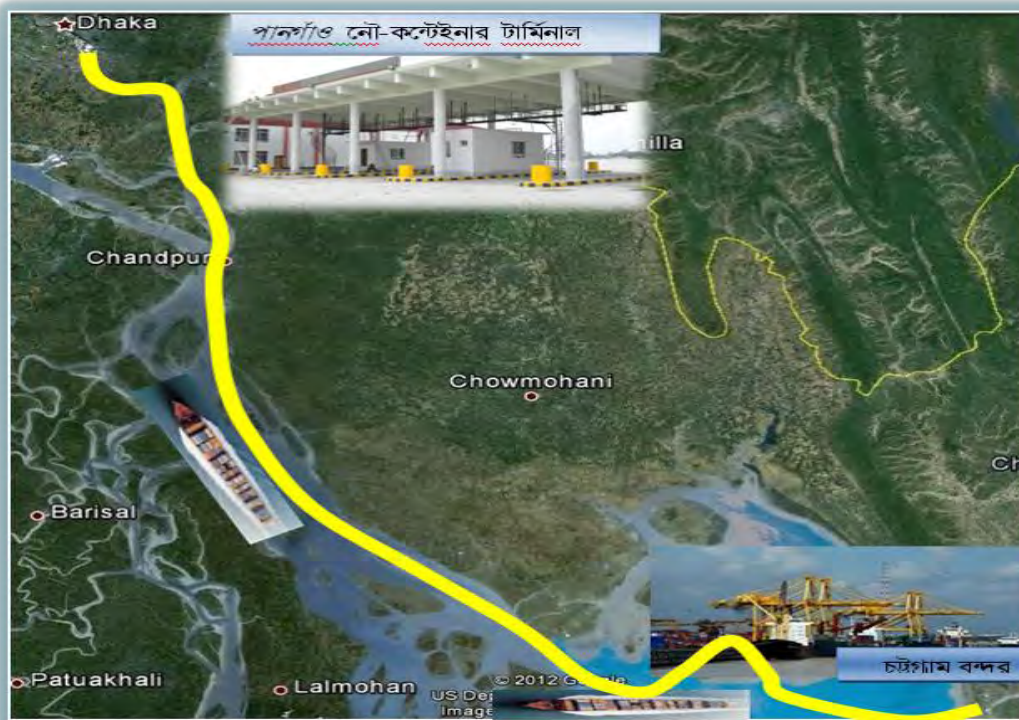


Figure 4.16: Waterway from Pangaon inland container terminal, Dhaka to Chittagong port container terminal

The Hydrographic Chart Index for the Dhaka-Chittagong route is shown in Figure 4.17.

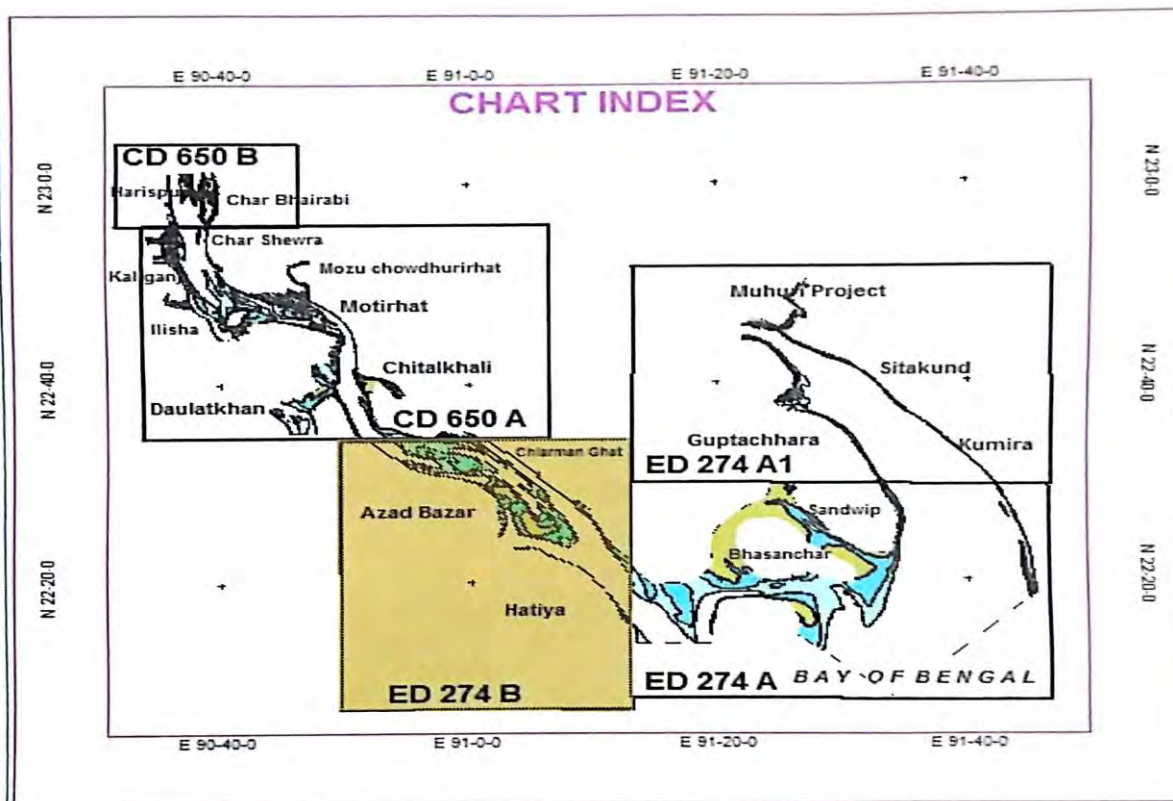


Figure 4.17: Hydrographic Chart Index for Dhaka-Chittagong route (BIWTA Hydrographic Chart, 2018)

From the Hydrographic Charts of February, 2018 which are collected from the Hydrography department of BIWTA, it is seen that the water depths in three places in this route are too small, the values are given in Table 4.10 and the charts can be seen from Figures 4.18, 4.19 and 4.20.

Table 4.10: Minimum depth of the shallow water regions in Dhaka-Chittagong waterway

SN	Name of Place	Nearest place	District	Minimum depth of water (m)	Reference
1.	Ilisha	Ramdaspur	Bhola	3.0	Figure 4.18
2.	Chairman Ghat	Hatia	Feni	3.3	Figure 4.19
3.	Bhasanchar	Sandwip Channel	Chittagong	3.2	Figure 4.20

In these hydrographic charts the navigable path of the ship is indicated by red coloured line in the white spaces, the sky (light) blue coloured spaces means very shallow water and both the navy (deep) blue and green coloured spaces indicates the restriction of navigable path. These are summarised in Table 4.11.

Table 4.11: Description of various colours in Hydrographic charts

SN	Name of Coloured spaces	Water depth (m)	Navigable
1.	White	Greater than 3.66	Yes
2.	Sky (light) blue	Less than 3.66	Blockage
3.	Navy (deep) blue	Less than 2.0	No
4.	Green	Less than 1.0	No

So, in hydrographic charts the red coloured circles on sky blue spaces means the blockage for the navigable path of the ship. During crossing the blockage following points should be checked under close observation:

- ❖ The even keel draft of the container ship is 3.8 metre. So, from Table 4.10, in these places this ship cannot run even in the low-tide time. Because from the Tide-Tables (BTT, 2018) in Ilisha near Char Ramdaspur the height of low-tide is reduced to only 0.36 metre in the date of 04 March, 2018 at 01:53 pm, this can be seen from Figure 4.21. And the minimum depth of water in Ilisha region is only 3.0 metre which can be seen from Figure 4.18. So, the ship must wait for high tide to avoid grounding because

$3.0 + 0.36 = 3.36$ metre which is less than 3.8 metre.

- ❖ Another study is that in Ilisha region from the tide table Figure 4.21, in 11 March, 2018 the minimum height of high tide is occurred at 01:35 pm which is only 1.47 metre. Then the total depth of water in that case is $3.0 + 1.47 = 4.47$ metre. So, in order to avoid grounding the ship must reduce her speed to 7 knots. Because from Table 4.7, it is seen that in very shallow water the aft draft of the ship increases with speed for the sinkage and trim effects. In the speed of 9 knots the dynamic aft draft is 4.89 metre, in 8 knots the dynamic aft draft is 4.26 metre and in 7 knots the dynamic aft draft is 4.11 metre. So, keeping the safety limit $4.47 - 4.11 = 0.36$ metre, 7 knots speed may be the maximum limit.
- ❖ The minimum water depth in Chariman Ghat near Hatia is 3.3 metre, from Figure 4.19, which is a restriction for the ship to run, but in high-tide the ship can run easily. Again, the minimum depth of water in Bhasanchar near Sandwip Channel is only 3.2 metre, Figure 4.20, and in the time of high-tide the minimum increase of water depth is 3.76 metre in 11 March, 2018 at 08:58 am, Figure 4.22. Therefore, the total depth of water is $3.2 + 3.76 = 6.96$ metre. So, no problem to run for the ship in high-tide upto her design speed 10 knots. But in the time of low-tide the ship can't run in this area without the help of Table 4.7.

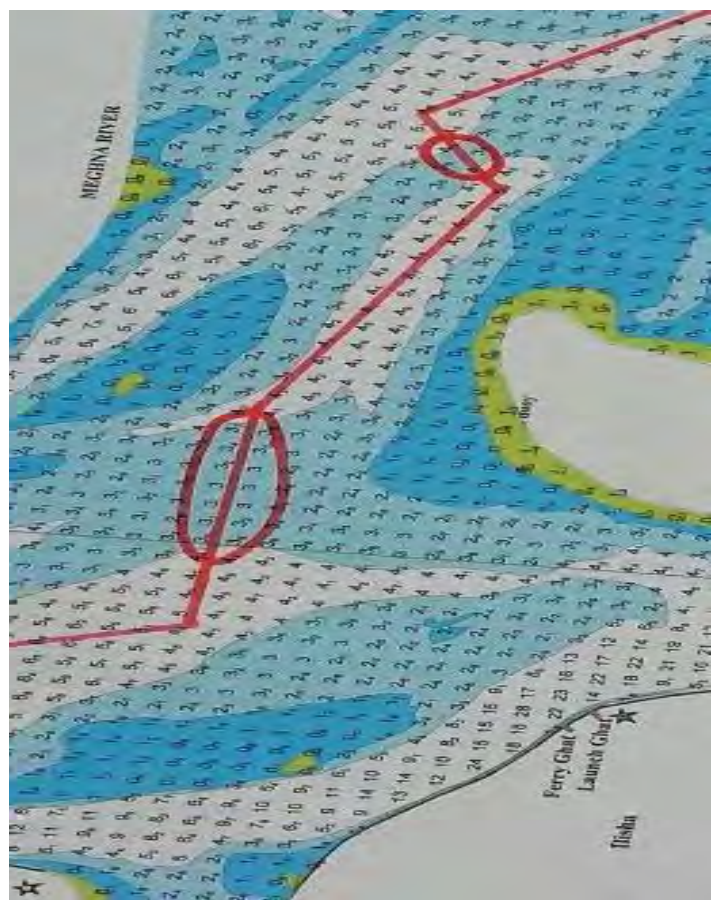
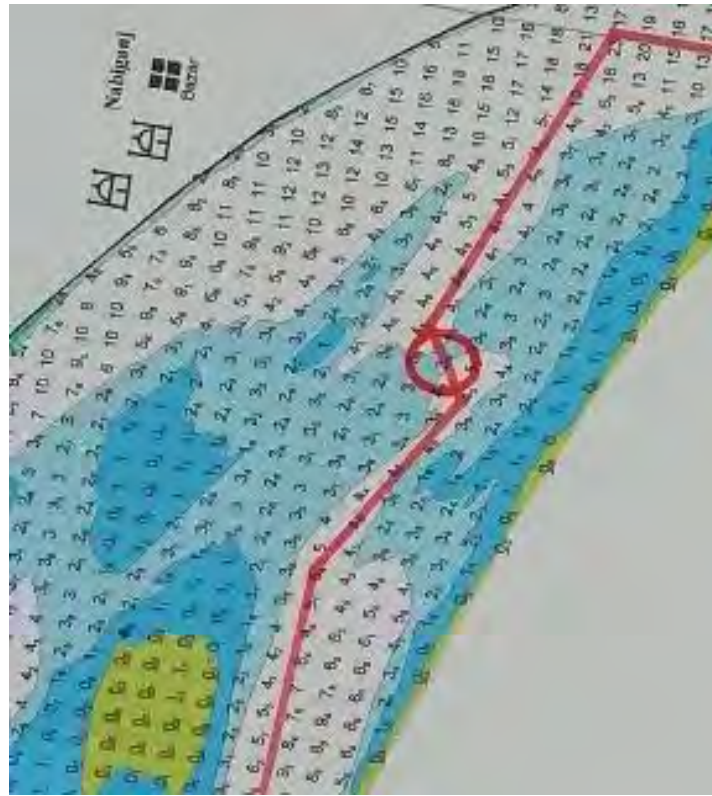
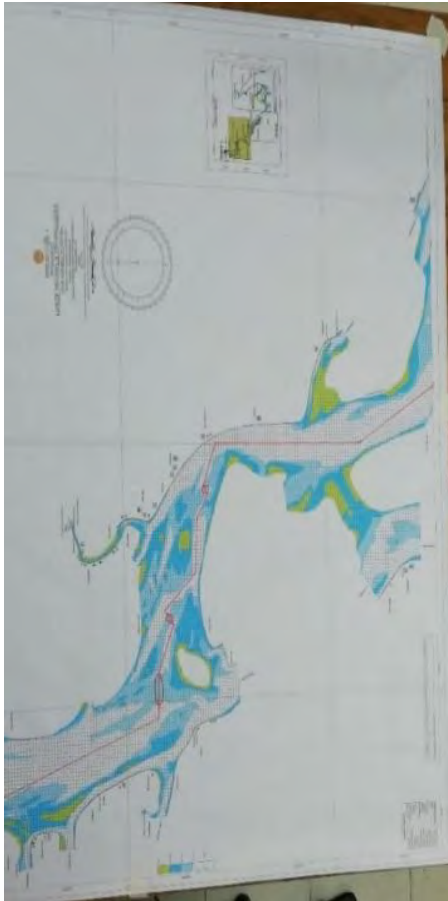


Figure 4.18: Enlarged figure of Hydrographic Chart CD 650 A (Ilisha region)

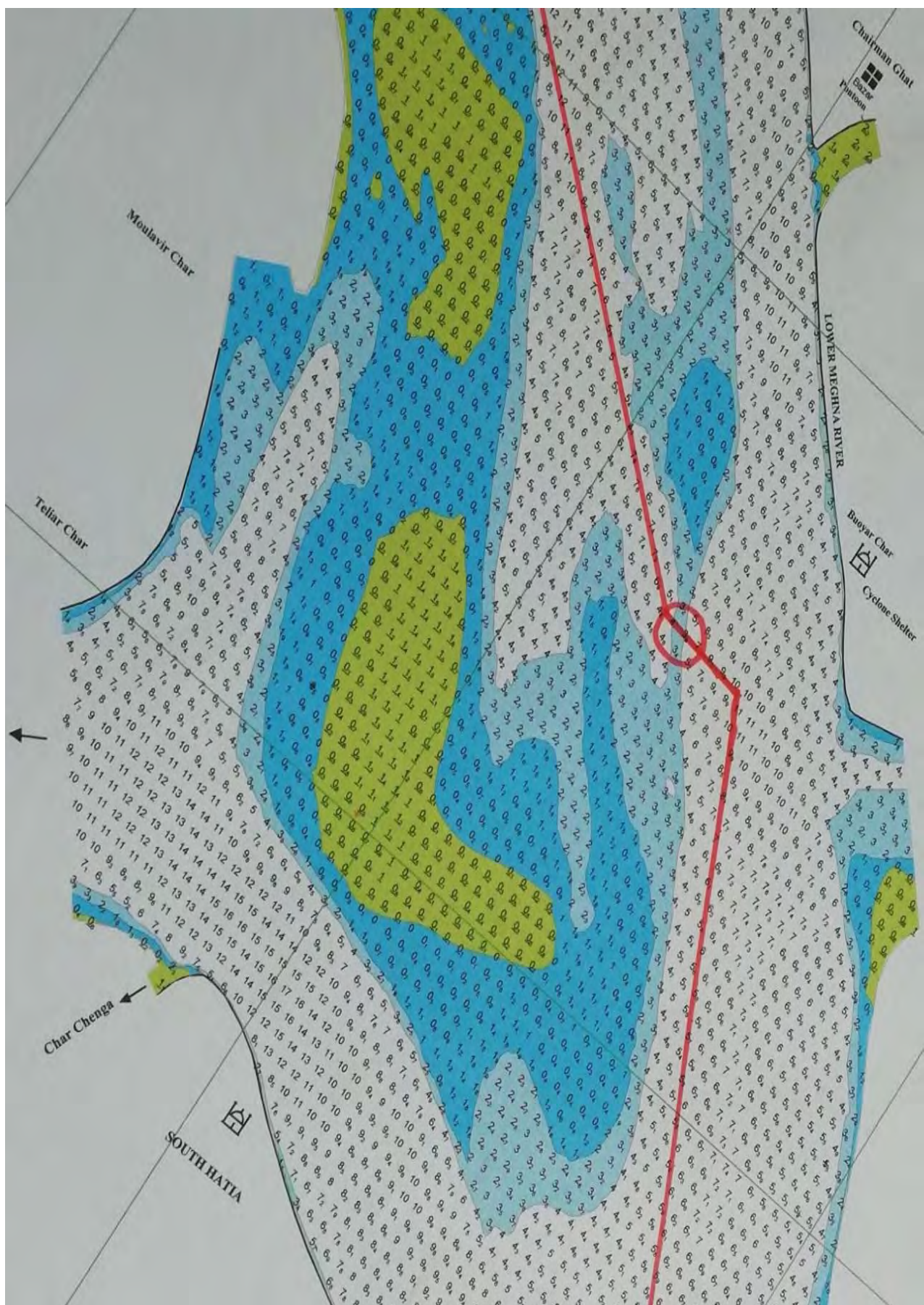


Figure 4.19: Enlarged figure of Hydrographic Chart ED 274 B (Chairman Ghat region)

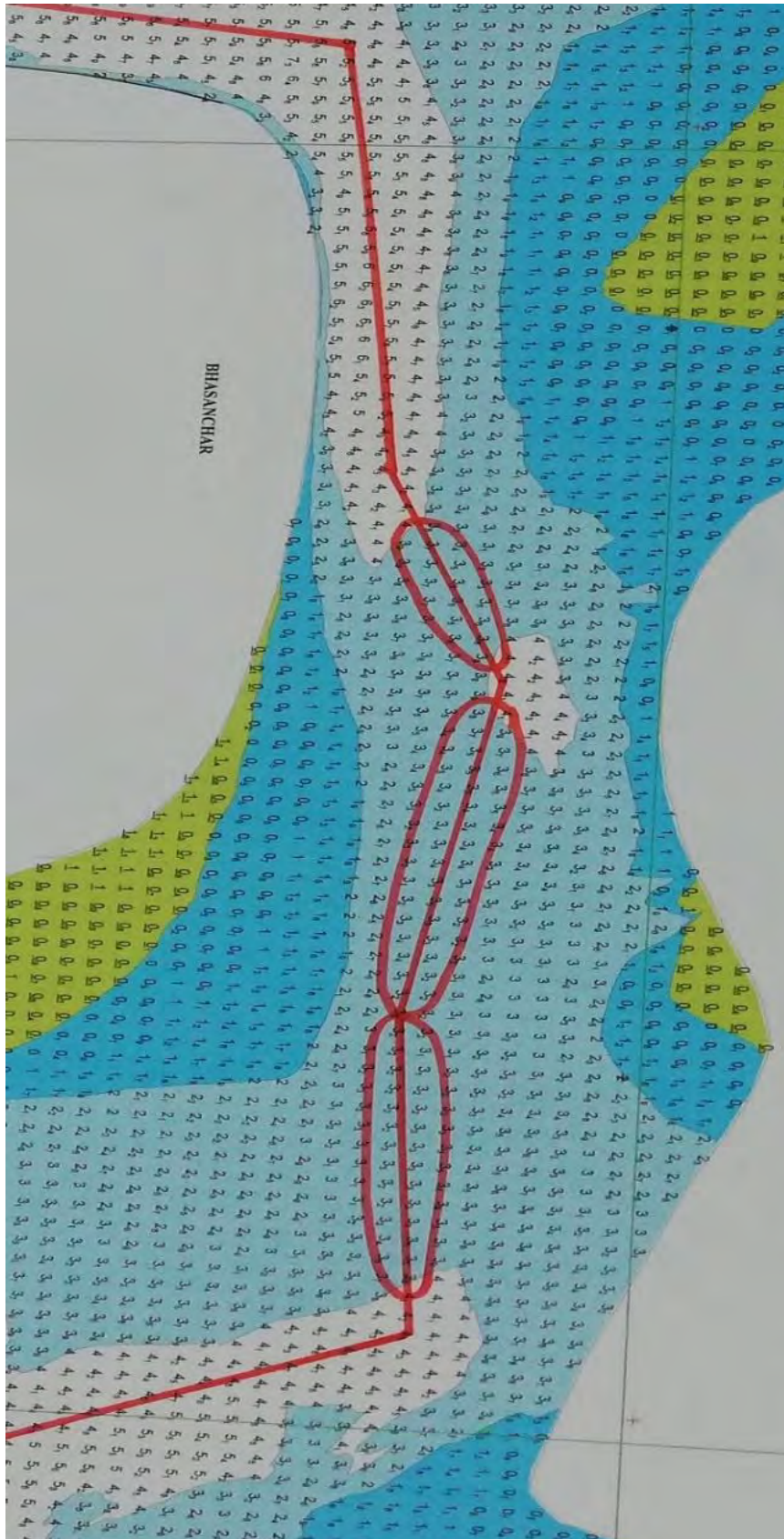


Figure 4.20: Enlarged figure of Hydrographic Chart ED 274 A (Bhasanchar region)

MEGHNA RIVER — CHAR RAMDASPUR									
MARCH						APRIL			
Time	Ht.m	Time	Ht.m	Time	Ht.m	Time	Ht.m	Time	
1	0411 2.49	12	0208 1.68	23	0334 0.64	1	0034 0.58	12	0248 2.20
Th	1201 0.43	Mo	0835 0.77	Fr	0817 2.40	Su	0505 2.86	Th	0953 0.88
	1631 2.38		1434 1.56		1546 0.68		1251 0.57		1512 2.23
			2054 0.73		2045 2.33		1720 2.94		2211 0.90
2	0015 0.45	13	0251 1.82	24	0427 0.74	2	0109 0.58	13	0322 2.41
Fr	0448 2.67	Tu	0944 0.71	Sa	0914 2.13	Mo	0540 2.89	Fr	1036 0.81
	1240 0.39		1516 1.73		1642 0.77		1324 0.60		1539 2.48
	1707 2.57		2156 0.68		2155 2.09		1756 2.96		2254 0.83
3	0054 0.42	14	0327 2.01	25	0539 0.83	3	0143 0.59	14	0351 2.60
Sa	0525 2.78	We	1038 0.63	Su	1031 1.86	Tu	0616 2.84	Sa	1114 0.76
	1317 0.37		1550 1.94		1810 0.86		1358 0.64		1604 2.71
	1743 2.68		2248 0.62		2345 1.94		1833 2.86		2333 0.77
4	0131 0.41	15	0359 2.23	26	0720 0.86	4	0218 0.62	15	0418 2.76
Su	0602 2.79	Th	1119 0.57	Mo	1252 1.76	We	0654 2.70	Su	1150 0.74
	1353 0.36		1619 2.17		1957 0.84		1432 0.70		1629 2.89
	1820 2.70		2329 0.58				1912 2.68		2200 0.86
5	0208 0.41	16	0428 2.43	27	0135 2.00	5	0255 0.68	16	0009 0.73
Mo	0640 2.71	Fr	1154 0.53	Tu	0851 0.78	Th	0733 2.49	Mo	0444 2.88
	1429 0.37		1643 2.38		1413 1.91		1508 0.78		1223 0.75
	1859 2.61				2118 0.76		1954 2.44		1657 3.03
6	0246 0.44	17	0005 0.54	28	0233 2.18	6	0336 0.78	17	0043 0.72
Tu	0720 2.54	Sa	0455 2.59	We	1001 0.67	Fr	0816 2.23	Tu	0513 2.97
	1506 0.42		1226 0.50		1501 2.14		1549 0.87		1256 0.79
	1941 2.43		1706 2.56		2223 0.67		2042 2.19		1728 3.11
7	0326 0.49	18	0038 0.52	29	0317 2.39	7	0422 0.88	18	0118 0.74
We	0803 2.31	Su	0519 2.70	Th	1055 0.59	Sa	0905 1.96	We	0547 3.00
	1546 0.49		1256 0.50		1538 2.39		1636 0.96		1329 0.85
	2028 2.18		1730 2.70		2314 0.61		2146 1.96		1804 3.12
8	0409 0.57	19	0109 0.51	30	0355 2.59	8	0518 0.98	19	0154 0.80
Th	0851 2.04	Mo	0544 2.77	Fr	1138 0.55	Su	1018 1.73	Th	0625 2.96
	1628 0.58		1326 0.51		1612 2.63		1739 1.03		1404 0.91
	2124 1.93		1757 2.78		2357 0.59		2338 1.83		1844 3.04
9	0458 0.67	20	0140 0.51	31	0430 2.75	9	0633 1.04	20	0235 0.87
Fr	0945 1.78	Tu	0614 2.79	Sa	1216 0.55	Mo	1254 1.67	Fr	0708 2.82
	1717 0.68		1356 0.53		1646 2.82		1902 1.06		1445 0.97
	2252 1.70		1829 2.79						1932 2.86
10	0558 0.76	21	0213 0.53			10	0113 1.86	21	0322 0.94
Sa	1108 1.54	We	0648 2.75			Tu	0758 1.02	Sa	0759 2.58
	1821 0.75		1428 0.57				1400 1.78		1536 1.03
			1906 2.72				2019 1.03		2030 2.61
11	0106 1.62	22	0251 0.57			11	0208 2.00	22	0421 1.00
Su	0715 0.80	Th	0729 2.61			We	0902 0.95	Su	0903 2.30
	1335 1.47		1504 0.61				1441 1.99		1643 1.08
	1941 0.77		1951 2.56				2120 0.97		2149 2.36

Figure 4.21: Bangladesh Tide Tables, 2018 for Ilisha region (Meghna River, Char Ramdaspur)

SATAL KHAL — SANDWIP											
MARCH						APRIL					
	Time	Ht.m		Time	Ht.m		Time	Ht.m		Time	Ht.m
1	0040	5.60	12	0406	1.60	23	0453	5.20	1	0143	6.16
Th	0744	0.48	Mo	1012	3.89	Fr	1155	0.77	Su	0846	0.30
	1301	5.40		1625	1.72		1719	5.32		1400	6.12
	2000	0.44		2236	4.40					2101	0.19
										2334	5.16
2	0121	5.93	13	0512	1.47	24	0034	0.89	2	0220	6.18
Fr	0828	0.29	Tu	1107	4.19	Sa	0548	4.72	Mo	0921	0.23
	1341	5.70		1730	1.52		1246	1.10		1436	6.15
	2042	0.23		2325	4.72		1821	4.91		2137	0.15
3	0201	6.15	14	0608	1.25	25	0137	1.19	3	0257	6.05
Sa	0907	0.15	We	1151	4.57	Su	0702	4.27	Tu	0956	0.25
	1420	5.89		1825	1.21		1353	1.43		1514	6.04
	2120	0.10					1950	4.59		2213	0.23
4	0240	6.21	15	0007	5.09	26	0254	1.39	4	0334	5.78
Su	0945	0.09	Th	0655	0.99	Mo	0847	4.09	We	1030	0.38
	1458	5.94		1229	4.96		1518	1.60		1552	5.80
	2158	0.06		1911	0.89		2130	4.62		2251	0.42
5	0319	6.09	16	0045	5.45	27	0417	1.37	5	0413	5.39
Mo	1022	0.11	Fr	0736	0.73	Tu	1013	4.34	Th	1106	0.63
	1538	5.83		1303	5.32		1645	1.50		1632	5.47
	2237	0.12		1951	0.61		2241	4.93		2332	0.73
6	0400	5.78	17	0120	5.76	28	0535	1.17	6	0453	4.95
Tu	1100	0.24	Sa	0814	0.52	We	1114	4.76	Fr	1143	0.97
	1619	5.57		1336	5.62		1801	1.20		1715	5.11
	2318	0.30		2028	0.39		2337	5.32			
7	0442	5.33	18	0152	5.97	29	0639	0.89	7	0015	1.10
We	1140	0.49	Su	0850	0.37	Th	1203	5.21	Sa	0538	4.50
	1704	5.21		1407	5.84		1859	0.85		1223	1.36
				2103	0.25					1803	4.74
8	0002	0.59	19	0223	6.07	30	0023	5.69	8	0105	1.45
Th	0530	4.81	Mo	0925	0.29	Fr	0728	0.63	Su	0634	4.10
	1222	0.82		1438	5.96		1245	5.62		1313	1.71
	1755	4.81		2139	0.19		1945	0.54		1909	4.43
9	0051	0.95	20	0255	6.04	31	0104	5.98	9	0203	1.72
Fr	0624	4.31	Tu	0959	0.28	Sa	0809	0.43	Mo	0758	3.86
	1308	1.20		1511	5.98		1323	5.93		1417	1.94
	1855	4.44		2216	0.22		2024	0.32		2036	4.32
10	0147	1.31	21	0329	5.88				10	0309	1.82
Sa	0733	3.92	We	1035	0.35				Tu	0926	3.94
	1403	1.55		1547	5.88					1531	1.97
	2011	4.19		2257	0.36					2151	4.47
11	0253	1.55	22	0408	5.60				11	0419	1.74
Su	0858	3.76	Th	1113	0.51				We	1029	4.26
	1512	1.75		1629	5.65					1644	1.78
	2133	4.18		2342	0.59					2248	4.78
										1806	5.18

Figure 4.22: Bangladesh Tide Tables, 2018 (Satal Khal, Sandhip)

Chapter 5

Conclusions and Future Works

5.1 Conclusions

In this thesis, a commercial popular Computational Fluid Dynamics (CFD) modelling software SHIPFLOW has been used to predict the flow around a benchmark KCS hull and a 158 TEU container ship. The KRISO Container Ship (KCS) hull is used to check the validity of the SHIPFLOW CFD code. On the other hand, the 158 TEU container ship hull is used to predict the hydrodynamic performances such as resistance, sinkage, trim and other values. Based on the predicted results and discussions following conclusions can be drawn:

- 1) From the Verification and Validation (V&V) study of total resistance coefficients for KCS hull, it is observed that when grid density is changed from coarse grids to finer grids, CFD predictions get closer to EFD results and after finding the validation uncertainty it is seen that simulation results are valid.
- 2) It is seen that from the simulation results, the shape of the graph of Wave Resistance Coefficient (C_W) and Frictional Resistance Coefficient (C_F) against Froude number follows the standard pattern.
- 3) The values of total Resistance calculated in SHIPFLOW are slightly lower than the experimental results in different range of speed. At the speed of 8 knot the calculated value is 48.2 kN and the experimental value is 49.7 kN, so the error is about 3%.
- 4) From the values of sinkage and trim, it is found that the sinkage is less than 5% of the draft and the absolute trim angle remains small (less than 1°) for various ship speed.
- 5) The successful squat calculation of SHIPFLOW gives the lower value of squat against the maximum standard value.
- 6) The values of WaveHeight increases with the speed of the ship which is seen from Kelvin wave patterns and wave profiles.
- 7) In the initial design stage, we can use the SHIPFLOW software to predict the resistance, sinkage and trim of a ship where the experimental results are costly and time consuming.

- 8) For 158 TEU container ship with draft 3.8 meter, three regions are found from the hydrographic charts of BIWTA where the depth of water is less than 3.8 meter. These very shallow water regions are Ilisha, Chairman Ghat and Bhasanchar.
- 9) To avoid grounding in those three regions, the ship must wait for high-tide and the speed of the ship must be reduced to a prescribed limit, for the effect of sinkage and trim on shallow water, that is given in Table 4.7.

5.2 Future Works

The following statements are given based on the work carried out in this thesis. These recommendations indicate guidelines for further exploring the results of CFD codes.

- 1) It is imperative to note that only the container ship have been checked in this instance, which implies that the range could be further enlarged and more rigorous validation is required against experimental results for many other ships.
- 2) Only the bare hull resistance is predicted in this thesis, if the appendages such as rudder and propeller can be included in mesh generation a more complete picture on the overall forces on the ship could be found.
- 3) The investigation of Dhaka-Chittagong waterway is done only from the hydrographic chart of February, 2018 and Tide Tables, 2018. So, a continuous investigation is required as the water depth is continuously changing.
- 4) For the dangerous three very shallow water regions in Dhaka-Chittagong waterway, capital dredging is urgently necessary as the normal dredging process is hampered by the heavy current specially in Bhasanchar region.

References

- Azcueta R. (2002), RANSE simulations for sailing yachts including dynamic sinkage and trim and unsteady motions in waves, High Performance Yacht Design Conference, Auckland.
- Ahmed, M. (2012), Transportation of export-import containers through inland waterways; Challenges & Opportunities, Shipwrights Bangladesh Limited.
- Bessho M. and Sakuma S. (1992), Trim and sinkage of two-dimensional shallow draft ships, Journal of the Kansai Society of Naval Architects, Japan, No.218.
- Barrass, D.C.B., and Derrett, C.D.R. (1999), "Ship Stability for Masters and Mates", 5th edition, Chapter 15, Trim, p-133.
- Barrass, D.C.B., and Derrett, C.D.R., Ship Squat (1999), "Ship Stability for Masters and Mates", 5th edition, Chapter 31, p-281.
- Bertram, V. (2000), Practical Ship Hydrodynamics, Oxford: Butterworth-Heinemann.
- Broberg, L., B. Regnstrom, and M. Ostberg (2007), SHIPFLOW Theoretical Manual, FLOWTECH International AB, Gothenburg, Sweden.
- Bartesaghi, S., and Viola, I. M. (2008), Hull Resistance and Wave Pattern Computation with RANS Technique on a Simplified Experimental Benchmark.
- Bangladesh Inland Water Transport Authority (BIWTA), [URL:http://www.biwta.gov.bd/](http://www.biwta.gov.bd/) accessed on 14 October 2018.
- Bangladesh Tide Tables (BTT) (2018), pp. 43-48 and 55-60, Department of Hydrography, BIWTA, 141-143 Motijheel Commercial Area, Dhaka, Bangladesh.
- BIWTA Hydrographic Chart (2018), Dhaka to Chittagong waterway charts, Department of Hydrography, BIWTA, 141-143 Motijheel Commercial Area, Dhaka, Bangladesh.
- Chowdhury, A.R.M.M, Kishi, Kunihiro and Satoh, Keiichi. (2002), An analysis of Container Trains Systems from Dhaka to Chittagong in Bangladesh. Japan Society of Civil Engineers.
- Doust, D. J., & O'Brien, T. P. (1959), Resistance and propulsion of trawlers, Trans. NECI Transactions, 75.
- Dagkinis, I., Nikitakos, N. (2015), "Slow Steaming Options Investigation Using Multi Criteria Decision Analysis Method", June 2015, Department of Shipping, Trade and Transport, University of Aegean, Greece.
- Froude., W. (1810-1879), Observations and suggestions on the subject of determining by experiment the resistance of ships", The Papers of William Froude, Royal Institution of Naval Architects.

Flowtech Int. (2010), SHIPFLOW User Manual. Gothenburg: FLOWTECH International AB.

Flowtech Int., XCHAP Theoretical Manual (2010), Gothenburg, FLOWTECH International AB.

Gourlay T.P. and Tuck E.O. (2001), The maximum sinkage of a ship. – Journal of Ship Research, vol.45, No.1, pp.50-58.

Guo, B. J., Deng, G. B., and Steen, S. (2013), Verification and Validation Of Numerical Calculation of Ship Resistance and Flow Field of a Large Tanker, Ships and Offshore Structures vol. 8, no. 1, pp. 3-14.

Havelock, T. H. (1908), The propagation of groups of waves in dispersive media with application to waves on water produced by a travelling disturbance, Proceedings of the Royal Society, London, Vol. 81.

Holtrop, J., & Mennen, G. G. J. (1978), A statistical power prediction method. International Shipbuilding Progress, 25, 253.

Harvald Sv. Aa. (1983), “Resistance and Propulsion of Ships”, A wiley-interscience publication, Chapter 4, pp (42-45).

Han, K. (2008), Numerical optimization of hull/ propeller/rudder interaction, Doctoral thesis, Shipping and Marine Technology, Chalmers University of Technology, Gothenburg, Sweden.

Habib, M. Z, Noor, A. U (2016), “Prospects of Inland Waterways for Freight Traffic Movement along Dhaka-Chittagong Corridor and Constraint Analysis of Full Operation of the Pangaon Inland Container Terminal (Pict)”, Proceedings of the 3rd International Conference on Civil Engineering for Sustainable Development (ICCESD 2016), 12~14 February 2016, KUET, Khulna, Bangladesh.

International Towing Tank Conference (ITTC), (1999), Recommended procedures and guidelines, 7.5-03-02-01, CFD, Resistance and Flow, Uncertainty analysis in CFD Examples for Resistance and Flow.

International Towing Tank Conference (ITTC), (2011), “The Specialist Committee on Computational Fluid Dynamics,” in Proceedings of 26th ITTC – Volume II, 2011.

Jones, D. A., and Clarke., D. B. (2010), Fluent Code Simulation of Flow around a Naval Hull: the DTMB 5415, Maritime Platforms Division, Defense Science and Technology Organization, DSTO-TR-2465.

Kelvin, L. (1905), Deep sea ship waves, Proceedings of Royal Society Edinburgh, No. 5.

Korkmaz, K.B. (2015), CFD predictions of resistance and propulsion for the JAPAN Bulk Carrier (JBC) with and without an energy saving device, Master’s Thesis, Department of Shipping and Marine Technology, Division of Marine Technology, CHALMERS University of Technology, Gothenburg, Sweden.

Larsson, L., and Janson, C. (1996), "A Method for the Optimization of Ship Hulls from a Resistance Point of View", Presented at 21st Symposium on Naval Hydrodynamics, June 24-28, 1996, Trondheim, Norway.

Larsson, L., & Raven, H. (2004), *Ship Resistance and Flow*. Gothenburg and Wageningen: Chalmers University of Technology, Gothenburg, Sweden.

Larsson, L., and Raven, H., C. (2010), *The Principles of Naval Architecture Series*, "Ship Resistance and Flow", 2010, Chapter 1: Introduction, pages 1-5.

Michell, J. H. (1898), The wave resistance of a ship, *Philosophical Magazine*, Series 5, Vol. 45, No. 272, London.

Menter, F.R. (1993), Zonal Two Equation $k-\omega$ Turbulence Models for Aerodynamic Flows, In 24th Fluid Dynamics Conference, Orlando, July 1993, AIAA paper-93-2906.

Mahmud, S.M.S, Rahman, M.W and Hasnat-e-Rabbi, S. (2006), *Transport System in Bangladesh: Issues and Options for Sustainable Development*, Accident Research Center (ARC), BUET, Dhaka, Bangladesh.

Moctar, B. E., Kaufmann, J., Ley, J., Oberhagemann, J., Shigunov, V., and Zorn, T. (2010), Prediction of Ship Resistance and Ship Motions Using RANSE, Gothenburg 2010, A Workshop on CFD in Ship Hydromechanics, Gothenburg, Sweden.

National Maritime Research Institute (NMRI), (2015), A Workshop on CFD in Ship Hydrodynamics, Tokyo, URL: <http://www.t2015.nmri.go.jp/>, accessed on 12 October, 2018.

Naz, N. (2017), Numerical Simulation of Flow around Ship Hull Considering Rudder-Propeller Interaction, M.Sc thesis, Department of Naval Architecture & Marine Engineering, Bangladesh University of Engineering & Technology, Dhaka, Bangladesh.

Orych, M. (2013), Development of a Free Surface Capability in a RANS Solver with Coupled Equations and Overset Grids, Licentiate Thesis, Department of Shipping and Marine Technology, Division of Marine Technology, CHALMERS University of Technology, Gothenburg, Sweden.

PIANC (1992), "Capability of Ship Manoeuvring Simulation Models for Approach Channels and Fairways in Harbours", Report of working group No. 20 of permanent technical committee II, Supplement to PIANC Bulletin No. 77, p-49.

Peng, H. (2001), Numerical Computation of Multi-hull Ship Resistance and Motion, Ph. D. Thesis, Dalhousie University, Halifax, Nova Scotia.

Purnamasari, D., Utama, K., A., P., Suastika, K. (2017), CFD Simulations to Calculate the Resistance of a 17.500-DWT Tanker, The 3rd International Seminar on Science and Technology, August 3rd 2017, Surabaya, Indonesia.

Pangaon Inland Container Terminal (PICT), (2018), [URL:http://www.pict.gov.bd/](http://www.pict.gov.bd/) accessed on 18 September 2018.

Regnström, B. (2008), Introduction to Overlapping Grids in SHIPFLOW, Flowtech International AB, Gothenburg, Sweden.

Suzuki K. (1979), Calculation of ship wave resistance with special reference to sinkage. – Proceedings of the Workshop on Ship Wave Resistance Computations, vol.2, pp.256-281.

Subramani A.K., Paterson E.G. and Stern F. (2000), CFD calculation of sinkage and trim. – Journal of Ship Research, vol.44, No.1, pp.59-82.

Svetak. J., SHIP SQUAT, (2001), M. Sc. Fakulteta za pomorstvo in promet, Portoroz, Pot pomorscakov 4, Traffic Engineering, Promet-Traffic-Traffico, Vol. 13, No. 4, p 247-251.

Shabnam, S. (2015), Computational of Ship Hull Resistance using Raynolds Averaged Navier Stokes Equations (RANSE) in Calm Water, M.Sc thesis, Department of Naval Architecture & Marine Engineering, Bangladesh University of Engineering & Technology, Dhaka, Bangladesh.

Saha, G. K., and Miazee, M. A. (2017), “Numerical and Experimental Study of Resistance, Sinkage and Trim of a Container Ship”, Procedia Engineering, vol. 194, pp. 67–73.

Sadrehaghighi, Ideen. (2018), Turbulence Modeling - A Review, CFD Open Series, Revision 1.65, Annapolis, Maryland, USA, DOI:10.13140/RG.2.2.35857.33129/2.

Todd, F. H. (1963), Series 60-Methodical experiments with models of single-screw merchant ships, DTMB Report 1712, Hoboken, NJ: Stevens Inst. of Tech.

Tuck E.O. (1967), Sinkage and trim in shallow water of finite width. – Schiffstechnik, vol.14, pp.92-94.

Tarafder S., Khalil G. (2006), Calculation of ship sinkage and trim in deep water using a potential based panel method, International Journal of Applied Mechanics and Engineering, vol.11, No.2, pp.401-41.

Valdenazzi, F., Harries, S., Janson, C. E., Leer-Andersen, M., Maisonneuve, J. J., Marzi, J. (2003), The FANTASTIC RoRo: CFD optimisation of the forebody and its experimental verification, Proceedings of the NAV2003 Conference, Palermo, Italy.

Vantorre, M. (2003), “Review of practical methods for assessing shallow and restricted water effects.” International Conference on Marine Simulation and Ship Maneuverability (MARSIM 2003), August 2003, Kanazawa, Japan: International Marine Simulator Forum.

Versteeg, H.K. & Malalasekera, W. (2007), “An Introduction to Computational Fluid Dynamics: The Finite Volume Method”, 2nd edition, Chapter-3, p-110.

White, F. (2008), Fluid Mechanics, 6th Edition, New York: McGraw-Hill.

Yasukawa H. (1993), A Rankine panel method to calculate steady wave-making resistance of a ship taking the effect of sinkage and trim into account, Transactions of the West Japan Society of Naval Architects, No.86, pp.27-35.

Appendix-A

A.1 SHIPFLOW input file for 158 TEU Container ship at 10 knot speed

xflow

```
title( title = "SHIPFLOW" )
```

```
program( all )
```

```
vship( fn = [0.192], rn = [432000000] )
```

```
hull( mono, xmacro, h1gr = "hull", fsflow, coarse )
```

```
offset( file = "TCCV_1", lpp = 72.87, xaxdir = -1, ysign = 1, xori = 72.87,  
zori = 3.8 )
```

end

xpan

```
iterati( maxit = 20 )
```

```
parall( nthread = 6 )
```

end

A.2 SHIPFLOW output file for 158 TEU Container ship at 10 knot speed

SHIPFLOW-XFLOW VERSION 5.1.00 2017-08-13 AT 14:03:11

```
*****
* THIS SOFTWARE IS A LICENSED PRODUCT OF FLOWTECH INTERNATIONAL AB,*
* AND MAY ONLY BE USED ACCORDING TO THE TERMS OF THAT LICENSE ON THE *
* SYSTEM IDENTIFIED IN THE LICENSE AGREEMENT. COPYRIGHT (C) 1990 BY *
* FLOWTECH INTERNATIONAL AB. ALL RIGHTS RESERVED. *
*****
```

Licensed under the SHIPFLOW EDUCATIONAL LICENSE AGREEMENT

--- To be used only in academic education ---

Revision: Rev. 9136

- COMMANDS AND KEYWORDS FOR XFLOW

Both input and default values are printed

- TITLE

titl = SHIPFLOW

- POST PROCESSOR

Default post-processor SHIPFLOW is used.

- PROGRAM

xmes

xpan

xbou

xgri

xcha

- HULLTYPE

mono

xmau

h1gr = hull

fsfl

bden = 5.00000E-01

fden = 5.00000E-01

trxd

xwlp = 6.00000E-01

- OFFSETFILE

file = ../TCCV_1

lpp = 7.28700E+01

xori = 7.28700E+01

yori = 0.00000E+00

zori = 3.80000E+00

ztem = 0.00000E+00

ztop = 0.00000E+00

xaxd = -1.00000E+00

ysig = 1.00000E+00

itte = 4

- IPOSITION

roll = 0.00000E+00
 trim = 0.00000E+00
 xcof = 5.00000E-01
 zvcg = 0.00000E+00

- OSFLOW

numb = 1
 flow = 0.00000E+00

- VSHIP

numb = 1
 fn = 1.92000E-01
 rn = 4.32000E+08

- SYMMETRY

xzpl

- FLUID

dens = 1.00000E+03
 grav = 9.80665E+00
 visc = 1.00400E-06

SHIPFLOW-XMESH VERSION 5.1.00 2017-08-13 AT 14:03:12

Licensed under the SHIPFLOW EDUCATIONAL LICENSE AGREEMENT

--- To be used only in academic education ---

- Estimated memory requirement for XPAN
 memory requirement in integer words: 31513221
 available memory (SHIPFLOWMEM): 200000000
 - Estimated disk space requirement for XPAN
 disk space in Mbyte : 1
 - COMMANDS AND KEYWORDS FOR XMESH
 Both input and default values are printed

- BODY

grno = 1
 high
 gene
 fsin
 onei
 offs = hull
 poin = 14
 stat = 79
 expa = 2
 str1 = 0
 df1 = 0.00000E+00
 dl1 = 0.00000E+00
 str2 = 5
 df2 = 5.00000E-03
 dl2 = 5.00000E-03

str3 = 0
df3 = 0.00000E+00
dl3 = 0.00000E+00
str4 = 5
df4 = 5.00000E-03
dl4 = 5.00000E-03
xtra = 0.00000E+00
ytra = 0.00000E+00
ztra = 0.00000E+00
xrot = 0.00000E+00
yrot = 0.00000E+00
zrot = 0.00000E+00
xsca = 1.00000E+00
ysca = 1.00000E+00
zsca = 1.00000E+00
velb = 0.00000E+00

- FREE

grno = 2
firs
gene
poin = 24
str1 = 1
df1 = 1.26800E-02
dl1 = 0.00000E+00
stau = 15
stru = 1
dfu = 0.00000E+00
dlu = 1.78571E-02
stam = 57
strm = 0
dfm = 0.00000E+00
dlm = 0.00000E+00
stad = 35
strd = 1
dfd = 1.78571E-02
dld = 0.00000E+00
xups = -3.65812E-01
xbow = 0.00000E+00
xste = 1.00000E+00
xdow = 1.84744E+00
y2si = 0.00000E+00
y4si = -9.04726E-01
smoo = 10
nbd2 = 1
ibd2 = 1
nbd4 = 0
nbde = 0
xu2 = -1.00000E-02
yu2 = 0.00000E+00
xd1 = 1.10000E+00

yd1 = 0.00000E+00
 Total no. of panels : 3562
 Total no. of nodes : 3784

SHIPFLOW-XPAN VERSION 5.1.00 2017-08-13 AT 14:03:12

Licensed under the SHIPFLOW EDUCATIONAL LICENSE AGREEMENT

--- To be used only in academic education ---

Non-lifting potential flow
 with free surface
 and without the dry transom stern option

- COMMANDS AND KEYWORDS FOR XPAN

Both input and default values are printed

- CONTROL

nonl
 itso
 eqsi = 1.00000E-05
 eqav = 5.00000E-03
 eqco = 1.00000E-03
 nodi
 sing
 four
 free
 save
 nola
 zrai = 7.60000E-01
 xshi = 3.00000E-01
 zfac = 7.50000E-01
 afss

- CONVERGENCE

eptr = 1.00000E-02
 epsi = 1.00000E-05
 epwa = 5.00000E-05
 wchm = 1.00000E+00

- EXFORCE

cvfo = 0.00000E+00
 cvli = 0.00000E+00
 cvbo = 0.00000E+00

- EXMOMENT

towx = LCB
 towz = VPoR
 towa = 0.00000E+00
 zmlt = 0.00000E+00
 zmbo = 0.00000E+00

- ITERATION

maxi = 20

- RELAXATION

rfr = 1.00000E+00
 rfsi = 1.00000E+00
 rfso = 7.00000E-01
 rfwa = 1.00000E+00

- TWCUT

xstt = 1.55791E+00
 xent = 1.78953E+00
 ytwc = -9.04726E-01
 stat = 8
 strt = 1
 dftw = 1.44765E-02
 dltw = 0.00000E+00
 nval = 100
 nwav = 100

Case no 1 : Flow Angle = 0.0 Fn = 0.192 Iteration no 1

- Iterations

IT (iterations) : 1

- Hull data, non-dimensionalized by Lpp

LPP (length) : 0.100000000000000E+01
 B (breadth) : 0.205855864955575E+00
 T (draught) : 0.519907814637945E-01
 WPA (water plane area) : 0.195505045686510E+00
 CWPA (water plane area coefficient) : 0.949718123060043E+00
 CB (block coefficient) : 0.838496610570712E+00
 CPRISM (prismatic coefficient) : 0.880361185564826E+00
 LCB (x - center of buoyancy) : 0.490172253147491E+00
 VCB (z - center of buoyancy) : -0.242731590587442E-01
 S (wetted surface area) : 0.270805648506232E+00
 V (displacement) : 0.897409993521186E-02

- Resistance coefficients (force/(0.5*density*Sref*U2))**

CW (Wave resist. coeff. press. int.) : 0.309035634912877E-02
 CWTWC (Wave resist. coeff. wave cut) : 0.866837506625795E-03
 Sref (Wetted surface at zero speed) : 0.270805648506232E+00

- Sinkage and Trim calculation

CZSINK (coefficient of sinking force) : -0.556971444932267E-01
 CMTRIM (coefficient of trim moment) : -0.180480254443207E-02
 XCOF (center of flotation) : 0.508859601608415E+00
 BML (metacentric radius, long.) : 0.166052316225333E+01
 TRIMAN (trim angle in degree) : -0.127446320623707E+00
 ZSINK (draft change at Lpp/2) : -0.144172507707137E-02
 ZSINKF (draft change at XCOF) : -0.142201815211494E-02
 ZSINKB (draft change at bow) : -0.255390403428939E-02

ZSINKS (draft change at stern) : -0.329546119853356E-03

Case no 1 : Flow Angle = 0.0 Fn = 0.192 Iteration no 2

- Iterations

IT (iterations) : 2

- Hull data, non-dimensionalized by Lpp

LPP (length) : 0.100000000000000E+01
 B (breadth) : 0.205849381071345E+00
 T (draught) : 0.544428558769014E-01
 WPA (water plane area) : 0.196037768978010E+00
 CWPA (water plane area coefficient) : 0.952335965052358E+00
 CB (block coefficient) : 0.825052332145637E+00
 CPRISM (prismatic coefficient) : 0.799852467646639E+00
 LCB (x - center of buoyancy) : 0.487124223477025E+00
 VCB (z - center of buoyancy) : -0.248771715871162E-01
 S (wetted surface area) : 0.273290370582940E+00
 V (displacement) : 0.924638474129487E-02

- Resistance coefficients (force/(0.5*density*Sref*U2))**

CW (Wave resist. coeff. press. int.) : 0.355390997582596E-02
 CWTWC (Wave resist. coeff. wave cut) : 0.200265437108438E-03
 Sref (Wetted surface at zero speed) : 0.270805648506232E+00

- Sinkage and Trim calculation

CZSINK (coefficient of sinking force) : -0.595200742086377E-01
 CMTRIM (coefficient of trim moment) : -0.193307814684063E-02
 XCOF (center of flotation) : 0.508181921260336E+00
 BML (metacentric radius, long.) : 0.167717627448832E+01
 TRIMAN (trim angle in degree) : -0.136360370673413E+00
 ZSINK (draft change at Lpp/2) : -0.153496531545783E-02
 ZSINKF (draft change at XCOF) : -0.151549285473975E-02
 ZSINKB (draft change at bow) : -0.272493403420332E-02
 ZSINKS (draft change at stern) : -0.344996596712339E-03

- Convergence test :

- Max wave change = 0.6111E-02 at panel no : 2898
 - Max wave elevation = 0.1676E-01 at panel no : 1493
 - Max dyn. BC residual = -.157586E-02 at panel no : 2828
 - Max tot. BC residual = -.613729E+00 at panel no : 2735
 - Norm dyn. BC residual = 0.455207E-04
 - Norm tot. BC residual = 0.624144E-02

- Convergence test :

- Change of sinkage = 0.9347E-04
 - Change of trim angle = 0.8914E-02

Case no 1 : Flow Angle = 0.0 Fn = 0.192 Iteration no 3

- Iterations

IT (iterations) : 3

- Hull data, non-dimensionalized by Lpp

LPP (length) : 0.100000000000000E+01
 B (breadth) : 0.205843193183604E+00
 T (draught) : 0.546069551708044E-01
 WPA (water plane area) : 0.196082171816411E+00
 CWPA (water plane area coefficient) : 0.952580305346865E+00
 CB (block coefficient) : 0.824294070511402E+00
 CPRISM (prismatic coefficient) : 0.811677379269198E+00
 LCB (x - center of buoyancy) : 0.486926823829443E+00
 VCB (z - center of buoyancy) : -0.249214660236283E-01
 S (wetted surface area) : 0.273385121926770E+00
 V (displacement) : 0.926545278921911E-02

- Resistance coefficients (force/(0.5*density*Sref*U2))**

CW (Wave resist. coeff. press. int.) : 0.255102641385439E-02
 CWTWC (Wave resist. coeff. wave cut) : 0.203358068838263E-03
 Sref (Wetted surface at zero speed) : 0.270805648506232E+00

- Sinkage and Trim calculation

CZSINK (coefficient of sinking force) : -0.611823100937539E-01
 CMTRIM (coefficient of trim moment) : -0.215396569425457E-02
 XCOF (center of flotation) : 0.508590080706494E+00
 BML (metacentric radius, long.) : 0.167793589678003E+01
 TRIMAN (trim angle in degree) : -0.152311805254675E+00
 ZSINK (draft change at Lpp/2) : -0.158029911043839E-02
 ZSINKF (draft change at XCOF) : -0.155746373389218E-02
 ZSINKB (draft change at bow) : -0.290947035611362E-02
 ZSINKS (draft change at stern) : -0.251127864763149E-03

- Convergence test :

- Max wave change = -0.4584E-02 at panel no : 2852
 - Max wave elevation = 0.1596E-01 at panel no : 1493
 - Max dyn. BC residual = -.230750E-03 at panel no : 2758
 - Max tot. BC residual = -.111564E+00 at panel no : 2782
 - Norm dyn. BC residual = 0.100295E-04
 - Norm tot. BC residual = 0.267753E-02

- Convergence test :

- Change of sinkage = 0.4197E-04
 - Change of trim angle = 0.1595E-01

Case no 1 : Flow Angle = 0.0 Fn = 0.192 Iteration no 4

- Iterations

IT (iterations) : 4

- Hull data, non-dimensionalized by Lpp

LPP (length) : 0.1000000000000000E+01
 B (breadth) : 0.205835358967216E+00
 T (draught) : 0.547790859819881E-01
 WPA (water plane area) : 0.196063170954106E+00
 CWPA (water plane area coefficient) : 0.952524250147582E+00
 CB (block coefficient) : 0.822506482983266E+00
 CPRISM (prismatic coefficient) : 0.815212267606187E+00
 LCB (x - center of buoyancy) : 0.486509953305773E+00
 VCB (z - center of buoyancy) : -0.249469729085747E-01
 S (wetted surface area) : 0.273197749410782E+00
 V (displacement) : 0.927414949890792E-02

- Resistance coefficients (force/(0.5*density*Sref*U2))**

CW (Wave resist. coeff. press. int.) : 0.177355336562163E-02
 CWTWC (Wave resist. coeff. wave cut) : 0.286590898387478E-03
 Sref (Wetted surface at zero speed) : 0.270805648506232E+00

- Sinkage and Trim calculation

CZSINK (coefficient of sinking force) : -0.607576274419323E-01
 CMTRIM (coefficient of trim moment) : -0.234816485383688E-02
 XCOF (center of flotation) : 0.508814520567478E+00
 BML (metacentric radius, long.) : 0.167743517097766E+01
 TRIMAN (trim angle in degree) : -0.166290213202873E+00
 ZSINK (draft change at Lpp/2) : -0.157238534038693E-02
 ZSINKF (draft change at XCOF) : -0.154680285391230E-02
 ZSINKB (draft change at bow) : -0.302354120750367E-02
 ZSINKS (draft change at stern) : -0.121229473270194E-03

- Convergence test :

- Max wave change = -0.9984E-03 at panel no : 1587
 - Max wave elevation = 0.1565E-01 at panel no : 1493
 - Max dyn. BC residual = -.652580E-04 at panel no : 1517
 - Max tot. BC residual = -.504198E-01 at panel no : 2853
 - Norm dyn. BC residual = 0.233354E-05
 - Norm tot. BC residual = 0.133906E-02

- Convergence test :

- Change of sinkage = 0.1066E-04
 - Change of trim angle = 0.1398E-01

Case no 1 : Flow Angle = 0.0 Fn = 0.192 Iteration no 5

- Iterations

IT (iterations) : 5

- Hull data, non-dimensionalized by Lpp

LPP (length) : 0.1000000000000000E+01
 B (breadth) : 0.205831315646170E+00

T (draught) : 0.548822823632692E-01
 WPA (water plane area) : 0.196057749224719E+00
 CWPA (water plane area coefficient) : 0.952516620754385E+00
 CB (block coefficient) : 0.820815009748359E+00
 CPRISM (prismatic coefficient) : 0.816016099106424E+00
 LCB (x - center of buoyancy) : 0.486129398755028E+00
 VCB (z - center of buoyancy) : -0.249472100031146E-01
 S (wetted surface area) : 0.273147056158557E+00
 V (displacement) : 0.927233050670260E-02

- Resistance coefficients (force/(0.5*density*Sref*U2))**

CW (Wave resist. coeff. press. int.) : 0.144449237015571E-02
 CWTWC (Wave resist. coeff. wave cut) : 0.303360840548059E-03
 Sref (Wetted surface at zero speed) : 0.270805648506232E+00

- Sinkage and Trim calculation

CZSINK (coefficient of sinking force) : -0.609913069746037E-01
 CMTRIM (coefficient of trim moment) : -0.239785422319966E-02
 XCOF (center of flotation) : 0.508901933168522E+00
 BML (metacentric radius, long.) : 0.167727578976385E+01
 TRIMAN (trim angle in degree) : -0.169910694321311E+00
 ZSINK (draft change at Lpp/2) : -0.157919363429515E-02
 ZSINKF (draft change at XCOF) : -0.155279494213459E-02
 ZSINKB (draft change at bow) : -0.306194415942340E-02
 ZSINKS (draft change at stern) : -0.964431091669026E-04

- Convergence test :

- Max wave change = -0.5936E-03 at panel no : 1564
 - Max wave elevation = 0.1548E-01 at panel no : 1493
 - Max dyn. BC residual = -.204140E-04 at panel no : 1517
 - Max tot. BC residual = -.280302E-01 at panel no : 1517
 - Norm dyn. BC residual = 0.488118E-06
 - Norm tot. BC residual = 0.647593E-03

- Convergence test :

- Change of sinkage = 0.5992E-05
 - Change of trim angle = 0.3620E-02

Case no 1 : Flow Angle = 0.0 Fn = 0.192 Iteration no 6

- Iterations

IT (iterations) : 6

- Hull data, non-dimensionalized by Lpp

LPP (length) : 0.100000000000000E+01
 B (breadth) : 0.205830408336763E+00
 T (draught) : 0.549178682526125E-01
 WPA (water plane area) : 0.196044209318956E+00
 CWPA (water plane area coefficient) : 0.952455037635665E+00
 CB (block coefficient) : 0.820401206487199E+00

CPRISM (prismatic coefficient) : 0.817573609063282E+00
 LCB (x - center of buoyancy) : 0.486036500668319E+00
 VCB (z - center of buoyancy) : -0.249513530367573E-01
 S (wetted surface area) : 0.273115042138574E+00
 V (displacement) : 0.927362428763367E-02

- Resistance coefficients (force/(0.5*density*Sref*U2))**

CW (Wave resist. coeff. press. int.) : 0.127773822823056E-02
 CWTWC (Wave resist. coeff. wave cut) : 0.311942687049652E-03
 Sref (Wetted surface at zero speed) : 0.270805648506232E+00

- Sinkage and Trim calculation

CZSINK (coefficient of sinking force) : -0.611776980026292E-01
 CMTRIM (coefficient of trim moment) : -0.241951299534028E-02
 XCOF (center of flotation) : 0.508920293398877E+00
 BML (metacentric radius, long.) : 0.167694261781600E+01
 TRIMAN (trim angle in degree) : -0.171527833730606E+00
 ZSINK (draft change at Lpp/2) : -0.158435280590924E-02
 ZSINKF (draft change at XCOF) : -0.155764789647344E-02
 ZSINKB (draft change at bow) : -0.308121553461548E-02
 ZSINKS (draft change at stern) : -0.874900772030109E-04

- Convergence test :

- Max wave change = -0.3786E-03 at panel no : 1564
 - Max wave elevation = 0.1541E-01 at panel no : 1493
 - Max dyn. BC residual = -.612169E-05 at panel no : 1518
 - Max tot. BC residual = -.146196E-01 at panel no : 1493
 - Norm dyn. BC residual = 0.184129E-06
 - Norm tot. BC residual = 0.352302E-03

- Convergence test :

- Change of sinkage = 0.4853E-05
 - Change of trim angle = 0.1617E-02

Case no 1 : Flow Angle = 0.0 Fn = 0.192 Iteration no 7

- Iterations

IT (iterations) : 7

- Hull data, non-dimensionalized by Lpp

LPP (length) : 0.100000000000000E+01
 B (breadth) : 0.205830248647785E+00
 T (draught) : 0.549358812779403E-01
 WPA (water plane area) : 0.196036651383876E+00
 CWPA (water plane area coefficient) : 0.952419057314230E+00
 CB (block coefficient) : 0.820220915935339E+00
 CPRISM (prismatic coefficient) : 0.818966438840075E+00
 LCB (x - center of buoyancy) : 0.485995220920108E+00
 VCB (z - center of buoyancy) : -0.249542048512641E-01

S (wetted surface area) : 0.273097155326256E+00
 V (displacement) : 0.927462020401186E-02

- Resistance coefficients (force/(0.5*density*Sref*U2))**

CW (Wave resist. coeff. press. int.) : 0.118802937047473E-02
 CWTWC (Wave resist. coeff. wave cut) : 0.316078450371772E-03
 Sref (Wetted surface at zero speed) : 0.270805648506232E+00

- Sinkage and Trim calculation

CZSINK (coefficient of sinking force) : -0.613010471089816E-01
 CMTRIM (coefficient of trim moment) : -0.243040831217188E-02
 XCOF (center of flotation) : 0.508932906996176E+00
 BML (metacentric radius, long.) : 0.167675337002446E+01
 TRIMAN (trim angle in degree) : -0.172346195003726E+00
 ZSINK (draft change at Lpp/2) : -0.158771892798804E-02
 ZSINKF (draft change at XCOF) : -0.156084866731270E-02
 ZSINKB (draft change at bow) : -0.309172320603765E-02
 ZSINKS (draft change at stern) : -0.837146499384316E-04

- Convergence test :

- Max wave change = -0.2304E-03 at panel no : 1564
 - Max wave elevation = 0.1539E-01 at panel no : 1493
 - Max dyn. BC residual = -.224968E-05 at panel no : 1518
 - Max tot. BC residual = -.880348E-02 at panel no : 1493
 - Norm dyn. BC residual = 0.725864E-07
 - Norm tot. BC residual = 0.204971E-03

- Convergence test :

- Change of sinkage = 0.3201E-05
 - Change of trim angle = 0.8184E-03

Case no 1 : Flow Angle = 0.0 Fn = 0.192 Iteration no 8

- Iterations

IT (iterations) : 8

- Hull data, non-dimensionalized by Lpp

LPP (length) : 0.100000000000000E+01
 B (breadth) : 0.205830248541803E+00
 T (draught) : 0.549457521390611E-01
 WPA (water plane area) : 0.196032491446875E+00
 CWPA (water plane area coefficient) : 0.952398847281482E+00
 CB (block coefficient) : 0.820131133174902E+00
 CPRISM (prismatic coefficient) : 0.819931732169849E+00
 LCB (x - center of buoyancy) : 0.485974350180951E+00
 VCB (z - center of buoyancy) : -0.249560115939067E-01
 S (wetted surface area) : 0.273086191698391E+00
 V (displacement) : 0.927527126201698E-02

- Resistance coefficients (force/(0.5*density*Sref*U2))**

CW (Wave resist. coeff. press. int.) : 0.114053561403654E-02
 CWTWC (Wave resist. coeff. wave cut) : 0.317565713960019E-03
 Sref (Wetted surface at zero speed) : 0.270805648506232E+00

- Sinkage and Trim calculation

CZSINK (coefficient of sinking force) : -0.613815155731416E-01
 CMTRIM (coefficient of trim moment) : -0.243521084898033E-02
 XCOF (center of flotation) : 0.508940670810542E+00
 BML (metacentric radius, long.) : 0.167664755083246E+01
 TRIMAN (trim angle in degree) : -0.172712203885323E+00
 ZSINK (draft change at Lpp/2) : -0.158988145073311E-02
 ZSINKF (draft change at XCOF) : -0.156293072289548E-02
 ZSINKB (draft change at bow) : -0.309707975882043E-02
 ZSINKS (draft change at stern) : -0.826831426457913E-04

- Convergence test :

- Max wave change = -0.1371E-03 at panel no : 1564
 - Max wave elevation = 0.1538E-01 at panel no : 1493
 - Max dyn. BC residual = -.796843E-06 at panel no : 1518
 - Max tot. BC residual = -.546354E-02 at panel no : 1471
 - Norm dyn. BC residual = 0.269801E-07
 - Norm tot. BC residual = 0.123156E-03

- Convergence test :

- Change of sinkage = 0.2082E-05
 - Change of trim angle = 0.3660E-03

Case no 1 : Flow Angle = 0.0 Fn = 0.192 Iteration no 9

- Iterations

IT (iterations) : 9

- Hull data, non-dimensionalized by Lpp

LPP (length) : 0.100000000000000E+01
 B (breadth) : 0.205830258421582E+00
 T (draught) : 0.549508238773892E-01
 WPA (water plane area) : 0.196030247664215E+00
 CWPA (water plane area coefficient) : 0.952387900435445E+00
 CB (block coefficient) : 0.820092648617321E+00
 CPRISM (prismatic coefficient) : 0.820547053448160E+00
 LCB (x - center of buoyancy) : 0.485965307316598E+00
 VCB (z - center of buoyancy) : -0.249571233351726E-01
 S (wetted surface area) : 0.273079621621018E+00
 V (displacement) : 0.927569257501601E-02

- Resistance coefficients (force/(0.5*density*Sref*U2))**

CW (Wave resist. coeff. press. int.) : 0.111479823414492E-02
 CWTWC (Wave resist. coeff. wave cut) : 0.318015061398884E-03
 Sref (Wetted surface at zero speed) : 0.270805648506232E+00

- Sinkage and Trim calculation

CZSINK (coefficient of sinking force) : -0.614286918464224E-01
 CMTRIM (coefficient of trim moment) : -0.243740170034691E-02
 XCOF (center of flotation) : 0.508945180316055E+00
 BML (metacentric radius, long.) : 0.167658933654745E+01
 TRIMAN (trim angle in degree) : -0.172881728490223E+00
 ZSINK (draft change at Lpp/2) : -0.159114064289545E-02
 ZSINKF (draft change at XCOF) : -0.156414985495542E-02
 ZSINKB (draft change at bow) : -0.309981833224209E-02
 ZSINKS (draft change at stern) : -0.824629535488089E-04

- Convergence test :

- Max wave change = -0.8114E-04 at panel no : 1564
 - Max wave elevation = 0.1538E-01 at panel no : 1493
 - Max dyn. BC residual = -.279131E-06 at panel no : 1518
 - Max tot. BC residual = -.339124E-02 at panel no : 1471
 - Norm dyn. BC residual = 0.980740E-08
 - Norm tot. BC residual = 0.740541E-04

- Convergence test :

- Change of sinkage = 0.1219E-05
 - Change of trim angle = 0.1695E-03

Case no 1 : Flow Angle = 0.0 Fn = 0.192 Iteration no 10

- Iterations

IT (iterations) : 10

- Hull data, non-dimensionalized by Lpp

LPP (length) : 0.100000000000000E+01
 B (breadth) : 0.205830222623601E+00
 T (draught) : 0.549534305323460E-01
 WPA (water plane area) : 0.196029020056071E+00
 CWPA (water plane area coefficient) : 0.952382101896411E+00
 CB (block coefficient) : 0.820076083087735E+00
 CPRISM (prismatic coefficient) : 0.820922824743021E+00
 LCB (x - center of buoyancy) : 0.485961127391000E+00
 VCB (z - center of buoyancy) : -0.249577567081259E-01
 S (wetted surface area) : 0.273075711968705E+00
 V (displacement) : 0.927594359078240E-02

- Resistance coefficients (force/(0.5*density*Sref*U2))**

CW (Wave resist. coeff. press. int.) : 0.110036274259843E-02
 CWTWC (Wave resist. coeff. wave cut) : 0.318045945772683E-03
 Sref (Wetted surface at zero speed) : 0.270805648506232E+00

- Sinkage and Trim calculation

CZSINK (coefficient of sinking force) : -0.614564530680980E-01
 CMTRIM (coefficient of trim moment) : -0.243842330408357E-02
 XCOF (center of flotation) : 0.508947781811489E+00
 BML (metacentric radius, long.) : 0.167655684730497E+01

TRIMAN (trim angle in degree) : -0.172962193448131E+00
 ZSINK (draft change at Lpp/2) : -0.159187773828443E-02
 ZSINKF (draft change at XCOF) : -0.156486653463622E-02
 ZSINKB (draft change at bow) : -0.310125761685505E-02
 ZSINKS (draft change at stern) : -0.824978597137995E-04

- Convergence test :

- Max wave change = -0.4841E-04 at panel no : 1564
 - Max wave elevation = 0.1537E-01 at panel no : 1493
 - Max dyn. BC residual = -.985024E-07 at panel no : 1518
 - Max tot. BC residual = -.208353E-02 at panel no : 1471
 - Norm dyn. BC residual = 0.350019E-08
 - Norm tot. BC residual = 0.444563E-04

- Convergence test :

- Change of sinkage = 0.7167E-06
 - Change of trim angle = 0.8046E-04

***** Convergence achieved after 10 iterations *****

SHIPFLOW-XBOUND VERSION 5.1.00 2017-08-13 AT 14:03:31

Licensed under the SHIPFLOW EDUCATIONAL LICENSE AGREEMENT

--- To be used only in academic education ---

- COMMANDS AND KEYWORDS FOR XBOUND

Both input and default values are printed

- CONTROL

save
 file = XBLIMIT

- INICON

sgro = 1
 turb
 poin = 1
 girt = 0.00000E+00
 t11 = 1.00000E-04
 h12 = 1.26628E+00
 beta = 0.00000E+00

- RESISTANCE

x11 = 5.00000E-02
 x12 = 9.00000E-01

- ROUGHNESS

h = 0.00000E+00
 c = 0.00000E+00

- TRACE

```

sgro = 1
grou = 1
stat = 100
stre = 10
ista = 10
idis = 1
s1 = 5.00000E-02
ds1 = 1.00000E-02
sn = 9.00000E-01
dsn = 0.00000E+00
jdis = 0
p1 = 5.00000E-02
dp1 = 0.00000E+00
pn = 9.50000E-01
dpn = 0.00000E+00

```

```

*** Warning: FREESURFACE option turned on
    Non-linear free-surface solution found in _XPDB

```

```

- Estimated memory requirements for XBOUND
memory in integer words      : 771212
available memory ( SHIPFLOWMEM ) :*****

```

- Sinkage and Trim calculation

```

XCOF ( center of flotation )      : 0.5089478E+00
TRIMAN ( trim angle in degrees )  : -0.1729622E+00
ZSINKF ( draft change at XCOF )   : -0.1564867E-02
ZSINK ( draft change at Lpp/2 )   : -0.1591878E-02
ZSINKB ( draft change at bow )    : -0.3101258E-02
ZSINKS ( draft change at stern )  : -0.8249786E-04

```

- Resistance coefficients (force/(0.5*density*Sref*U2))**

```

CW ( Wave resist. coeff. )       : 0.1100363E-02
Sref ( Wetted surface at zero speed ) : 0.2708056E+00

```

- Total skin friction coefficient:

```

CF ( Total skin friction coefficient ) : 1.769E-03
AREA ( Area for normalization )      : 1.259E-01

```

SHIPFLOW-XCHAP VERSION 5.1.00 2017-08-13 AT 14:03:32

Licensed under the SHIPFLOW EDUCATIONAL LICENSE AGREEMENT

--- To be used only in academic education ---

INDATA SECTION

- CONTROL

```

maxi = ***
cfl = 1.00000E+00
limi
sche = FROMM

```

rela = ADI
 disc = 0.00000E+00
 conv = 1.00000E-06
 refi = 1.00000E+00
 easm
 stre

- FRAME

imax = 0
 jmax = 0
 kmax = 0
 xste = 1.50000E+00
 zsli = 0.00000E+00

*** XGRID STARTED BY XCHAP**

- Coordinate transformation

Sinkage and trim will be taken from the XPDB-file,
 sinkage : -1.56487E-03
 trim : 0.000 + -0.173 (initial + correction)
 xcof : 0.509

- COMMANDS AND KEYWORDS FOR XGRID

Both input and default values are printed

- OUTPUT

This card was not found.
 Default output will be used:
 Interpolated grid -> XVGRID-file
 Coarse grid -> XGPOST-file
 Iteration history turned off

- OFFSET

h1gr = hull

- SIZE

This card was not found.
 ksim = 135 (default)
 etam = 59 (default)
 aeta = 0 (default)
 ueta = 0 (default)
 zeta = 84 (default)
 habo = 0.00000E+00 (default)
 hund = 0.00000E+00 (default)

- COARSE

This card was not found.
 ksic = 135.0 (default)
 zeta = 84.0 (default)
 fatt = 1.00000E+00 (default)

- XDISTR

This card was not found.
 xsta = 5.00000E-01 (default)

NM = 62 (default)
 xapu = 8.80000E-01 (default)
 NA = 38 (default)
 xapd = 9.90000E-01 (default)
 NW = 34 (default)
 xend = 1.80000E+00 (default)

- RADIUS

This card was not found.
 radi = 3.00000E+00 (default)
 cent = 0.00000E+00 (default)
 rsti = 0.00000E+00 (default)

- YPLUS

This card was not found.
 No wall laws assumed
 ytar = 8.30000E-01 (default)
 yexp = 1.00000E+00 (default)

- SKIN

The "skin" thickness at the keel is defined by:

x	thickness
0.90000	6.88748E-08
1.2000	6.88748E-08

 The "skin" thickness at the waterline is defined by:

x	thickness
0.90000	6.88748E-08
1.0000	6.88748E-08

- SINGUL

The singul(keel) card was not found.
 The default rule for monohull is used
 The singul(water) card was not found.
 The default line that follows the centre of the grid will be used.

- ETASMOOTH

This card was not found.
 The eta-boundary smoothing has been turned off.
 time = 1.00000E+00 (default)
 zeta = 16.0 (default)

- POISSON

This card was not found.
 The poisson solver has been turned on.
 maxi = 60 (default)
 ycri = 1.00000E-09 (default)
 zcri = 1.00000E-09 (default)
 orfy = 1.00000E+00 (default)
 orfz = 1.00000E+00 (default)

- NEUMANN

This card was not found.

The Neumann b.c. at the eta-boundaries has been turned off.

neuw = 20 (default)

neuh = 1 (default)

neum = 40 (default)

- IMPROVE

This card was not found.

impw = 4 (default)

imph = 1 (default)

impm = 40 (default)

angs = 1.00000E-03 (default)

conf = 33.0 (default)

- FEEDBACK

No feedback card was found, default values will be used.

--END OF ECHO

- Estimated memory requirements for XGRID

memory in integer words : 10822866

available memory (SHIPFLOWMEM): 200000000

- Estimated memory requirements for XGRID

memory in integer words : 18806496

available memory (SHIPFLOWMEM): 200000000

- Poisson solver iteration history:

	max change	max change
iter.	of y	of z
1	7.43141E-03	6.92620E-03
2	4.52850E-03	4.94779E-03
3	3.62458E-03	3.65077E-03
4	3.02732E-03	2.90686E-03
5	1.77765E-03	1.63275E-03
6	3.95469E-03	3.24542E-03
7	5.08718E-03	4.13220E-03
8	5.46986E-03	4.67212E-03
9	5.48817E-03	4.82654E-03
10	5.37825E-03	4.93842E-03
11	5.23652E-03	4.87674E-03
12	5.04795E-03	4.75602E-03
13	4.85105E-03	4.66825E-03
14	4.64815E-03	4.55033E-03
15	4.41295E-03	4.42964E-03
16	4.17170E-03	4.30745E-03
17	3.89891E-03	4.20097E-03
18	3.62649E-03	4.10423E-03
19	3.32933E-03	3.99807E-03
20	3.09361E-03	3.88497E-03
21	2.90539E-03	3.78057E-03
22	2.81976E-03	3.68396E-03
23	2.72436E-03	3.58435E-03
24	2.62453E-03	3.48513E-03
25	2.55236E-03	3.38715E-03

26	2.51335E-03	3.29238E-03
27	2.41455E-03	3.21224E-03
28	2.52095E-03	3.13273E-03
29	2.73309E-03	3.05412E-03
30	2.90662E-03	2.97628E-03
31	2.97626E-03	2.89873E-03
32	2.88908E-03	2.83092E-03
33	2.80515E-03	2.75804E-03
34	2.60389E-03	2.68019E-03
35	2.39512E-03	2.59711E-03
36	2.18651E-03	2.50675E-03
37	2.00676E-03	2.41438E-03
38	1.81707E-03	2.34409E-03
39	1.63383E-03	2.27359E-03
40	1.47767E-03	2.19730E-03
41	1.33732E-03	2.11956E-03
42	1.26306E-03	2.03907E-03
43	1.22436E-03	1.95951E-03
44	1.18199E-03	1.88291E-03
45	1.10170E-03	1.85484E-03
46	1.06142E-03	1.82991E-03
47	1.04026E-03	1.80617E-03
48	1.02898E-03	1.78269E-03
49	1.01947E-03	1.75946E-03
50	1.00954E-03	1.73647E-03
51	9.99222E-04	1.71372E-03
52	9.88524E-04	1.69199E-03
53	9.77635E-04	1.67078E-03
54	9.67239E-04	1.64980E-03
55	9.57823E-04	1.62910E-03
56	9.48233E-04	1.60869E-03
57	9.38408E-04	1.58861E-03
58	9.28989E-04	1.56891E-03
59	9.19600E-04	1.54960E-03
60	9.10052E-04	1.53090E-03

- Maximum number 60 (= maxit) iterations reached.

- Calculation of inlet profiles:

Reading XBDB file: config_XBDB
 created: 2016-08-13 at 14:03:31
 text card: SHIPFLOW
 number of data points: 1170
 x11 = 5.000E-02 (x12 = 9.000E-01)
 Reynolds number: 4.320E+08
 Data interpolated from section: 1

OVERLAPPING GRID SECTION

No of frames : 1
 No of grids : 1
 No of points : 669060
 No of interpolation cells : 0
 No of discretization cells: 744372

No of outside cells : 0
Total no of cells : 744372
Standard deviation for forces in XCHAP
(Displayed in percent of average force)
std(CPV)= : 0.62 %
std(CF)= : 0.01 %
Datapoints : 87

- Resistance:

CF (Frictional resist. coeff.) : 1.601E-03
CPV (Viscous pres. resist. coeff.) : 6.053E-04
CV (Viscous resist. coeff.) : 2.206E-03
CW (Wave resist. coeff.) : 1.100E-03
CT (Total resist. coeff.) : 3.306E-03
K (Form factor) : 0.295
S (Wetted surface / L**2) : 0.2708

SHIPFLOW started: 2017-08-13 at 14:03:11, ended: 2017-08-13 at 20:19:12